UNIVERSITY OF PARDUBICE

FACULTY OF TRANSPORT ENGINEERING

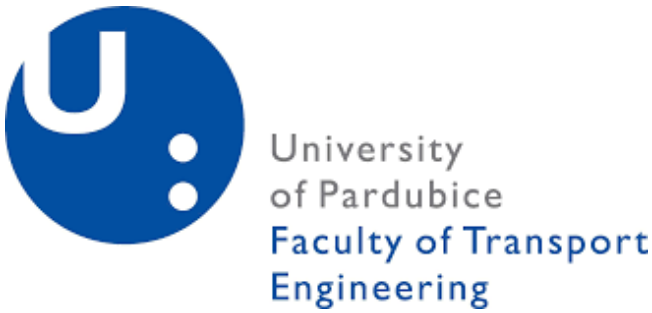

ANTI-SLIP CONTROL OF TRACTION MOTOR OF RAIL VEHICLES

Ing. Abdulkadir Zirek

Doctoral Thesis

2019

Programme of Study:

P3710 Technique and Technology in Transport and Communications

Branch of study:

3706V005 Transport Means and Infrastructure

Dissertation Title:

Anti-slip Control of Traction Motor of Rail Vehicles

Author:

Ing. Abdulkadir ZIREK

Supervisor:

Doc. Ing. Michael Lata, Ph.D.

Specialist supervisor:

Prof. Ing. Jaroslav Novák, CSc.

The dissertation has arisen at the supervising:

Department of Transport Means and Infrastructure

AUTHOR'S DECLARATION

I hereby declare:
This thesis was prepared individually. All the literary sources and the information I used in the thesis are listed in the bibliography.

I was familiar with the fact that rights and obligations arising from the Act No. 121/2000 Coll., the Copyright Act, apply to my thesis, especially with the fact that the University of Pardubice has the right to enter into a license agreement for use of this thesis as a school work pursuant to § 60, Section 1 of the Copyright Act, and the fact that should this thesis be used by me or should a license be granted for the use to another entity, the University of Pardubice is authorized to claim from me a reasonable contribution to cover the costs incurred during the making of the thesis, according to the circumstances up to the actual amount thereof.

I agree with the reference-only disclosure of my thesis in the University Library.

In Pardubice on …../…./…..

Abdulkadir ZIREK

ACKNOWLEDGEMENTS

First and foremost, I would like to express my very great appreciation to my supervisor doc. Ing. Michael Lata, Ph.D. and my colleague doc. Ing. Petr Voltr, Ph.D. for their patient guidance and useful critiques of this research work.

I would also like to thank my co-supervisor Prof. Ing. Jaroslav Novák, CSc., who provided an insight into the inception of my research.

I would like to express my very great appreciation to Anadolu University and Eskisehir Technical University for the financial support to my Ph.D. study.

I would also like to extend my thanks to my colleagues in Pardubice and Eskisehir for their help and motivation during this research.

Last but not the least, I would like to thank my family and my girlfriend for supporting me spiritually throughout my Ph.D. study.

Abdulkadir ZIREK

ABSTRACT

Railway transport is becoming an increasingly preferable transportation system worldwide. Due to the demand and emerging technologies in the railway sector, more powerful rail vehicles are produced. The recent development in power capacity of the vehicles enables them reaching high torques in a short time. On the other hand, the traction ability of these vehicles is limited by environmental conditions (i.e. rain, snow, leaves and mud) and human influences. Because of the mentioned reasons, wheel slip becomes one of the most important factors influencing the safety, traction performance and lifetime of the rail vehicles. Hence, this work deals with the use of anti-slip control methods for rail vehicles. Initially, to give readers a general picture of the research covered in the thesis, the adhesion and slip mechanism are explained. Furthermore, the slip detection methods and slip control methods based on the literature review are introduced. To verify the validity of the anti-slip control schemes, a numerical model of a tram wheel roller rig that includes nonlinear effects caused by time delay and disturbances to match the values of the experimental test setup has been generated using MATLAB editor. The provided numerical model consists of a PMSM, an AM, a wheel, a roller and two drive shafts. Freibauer and Polach adhesion force model has been employed to determine the coefficient of adhesion and adhesion force taking place between the wheel-roller. Five wheel slip control strategies -wheel slip control based on single threshold (WSCST), wheel slip control based on multiple thresholds (WSCMT), wheel slip control based on angular acceleration of wheel (WSCAA), PI wheel slip control (PI-WSC), and sliding mode wheel slip control (SM-WSC)- are suggested. In addition to the simulation calculations, this work includes an experimental part in which extensive experiments are carried out on laboratory test equipment where the anti-slip algorithms are implemented and tested. The validity of the developed numerical model is proven with the comparison of the simulation and experimental results. The performances of all the wheel slip control methods are evaluated through the mathematical model and experimental setup. The influences of different roller speeds and control parameters are analysed via validated numeric model.

Keywords: adhesion, wheel slip, anti-slip, acceleration, roller rig, control, PMSM, sliding mode.

NÁZEV: Protiskluzová regulace trakčního motoru železničního vozidla

SOUHRN

Železniční doprava se stává celosvětově preferovanějším dopravním systémem. Vzhledem k poptávce a vznikajícím technologiím v železničním sektoru se vyrábějí hnací vozidla se stále vyšším výkonem. Nedávný vývoj výkonové kapacity vozidel umožňuje v krátkém čase dosáhnout vysokých točivých momentů při rozjezdu. Na druhé straně je trakční schopnost těchto vozidel omezena podmínkami prostředí (tj. deštěm, sněhem, listy a bahnem) a lidskými vlivy. Z uvedených důvodů se prokluzování kol stává jedním z nejdůležitějších faktorů ovlivňujících bezpečnost, trakční výkon a životnost kolejových vozidel. Tato práce se proto zabývá využitím metod protiskluzového řízení pohonu kolejových vozidel. Nejprve jsou vysvětleny mechanismy adheze a skluzu. Dále jsou uvedeny metody detekce skluzu a metody regulace. Pro ověření platnosti schémat protiskluzové regulace byl pomocí editoru MATLAB vytvořen numerický model zkušebního laboratorního zařízení tramvajového kola, který obsahuje také nelinearity. Uvedený model se skládá ze synchronního motoru s permanentními magnety, asynchronního motoru, tramvajového kola, kladky (rotující kolejnice) a dvou hnacích hřídelí. Jednu z nelinearit tvoří model mechanismu adheze. Zde je použit model Freibauera a Polacha. Pro detekci a řízení skluzu je použito pět strategií (algoritmů): řízení skluzu kol na základě jednoduché prahové hodnoty (WSCST), řízení skluzu kol na základě více prahových hodnot (WSCMT), řízení prokluzu kol na základě úhlového zrychlení kola (WSCAA), PI regulace skluzu kol (PI-WSC) a metoda Sliding Mode Control (SM-WSC). Kromě simulačních výpočtů práce obsahuje experimentální část, kde jsou provedeny rozsáhlé experimenty na zkušebním laboratorním zařízení, kde byly uvedené protiskluzové algoritmy implementovány a testovány. Platnost vyvinutého numerického modelu je prokázána porovnáním simulačních a experimentálních výsledků. Vyhodnoceny jsou vlivy různých parametrů a chování systému při těchto protiskluzových metodách.

Klíčová slova: adheze, prokluz kola, protiskluz, zrychlení, zkušební zařízení tramvajového kola a rotující kolejnice, řízení, PMSM.

TABLE OF CONTENT

LIST OF FIGURES

LIST OF TABLES

LIST OF SYMBOLS

μ	:	Coefficient of adhesion
T	:	Traction force
N	:	Normal load force
v_t	:	Vehicle longitudinal speed
w_s	:	Wheel slip speed
ω	:	Wheel rotational speed
s	:	Relative slip
r_w	:	Radius of wheel
ω_a	:	Rotational speed of AM
ω_r	:	Roller rotational speed
ω_w	:	Wheel rotational speed
ω_p	:	Rotational speed of PMSM
T_a	:	Asynchronous motor torque
T_r	:	Roller torque
T_w	:	Wheel torque
T_p	:	PMSM motor torque
J_r	:	Roller moment of inertia
J_w	:	Wheel moment of inertia
J_p	:	PMSM rotor moment of inertia
J_a	:	AM rotor Moment of inertia
F_{adh}	:	Adhesion force acting on contact area
k_{s1}, k_{s2}	:	Torsional stiffnesses of the shafts
b_{s1}, b_{s2}	:	Torsional damping parameters of the shafts
h_1, h_2	:	Angular play in CV joints
x_1, x_2	:	Angular displacements in joints
r_r	:	Radius of roller
i_a, i_b, i_c	:	Three phase currents

i_α	:	α-axis current on stationary orthogonal reference frame
i_β	:	β-axis current on stationary orthogonal reference frame
i_0	:	Homopolar current
i_d	:	d-axis current on rotating reference frame
i_q	:	q-axis current on rotating reference frame
θ	:	Angle between a-axis and d-axis
v_1, v_2, v_3	:	Switching variable of inverter
V_{an}, V_{bn}, V_{cn}	:	Three-phase voltages
V_{dc}	:	DC link voltage
i_{ref}	:	Desired current
i_{act}	:	Actual current
Δi	:	Current hysteresis band
i_e	:	Error between actual and desired currents
V_0-V_8	:	Switching status of active and zero vector
S_1-S_6	:	Power switches of inverter
V_{ref}	:	Reference voltage
V_α	:	α-axis voltages on stationary orthogonal reference frame
V_β	:	β-axis voltages on stationary orthogonal reference frame
α	:	Phase angle
T_1	:	Switching time duration of first adjacent vector
T_2	:	Switching time duration of second adjacent vector
T_0	:	Switching time duration of zero vectors
T_z	:	Switching period
n	:	Number of sectors
f_s^*	:	Reference frequency
f_n	:	Rated electrical frequency of AM
f_{min}	:	Minimum frequency of AM
V_s^*	:	Magnitude reference stator voltage

V_n	:	Rated voltage of AM
V_{min}	:	Minimum voltage of AM
V_d	:	d-axis voltage of PMSM
V_q	:	q-axis voltage of PMSM
φ	:	Amplitude of flux induced by permanent magnet of rotor in stator phases
L_d	:	d-axis self-inductances of PMSM
L_q	:	q-axis self-inductances of PMSM
R	:	Stator resistance of PMSM
ω_e	:	Electrical speed of PMSM rotor
p	:	Number of pole pairs of PMSM
θ_e	:	Electrical Position of PMSM rotor
$\varphi_{ds}, \varphi_{qs}, \varphi_{dr}, \varphi_{qr}$	:	Flux linkages of AM
V_{ds}, V_{qs}	:	d-q axis stator voltage of AM
V_{dr}, V_{qr}	:	d-q axis rotor voltage of AM
i_{ds}, i_{qs}	:	d-q axis stator current of AM
i_{dr}, i_{qr}	:	d-q axis rotor current of AM
R_s	:	Stator resistance of AM
R_r	:	Stator resistance of AM
ω_{er}	:	Electrical speed of AM rotor
ω_{es}	:	Speed of AM reference frame
ω_{er}	:	electrical angular speed of AM rotor
ω_a	:	Mechanical speed of AM rotor
θ_{es}	:	Reference frame position of AM
L_s	:	Stator self-inductance of AM
L_r	:	Rotor self-inductance inductance of AM
L_m	:	Magnetising inductance of AM
T_a	:	Electromagnetic torque of AM
P	:	Number of pole pairs of AM

f	:	Variable coefficient of friction
ε	:	Scaled slip
a	:	Contact half-length
K_t	:	Tangential stiffness of surface layers
p_{max}	:	Maximum Hertzian pressure in contact
k_{red}	:	Reduction factor of brush contact model
f_0	:	Static coefficient of friction
A	:	Ratio of friction coefficients f_∞ / f_0
B	:	Coefficient of exponential friction decrease
C_1	:	Sensitivity parameter
T_{ref}^*	:	Reference torque output of controller
T_{cont}	:	Final output torque request
dt	:	Resolution time of speed sensor
A_{dec}	:	Deceleration rate parameter
A_{inc}	:	Increment rate parameter
dt	:	Resolution time of speed sensor
s_{th}	:	Slip threshold value
s_{act}	:	Actual slip occurs between wheel and roller
s_{th1}	:	First threshold value
s_{th2}	:	Second threshold value
α_{act}	:	Actual angular acceleration of wheel
α_{th}	:	Threshold value of angular acceleration
u	:	Output torque request of PI controller
s_d	:	Desired wheel slip
K_p	:	Proportional gain of PI controller
K_i	:	Integral gain of PI controller
k	:	Iterative step
e	:	Error between actual slip and desired slip

S	:	Sliding surface
D	:	Design parameter that determines convergence rate of tracking error
K	:	Design parameter that is adjusted in compliance with number of uncertainties and the disturbance in system
d	:	Disturbance due to vibration in system
V	:	Lyapunov function

ABBREVIATIONS

AM	:	Asynchronous Motor
CoA	:	Coefficient of Adhesion
CoF	:	Coefficient of Friction
FOC	:	Field Oriented Control
GPS	:	Global Positioning Systems
VÚKV	:	Výzkum, Vývoj a Zkušebnictví Kolejových Vozidel
PMSM	:	Permanent Magnet Synchronous Motor
PWM	:	Pulse Width Modulation
AMSC	:	Asynchronous Motor Scalar Control
SVPWM	:	Space Vector Pulse Width Modulation
THD	:	Total Harmonic Distortion
ASR	:	Acceleration based Slip Regulation
PID	:	Proportional, Integral and Derivative
WSCST	:	Wheel Slip Control based on a Single Threshold
WSCMT	:	Wheel Slip Control based on Multiple slip Thresholds
WSCAA	:	Wheel Slip Control based on Angular Acceleration of wheel
PI-WSC	:	PI Wheel Slip Control
SM-WSC	:	Sliding Mode Wheel Slip Control
VSI	:	Voltage Source Inverter

1 INTRODUCTION

The term of 'Railway transport' is defined as conveying people, livestock and general goods using a vehicle mounted on a rail system. In the last century, the importance of railway transport has increased considerably since it is an environmentally friendly and economical mode of transport. The railway transportation systems are considered as an essential feature of all modern economies. In developed countries, railway systems have *10%* of the entire transport network [1]. Furthermore, the railway is known as one of the safest methods of transportation.

Railway transport has become a more prevalent transportation system worldwide. In the early age of railway transport, the power of rail vehicles was limited. Hence, sophisticated vehicle control methods were not required. Due to the demand and emerging technologies in the railway sector, more powerful rail vehicles are produced. The recent development in the power capacity of the vehicles drive systems enables them reaching high torques in a short time. The vehicles tractive effort is transferred to the rail in a small contact area that provides the vehicle with an advantage due to the lower power losses caused by friction in wheel-rail contact [2]. On the other hand, the traction ability of these vehicles is limited to environmental conditions (i.e. rain, snow, leaves and mud) and human influences. Besides, it is a well-known fact that the adhesion between wheel and rail decreases with the increase of the running speed under contaminated surface conditions [3]. Hence, the wheel slip occurs when tractive effort exceeds the available adhesion, whereas sliding occurs when the braking effort exceeds the available adhesion. If the slip/slide reaches the high value, it causes severe wear of wheel and rail surfaces increases mechanical stress in the system and affects stability. The presence of high wheel slip is an undesired situation which reduces the safety, traction performance and wheel-rail lifetime.

It is a known fact that anti-slip control methods help to improve the traction performance of vehicles. Moreover, vehicle safety largely depends on the development of such systems. Therefore, the development of wheel slip protection systems becomes inevitable.

In the early age of railway transportation, the vehicles were equipped with the sander which improves the adhesion conditions. However, the sanding increases 10 to 100 times the wheel and rail wear [2], [4]. Thus, new strategies were sought out to be used for rail vehicles.

After the 1980s, with the rapid development of automatic control strategies and electronic technologies, the microprocessors with online processing were used for the detection of wheel slip and torque adjustment [5]. The first developed wheel slip control methods are the re-adhesion controller. The conventional re-adhesion control methods use the wheel slip speed or acceleration criterions to detect wheel slip. The methods do not require exact information of the wheel-rail contact condition for wheel slip detection and compensation of poor adhesion [5]. However, such strategies do not stop the wheel slip formation but suppress it. Due to the requirements of the trains hauled by locomotives, more advanced wheel slip control strategies are developed. The methods aim to stabilize the wheel slip at the peak of the slip curve to establish the optimum utilization of the adhesion characteristic. Although there is a vast amount of literature on both re-adhesion and wheel slip control strategies, there is still a need for further investigations.

1.1 Purpose of the Thesis

Due to the reasons that have been mentioned earlier, re-adhesion control strategies and wheel slip control strategies are studied in this thesis. Initially, the principles of the adhesion and slip mechanism are summarised to give the reader a general picture of the research covered in work. Besides, the available information in the literature about anti-slip protections systems and control systems for the use of the railway vehicle is briefly introduced. Each technique is investigated with its pros and cons for further development. After that, using information gathered from the literature, efficient, practical and viable solutions are proposed for an anti-slip control mechanism in this study. The algorithms are developed such a way that they are not only stabilising the wheel slip but also help to establish better utilisation of the adhesion characteristic regardless of the severity of contaminants between the wheel and the roller. To verify the validity of the control schemes, A proper numerical model of a tram wheel has been designed roller rig. The numerical model, which includes nonlinear effects caused by time delay and disturbances, is generated to match the values of the experimental test setup. The model consists of five main components: the mechanical model of the torsional system, the dynamic model of the PMSM, dynamic model of the AM, the Freibauer/Polach adhesion force model, and the anti-slip control model. Validation of the developed numerical model is carried out by comparing the simulation results and experimental results. Moreover, the derived algorithms are

implemented to both a full-scale tram wheel roller rig and its numerical model. It is expected that the proposed algorithms would work well, under different wheel-roller contact conditions (i.e. water, grease and water and grease), and the performance results of the refined algorithms with the numerical model and experimental setup are in good agreement. Finally, the performance of the wheel slip control strategies is evaluated through the validated numerical model with various roller speeds and control parameters.

To conclude, the basic premises of this study can be summarised as follows:

(i) Summarising a large number of published studies on the wheel slip, adhesion and slip control methods.

(ii) Reproducing a numerical model of the tram wheel roller rig in MATLAB environment that can be used for performance evaluation of the wheel slip control strategies.

(iii) Proposing algorithms to control the wheel slip mechanism and establishing optimum utilisation of adhesion.

(iv) Validation of reproduced numeric model.

(v) Verifying the functionality of proposed wheel slip control algorithms by either the validated numerical model or experimentally obtained results from the tram wheel roller rig.

(vi) Performance evaluation of the proposed wheel slip control algorithms with different speeds and control parameters.

2 THEORETICAL BACKGROUND

In this section, initially, the adhesion and slip mechanism are explained to give the reader a general picture of the research covered in the thesis. In addition to this, the wheel slip detection methods and wheel slip control methods based on the literature review are introduced with their pros and cons.

2.1 Adhesion Phenomenon

The general scientific description of adhesion force is the attachment between two contacting surfaces [6]. In tribological perspective, the adhesion is the force required to separate two surfaces that are in contact and is usually used to describe how well surface coatings or paints are bounded to surface they coat [7]. In railway terminology, the adhesion force is defined as the maximum traction/braking force exerted during wheel-rail contact [8].

The adhesion is the fundamental phenomenon that influences the tractive and braking performance of rail vehicles [2]. Hence, there is a vast amount of literature on the adhesion phenomenon [8]–[14]. Fletcher and Lewis [9] analysed adhesion using twin disk machine. In their research, they investigated slip-adhesion curve at a deficient level of slip (creep). Zhu et al. [10] present an experiment performed with a mini-traction machine to investigate the problem of low adhesion in wheel-rail contact for low speeds. However, the main limitation of the studies mentioned above is that the adhesion tests were carried out for low speeds levels. In Chinese National Traction Power laboratory, full-scale roller rig was used for the research of adhesion at higher speeds [11].

In our study, a full-scale tram wheel roller rig, which is similar to the one used by Zhang et al. [11], is used. However, in our setup, the vehicle is represented by a single wheel only, and there is no real simulation of the suspension system or bogie frame. The design of the tram wheel roller rig provides us with a wide range for adhesion research possibility.

The results obtained from the studies mentioned above allow the possibility to put forward common laws about the process of the adhesion [15]:

- The force of external friction is the basis of the adhesion;
- It is impossible to realise the adhesion in contact point without wheel slip;
- The coefficient of the adhesion decreases when the velocity of the vehicle increases due to the dynamic characteristic of the wheel-rail interaction;
- The critical wheel slip, which corresponds to the point where the maximum adhesion is observed, depends on the friction conditions of the contact;
- The coefficient of the adhesion decreases when the normal load increases;
- When the friction condition of the contact begins to get worse, the coefficient of adhesion drops and critical slip is shifted to the zone of larger value.

The coefficient of the adhesion is usually represented by the ratio of the traction force (T) and the normal force (N). The forces and velocities acting on a driven wheel are presented in Figure 1. The coefficient of the adhesion can be calculated using Eq. 1.

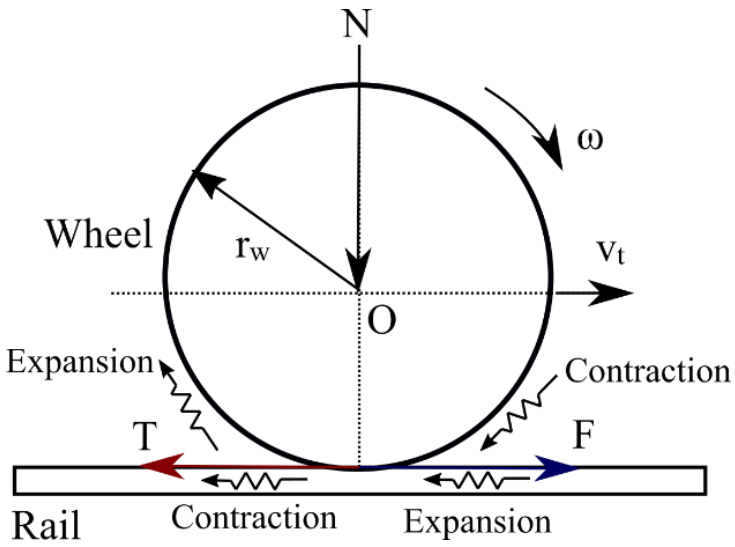

Figure 1. The forces and velocities acting on a driven wheel.

$$\mu = \frac{T}{N} \qquad \textit{Eq. 1}$$

where T is traction force, N is normal load force, and μ is the coefficient of adhesion.

The loss of adhesion between wheel and rail have serious influences on the traction and braking effort of the vehicles. As it is mentioned below, poor adhesion causes wheel slip during

the traction process and lead to the damage of wheel and rail [12]. Recently, various approaches have been proposed to outline the reasons for the loss of the adhesion [3], [16]–[19]. Taken together, these studies show that the loss of adhesion may occur due to the presence of water (rain, snow, dew), oil, and leaf contaminants. Moreover, the temperature is another factor which influences the adhesion.

2.2 Slip Phenomena

Slip is widely considered to be one of the most critical topics in vehicle dynamic and vehicle traction control areas. The most common definition of the wheel slip in the railway area is the normalised difference of the angular and longitudinal velocities of the vehicle. The wheel slip occurs when the tractive effort of the vehicle exceeds the adhesion force, whereas sliding occurs when the braking force exceeds the adhesion force. The main reason for the wheel slip/slide is the adhesion force. During the slip/slide event, the contact between the wheel and rail is not enough to transmit the provided traction/braking force supplied by the drivers. For the longitudinal movement of the vehicle, the force produced by the vehicle motor is transmitted to the rail via wheels. The forces that act on the wheel cause stress. The stress on wheel results in contraction and extension on the wheel, which leads slip between the wheel and rail [20]. The forces and velocities acting on a driven wheel can be seen in Figure 1.

The CoA is defined as a function of the slip at the contact point of the wheel and rail [21]. Therefore, the slip must be well-defined. The slip velocity and relative slip (hereinafter is referred to as wheel slip) can be calculated using the Eq. 2 and Eq. 3 as given below.

$$w_s = \omega \cdot r_w - v_t \qquad \textit{Eq. 2}$$

$$s = \frac{\omega \cdot r_w - v_t}{v_t} \qquad \textit{Eq. 3}$$

where w_s is slip speed, v_t is the vehicle longitudinal speed, ω is the wheel rotational speed, r_w is wheel radius, and s is the wheel slip.

The curve showing the relation between the wheel slip and adhesion is indicated in Figure 2. This curve is known as the slip-adhesion curve (slip curve) in railway terminology.

When no tangential force is transmitted, wheel slip in wheel-rail contact is zero. This situation is defined as “free rolling”. However, free rolling is not possible since the deformation between wheel and rail causes a certain wheel slip [7]. The direction of rolling is the leading edge, and the other side is the trailing edge. When the driving force of the vehicle motor increase, the wheel slip starts to form from trailing edge and spreads toward the leading edge. The wheel slip increases linearly to a certain point; meanwhile, sticking zone decreases and slip zone increases. After reaching the peak of the curve, the wheel comes up to the full sliding region [7]. This point is where the adhesion between the wheel and rail reaches the maximum. Moreover, the coefficient of adhesion is assumed to be equal to the coefficient of the friction at the peak point of the slip-adhesion curve. Therefore, the determination of the peak point of the slip curve is one of the main aims of the current studies in the area of slip control [20]. Figure 2 is used for showing the behaviour of the wheel-rail contact on the slip curve. However, it should be noted that the coefficient of adhesion is always lower than the coefficient of friction due to the effects of lateral forces, spin forces and uneven load distributions.

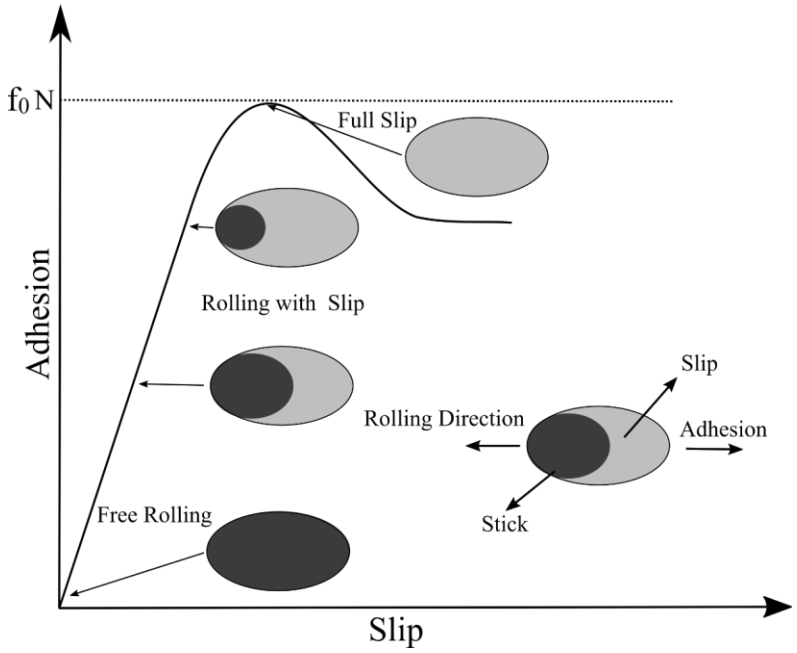

Figure 2. The slip-adhesion curve during the rolling [7].

2.2.1 Problem Formulation

The adhesion is the function of the wheel slip, as mentioned in the above section. A certain amount of wheel slip is required to transfer the tractive effort from the wheel to the rail. As it is illustrated in Figure 3, the slip curve has a nonlinear characteristic. The area on the left side of the peak of the slip curve is called adhesion zone and the area on the right side of the peak is the slip zone. The adhesion zone is stable, and adhesion increases when the wheel slip increases. On the other hand, the slip zone is nonstable part of the curve, and adhesion decreases when the wheel slip increases. Most of the wheel slip control methods aim to keep the slip in the stable part of the curve. While the goals of the optimisation method are to control the slip toward the peak of the curve where the maximum traction effort is achieved at [22]. Therefore, in this study, conventional and novel wheel slip control strategies are implemented to control the wheel slip toward the peak of the slip curve. The operation zone of the controllers is limited with the stable and the unstable parts of the slip curve near the maximum point [2]. The behaviour of the slip curve depends on two essential factors that are the condition of the wheel-rail contact and the vehicle velocity. Hence, the wheel slip control methods must be developed considering the effect of different friction conditions and vehicle velocity.

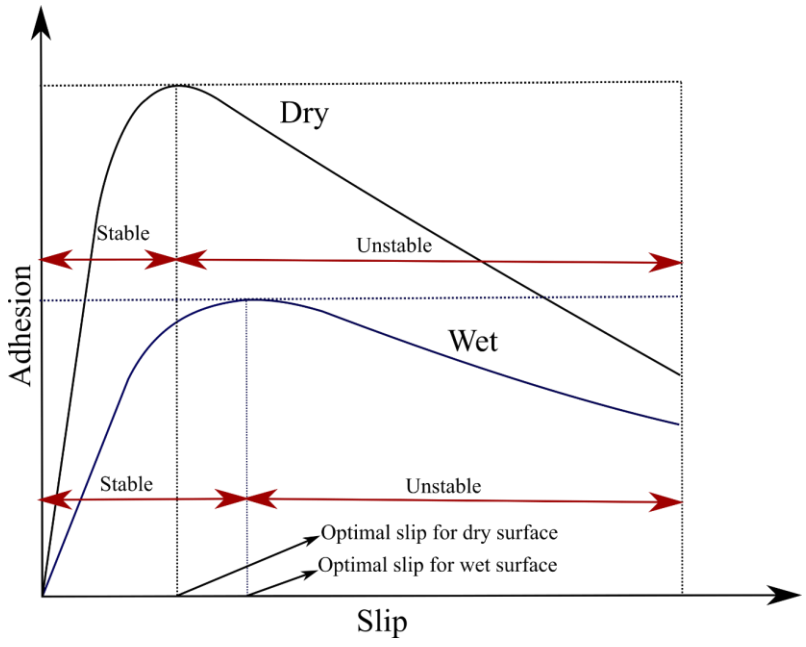

Figure 3. Slip-adhesion curve illustrating the characteristic of CoA under dry and wet contact conditions.

2.3 Wheel Slip Identification Methods

Identification of the wheel slip is one of the most challenging issues of the control methods. The problem arises due to the unknown longitudinal velocity of the vehicle. Several techniques have been proposed for identification of the wheel slip. Some of the techniques are summarised as follows:

- Current-based wheel slip detection of the all-wheel driving vehicle [23]
- Using the speed difference of driven and non-driven wheels [24].
- Method based time-frequency analysis [25]
- Linear, nonlinear and Kalman filters [26], [27].
- Nonlinear observers [28], [29].
- Using global positioning Systems (GPS) [30].
- Use of the optical-based sensor [31].

Fast and accurate determination of wheel slip is critical for control algorithms since the termination of slip starts right after the detection. The identification of the wheel slip on the experimental tram wheel roller rig is straightforward. The wheel and roller angular speeds are measured via rotary encoders that are mounted on the shafts. In the sequel of measuring, angular velocities of wheel and roller are multiplied with their radii, subtracted from each other and divided to reference speed. One can choose wheel speed, roller speed or the average of both as the reference.

2.4 Wheel Slip Control Methods

Recently, various wheel slip control methods have been put forward to solve the issue of high slip between the wheel and rail. Pichlík [2] classified the wheel slip control method in two categories which are used for the electric multiple units (EMU) and the locomotives. According to Pichlík, the wheel slip control methods that are used in EMU aim to prevent the high value of slip velocity; thus these methods reduce the power loses and wear of the vehicle wheels and rails. The wheel slip control methods for locomotive aim to achieve maximum adhesion rather than preventing the wheel slip [24]. Kondo explains the reason for this classification due to axle loads of the EMU and locomotive [32]. Since the axle loads of the

EMU is lower than the locomotive, the adhesive region is too narrow to precisely control the adhesion at the peak of the slip curve. The wheel slip control methods for EMU and locomotives are the main interest of this work. Therefore, the current work deals with wheel slip control algorithms in general. Frylmark and Johnsson have summarised the most common wheel slip control methods, as indicated in Figure 4 [22]:

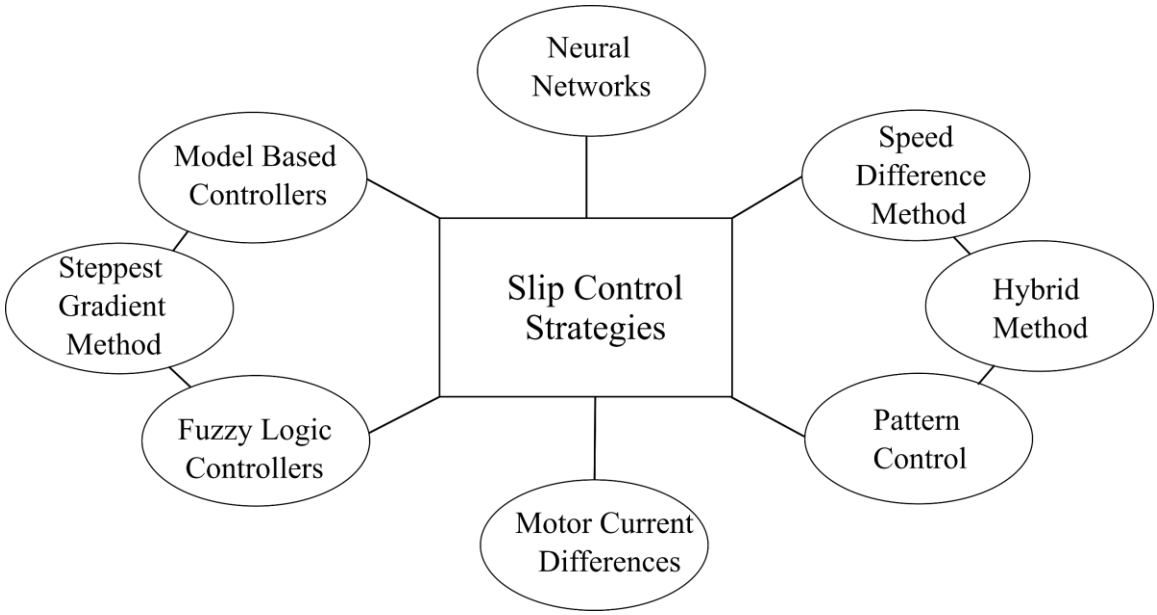

Figure 4. The wheel slip control strategies [22].

Besides the strategies mentioned above, angular acceleration-based control methods and PID (proportional, integral and derivative) control methods are some of the other control strategies used for the slip control. The basic principles of the mentioned methods are described in the following sections.

2.4.1 Wheel Slip Controller Based on a Certain Slip Threshold Value

This method is a conventional wheel slip control strategy that is known as pattern control [33]. The wheel slip is detected when its value exceeds a specific threshold value. The torque of the motor is reduced according to the specific pattern to prevent the wheel from the high slips. Following this, the wheel slip value reaches a peak and deceleration starts. When the wheel slip value gets lower than the threshold value, the torque drops stops, and torque starts to rise again. The action of the controller takes place periodically until the bad track condition disappears.

The advantage of this method is simplicity. However, the technique does not stop the wheel slip but suppresses. Hence, the periodic oscillations and excessive torque drops can be listed as the disadvantages of the technique. The correct setting of the control parameters is required to reduce the effect of the described disadvantages.

2.4.2 Wheel slip Controller based on Motor Current Differences

The wheel slip controller based on motor current differences has recently been proposed by Yamashita and Watanabe [34]. The conventional wheel slip control methods use the speed sensor for detection of the wheel slip. This method provides detection of the wheel slip by observing the motor current differences in a multiple motor drive. The wheel slip can be detected in two ways. The first method is based on the constant flux control. If the flux is kept constant, the motor slip frequency is proportional to the q-axis current component of the motor. The slip frequency of each motor can be calculated using the vector control approach. The inverter frequency and motor slip frequency are used to estimate the rotational speed of the motor. Time differential of the estimated rotational speed provides the wheel axle acceleration by which wheel slip is detected. The current difference in motors is the second method for detection of the wheel slip. Reducing the cost of the controller, the probability of failure and the complexity of the controller are the advantages of this method. On the other hand, this method does not eliminate the wheel slip, but it suppresses. Thus, the control system suffers from the frequent wheel slip oscillations and excessive torque drops. These can be listed as the drawbacks of the method.

2.4.3 Wheel Angular Acceleration Based Wheel Slip Control Method

An alternative way of wheel slip control is the wheel angular acceleration-based control method. It is also known as the acceleration slip regulation (ASR) method. ASR is widely used in four in-wheel motor drive electric vehicles to improve acceleration performance [35]–[37]. Moreover, ASR is used in rail vehicles as a part of the hybrid wheel slip control method to eliminate the disadvantages of the individual control methods [24]. The ASR method is preferred due to its advantages. The advantages of the ASR can be summarised as follows:

- It does not need longitudinal speed information.

- Adhesion measurement is not required.
- Implementation of the method is simple.
- The total cost is lower compared to other wheel slip control methods.
- The start of the wheel slip can be detected earlier.

The wheel slip is detected using the wheel rotational acceleration signal from the rotor of the traction motor. If the acceleration signal exceeds a certain threshold value, the wheel slip is deemed to have occurred. Thus, the torque of the motor is reduced to prevent wheel slip and restore the adhesion. The torque reduction continues until the acceleration signal gets lower than the threshold value. The action of the controller repeats until the adverse wheel-rail contact conditions disappear [38]. Similar to the previously mentioned methods, ASR controller suppresses wheel slip. Hence, excessive torque drops are the weakness of the conventional ASR controller.

2.4.4 Hybrid Wheel Slip Control Methods

The hybrid wheel slip control methods are composed of two or more control methods. The arrangements are developed to eliminate the disadvantage of the individual control strategy. The hybrid control methods have higher efficiency than individual methods. Doh-Young Park et al. [33] have proposed a hybrid wheel slip control method which is a combination of speed difference, pattern and acceleration control methods. Each of the control strategies is activated according to the different wheel slip levels [5]. The author claims that the proposed method has the advantages of reducing wheel slip and improving traction performance.

2.4.5 Neural Network Wheel Slip Control Methods

Recently, there has been considerable progress in vehicle stability, handling and ride comfort due to the number of the modern control theory application in vehicle dynamics. However, the on-line determination of some parameters that are required for the control application is challenging [39]. Neural Networks is an approach for estimating the parameters that cannot be measured on-line, such as the adhesion coefficient [22]. Ćirović et al. employed dynamic neural networks for improving the control of the longitudinal wheel slip [40]. The

nonlinear relationship between the brake actuation pressure and longitudinal wheel slip during a braking cycle is modelled under the different braking condition and vehicle load states by dynamic neural network method. The author claims in his work, the proposed method could be employed for increasing vehicle safety, improving vehicle stability and keeping the wheel slip at the desired level.

2.4.6 Fuzzy Logic Based Wheel Slip Control Methods

Highly nonlinear, time-varying, and complex nature of the slip curve makes the wheel slip control a challenging task. In order to overcome the described difficulties, fuzzy logic controllers have been offered to control the wheel slip [41]–[44]. The fuzzy logic modelling provides managing the complex systems and representing complex relations by using a linguistic approach. The mathematical model of the systems is not required for fuzzy logic controllers. The expert knowledge in the form of linguistic rule and measured data are used to develop fuzzy logic controllers [41]. Frylmark and Johnsson claim the major advantage of the fuzzy logic controllers is that they can include experienced human expert linguistic rules, describing how to design the slip control system. The linguistic rules are essential when access to the measured data is limited [22].

The fuzzy logic controllers can be implemented to rail vehicles for various applications. Bauer and Tomizuka [44] present two fuzzy logic controllers. The first one estimates the peak of the slip curve and regulates the wheel slip at peak while the second one maintains the wheel slip at the desired value. Garcia-Rivera et al. [42] have developed a nonlinear PD (proportional and derivative) controller using rule-based fuzzy logic. Cheok and Shiomi [41] designed a fuzzy logic antiskid controller using both linguistic rule-based on expert knowledge and measured training data.

2.4.7 PID Wheel Slip Control Methods

The PID (proportional, integral and derivative) controller is the most common control method in the railway industry [22]. The PID controller has a simple structure and does not require a system model. The controller continuously calculates the error between the desired reference point and measured process variable. The corrections are applied to the system based

on the calculated error. There are several control tuning methods available in the literature for the PID controller.

Aparow et al. [45] have implemented a conventional PID controller to deal with the strong nonlinearity in the design of the anti-lock braking system(ABS) controller. A reference slip value is selected from the slip curve as a control signal. In order to obtain the optimum braking performance, the control signal is selected close to the peak of the slip curve. The results that are presented in work show that the PID controller is a very useful controller for the ABS control system.

The most critical part of the PID control is the reference wheel slip value. The maximum point of the adhesion differs between dry, wet, and greasy rails. Since there are different optimum points for each contact conditions, the stability cannot be guaranteed with the PID controllers due to their linear characteristics [22]. Therefore, the PID controllers can be combined with fuzzy logic systems and adhesion prediction systems to ensure the stability of the process.

3 METHODS AND METHODOLOGY

On-track tests of railway vehicles are challenging, time-consuming and expensive processes. In keeping with the purpose of the study, the whole vehicle can be reduced to one powered bogie or a single wheelset [46]. Since the dynamics of the drive system are the main interest, a full-scale tram wheel roller rig is used for validation of the control algorithms. For experimental tests, the vehicle is replaced by a tram wheel that is connected to a permanent magnet synchronous motor with the rail being replaced by a roller connected to an asynchronous motor. These substitutions differ from the real case. More detailed information about the replacements and their effects are presented by Voltr [47] and Gerlici et al. [48].

In this thesis, the performances of the wheel slip control algorithms are investigated using a full-scale tram wheel roller rig and its numerical model that is generated in MATLAB editor. Therefore, in this section of the work, the structure of the experimental test stand is explained, and the numerical model of the test stand that is built up based on the described arrangement is clarified in detail.

3.1 Experimental Setup

The experiments are performed on the tram wheel roller rig, which was constructed by VÚKV (Výzkum, Vývoj a Zkušebnictví Kolejových Vozidel) and was renewed by the Faculty of Transport Engineering for further research. The tram wheel roller rig is composed of three main parts; a tram wheel, a roller, and a mainframe. The roller, which is manufactured from a railway wagon wheel, represents the rotating rail [49]. A schematic view and photos of the full-scale tram wheel roller rig are presented in Figure 5 and Figure 6.

Two rotating bodies (tram wheel and roller) are placed toward each other in a perpendicular direction. The wheel is attached to a swinging arm where an air spring is located on the top to provide vertical force to press the wheel toward the roller. The swinging arm allows the movement of the wheel in the vertical axis, while relatively stiff guiding is provided in the lateral axis. The roller is mounted in the bearings of the base plate that allows for setting the angle of attack [46]. Traction is provided by a torque-controlled PMSM, type STM 225-S24.

The roller is connected to an AM, which keeps the system at a constant speed by providing opposing torque.

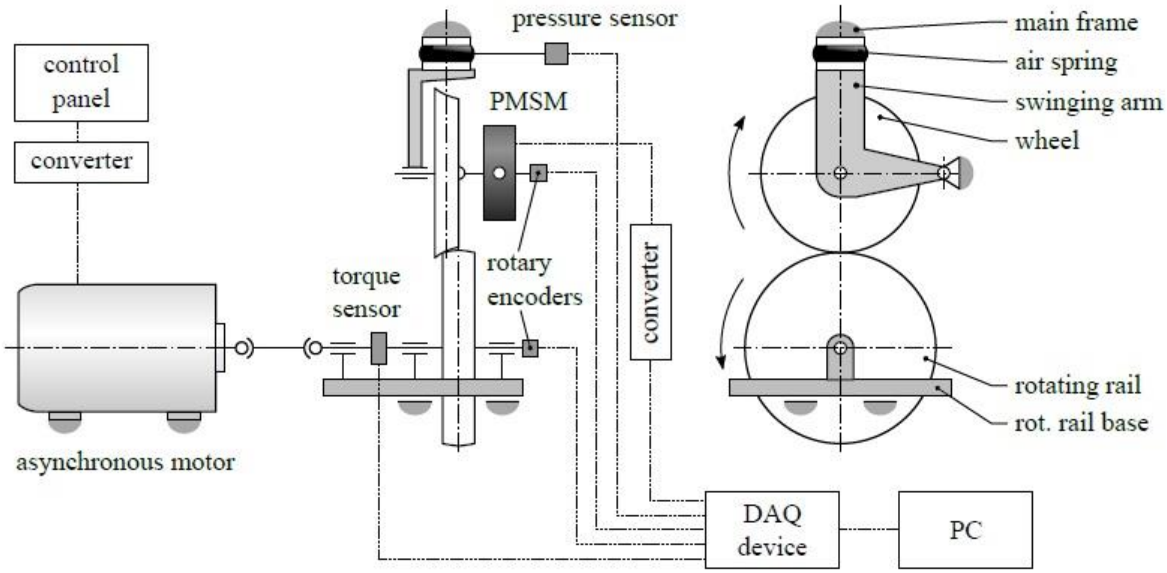

Figure 5. Schematic view of full-scale tram wheel roller rig measurement configuration [50].

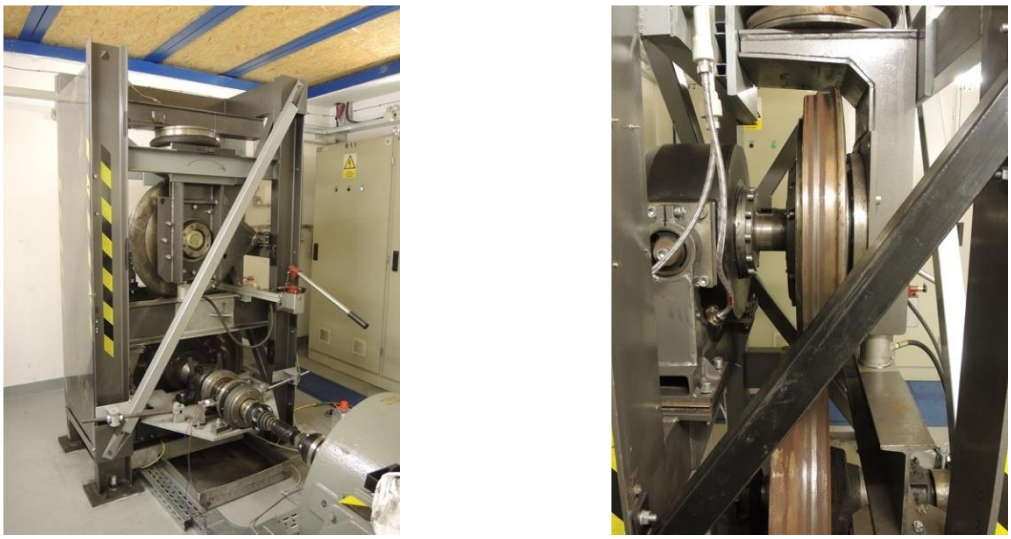

Figure 6. The full-scale tram wheel roller rig [46],[51].

In order to measure the wheel and roller angular speeds, incremental rotary encoders of type IRC315 are mounted on both shafts. The air pressure, which is provided to press the wheel toward the roller, is monitored by a DMP331 type pressure transducer. The adhesion force

between wheel and roller is monitored by a torque transducer placed on the roller shaft. The coefficient of adhesion (μ or CoA) is calculated using the measurement from the torque transducer and the pressure transducer.

The output of all the rotary encoders, transmitter and torque transducer are connected to a data acquisition device (DAQ-type NI USB-6341). The signals from the DAQ are transmitted at a *200 Hz* sampling rate of measurement to the PC where the data is saved as a binary file by a program that utilises the NI DAQmx libraries. The saved files are converted to physical quantities based on the calibration measurement defined for the experiment [46]. Although the signals are recorded with *200 Hz* sampling frequency, the control actions are only performed at *25 Hz* frequency.

The measured signals are observed to include parasitic contents. The primary sources of these disturbances are electromagnetic noise (high frequencies) and mechanical imperfections of the roller rig (low frequencies). The former is removed by low pass filtering; the latter is also easily eliminated since its dominant frequency is equal to the frequency of rotation of the roller [46], [49].

3.2 The Numerical Model of Tram Wheel Roller Rig

In order to evaluate the performance of the developed wheel slip control methods, a numerical model representing the tram wheel roller rig has been created in the MATLAB environment. The numerical model consists of five main components: the mechanical model of the torsional system, the dynamic model of the PMSM, dynamic model of the AM, the Freibauer/Polach adhesion force model, and the anti-slip control model. The finite difference method is used for the calculation of the dynamic equations. The step time of integration is selected as *20 μs*, to guarantee the accuracy of the calculations. However, the control action of the anti-slip control model is limited to the period of *0.04 ms* to simulate the control action of the controller in the real tram wheel roller rig. The complete structure of the developed numerical model tram wheel roller rig is depicted in Figure 7.

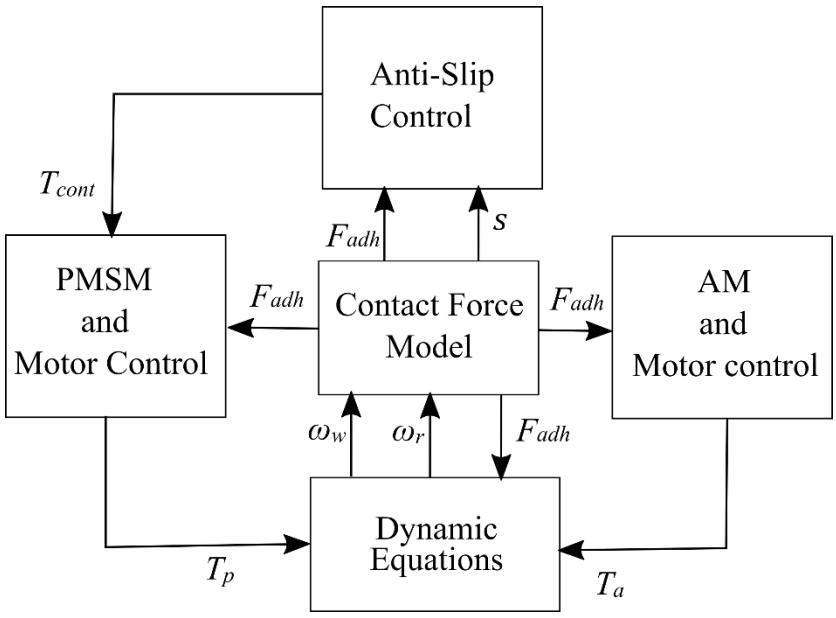

Figure 7. Complete structure of the developed numerical model of the tram wheel roller rig.

In order to obtain a suitable numerical model, the following assumptions are made:

- The stator windings are balanced with sinusoidal magnetomotive force.
- Saturation is neglected.
- Eddy-currents and hysteresis losses are neglected.
- The inductances are constant and independent of the rotor position.
- Devices used in the power-electronic circuit are ideal.

3.2.1 Dynamic Model of the Tram Wheel Roller Rig

A simple dynamic model of the tram wheel roller rig is depicted in Figure 8. It includes flexibilities of drive shafts and inertia of the rotating bodies; however, rolling resistance and resistances in bearings are neglected.

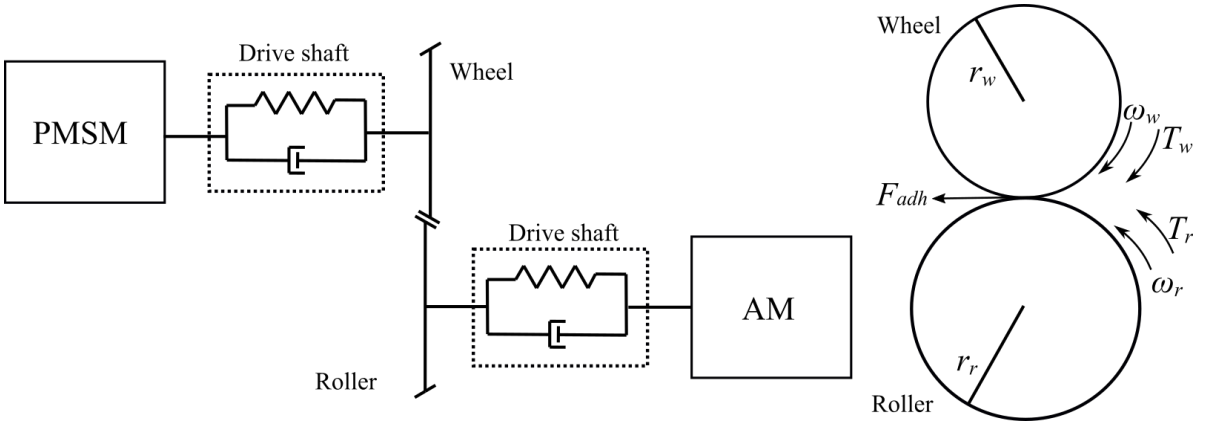

Figure 8. The dynamic model of the tram wheel roller rig.

The equations of motion of the tram wheel roller rig model are presented as follows:

$$\dot{\omega_a} = \frac{T_a - T_r}{J_a} \qquad \textit{Eq. 4}$$

$$\dot{\omega_r} = \frac{T_r - F_{adh} \cdot r_r}{J_r} \qquad \textit{Eq. 5}$$

$$\dot{\omega_w} = \frac{-T_w - F_{adh} \cdot r_w}{J_w} \qquad \textit{Eq. 6}$$

$$\dot{\omega_p} = \frac{T_p + T_w}{J_p} \qquad \textit{Eq. 7}$$

$$T_r = k_{s1} sgn(x_1)(|x_1| - h_1) + b_{s1}\dot{x_1}$$
$$T_w = k_{s2} sgn(x_2)(|x_2| - h_2) + b_{s2}\dot{x_2} \qquad \textit{Eq. 8}$$

where T_a is the AM torque, T_r is torque at the roller shaft, T_w is torque at the wheel shaft, T_p is the PMSM torque, J_a is the AM rotor moment of inertia, J_r is the roller moment of inertia, J_w is the wheel moment of inertia, J_p is the PMSM rotor moment of inertia, F_{adh} is the adhesion force acting in the contact area, ω_a is the rotational speed of AM, ω_r is the roller rotational speed, ω_w is the wheel rotational speed, ω_p is the rotational speed of the PMSM rotor, r_r is the radius of the roller, r_w is the radius of the wheel, k_{s1} and k_{s2} are torsional stiffnesses of the shafts, b_{s1} and b_{s2} are torsional damping parameters of the shafts, h_1 and h_2 represent angular play in CV joints and x_2 and x_1 are angular displacements in the joints [50]. Values of the dimensions and inertial parameters of the roller rig are shown in Table 1.

Table 1: Inertia and radii of the components of the tram-wheel roller rig

$J_w\ [kgm^2]$	$J_r\ [kgm^2]$	$J_p\ [kgm^2]$	$J_a\ [kgm^2]$	$r_w\ [m]$	$r_r\ [m]$
17.86	47.20	0.95	6.6	0.3482	0.4522

Wheel slip is defined as the normalised difference between the wheel speed and vehicle speed. The wheel slip that occurs between the wheel and roller is calculated using the data provided by rotary encoders. In order to obtain the wheel slip speed and wheel slip ratio, the following equations are used:

$$w_s = \omega_w \cdot r_w - |\omega_r| \cdot r_r, \qquad s = \frac{\omega_w \cdot r_w - |\omega_r| \cdot r_r}{|\omega_r| \cdot r_r} \qquad Eq.\ 9$$

where w_s is the slip speed, and s is wheel slip.

3.2.2 Electric Motor Control Methods

The control of the AM in experimental tram wheel roller rig is provided by scalar control (open-loop voltage/frequency) while field-oriented control (FOC) is employed for the control of the PMSM. However, for the simulations, FOC is replaced with hysteresis current control due to its simple structure. In this section of the thesis, the current motor control methods of the PMSM and AM are presented in detail.

3.2.2.1 Coordinate Transformations

The vector control architectures related to the PMSM and the AM use Clarke and Park transformations. The transformation helps to simplify the analysis of three-phase circuits. Therefore, in this section, the most common transformation methods are introduced.

Clarke and Inverse Clarke Transformation: Clarke transformation translates three-phase quantities from the three-phase reference frame to the two-axis orthogonal stationary reference frame while inverse Clarke transformation converts the two-axis quantities in a stationary reference frame to three-phase components in a three-phase reference frame [52]. The graphical representation of the Clarke transformation is indicated in Figure 9.

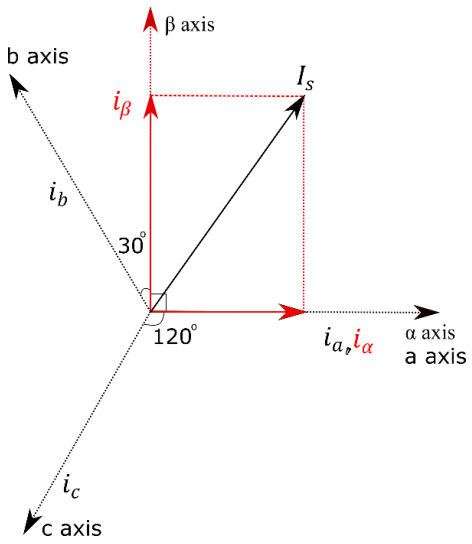

Figure 9. Clarke transformation.

The following equation expresses the Clarke transformation:

$$\begin{bmatrix} i_\alpha \\ i_\beta \\ i_0 \end{bmatrix} = \frac{2}{3}\begin{bmatrix} 1 & -\frac{1}{2} & -\frac{1}{2} \\ 0 & \frac{\sqrt{3}}{2} & -\frac{\sqrt{3}}{2} \\ \frac{1}{2} & \frac{1}{2} & \frac{1}{2} \end{bmatrix}\begin{bmatrix} i_a \\ i_b \\ i_c \end{bmatrix} \qquad \textit{Eq. 10}$$

where i_a, i_b and i_c are the three-phase quantities and i_α and i_β are the stationary orthogonal reference frame quantities.

The following equation expresses the inverse Clarke transformation:

$$\begin{bmatrix} i_a \\ i_b \\ i_c \end{bmatrix} = \begin{bmatrix} 1 & 0 & 1 \\ -\frac{1}{2} & \frac{\sqrt{3}}{2} & 1 \\ -\frac{1}{2} & -\frac{\sqrt{3}}{2} & 1 \end{bmatrix}\begin{bmatrix} i_\alpha \\ i_\beta \\ i_0 \end{bmatrix} \qquad \textit{Eq. 11}$$

Park and Inverse Park Transformation: Park transformation is used to transform two-axis orthogonal stationary reference frame quantities into rotating reference frame quantities. Inverse Park transformation transforms the rotating reference frame quantities into two-axis orthogonal

stationary reference frame quantities [52]. The Park transformation is graphically depicted in Figure 10.

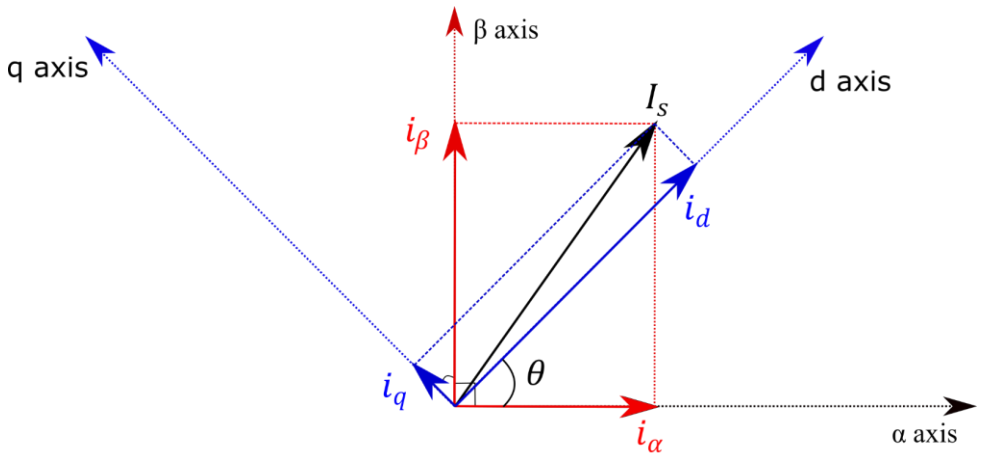

Figure 10. Park transformation.

The mathematical expression of the Park transformation is given in the following equation:

$$\begin{bmatrix} i_d \\ i_q \\ i_0 \end{bmatrix} = \begin{bmatrix} cos(\theta) & sin(\theta) & 0 \\ -sin(\theta) & cos(\theta) & 0 \\ 0 & 0 & 1 \end{bmatrix} \begin{bmatrix} i_\alpha \\ i_\beta \\ i_0 \end{bmatrix} \qquad \textit{Eq. 12}$$

where i_d and i_q are the rotating reference frame quantities and θ is the angle between a-axis and d-axis.

The inverse Park transformation is expressed by the following equation:

$$\begin{bmatrix} i_\alpha \\ i_\beta \\ i_0 \end{bmatrix} = \begin{bmatrix} cos(\theta) & -sin(\theta) & 0 \\ sin(\theta) & cos(\theta) & 0 \\ 0 & 0 & 1 \end{bmatrix} \begin{bmatrix} i_d \\ i_q \\ i_0 \end{bmatrix} \qquad \textit{Eq. 13}$$

Park-Clark and Inverse Park-Clark transformation: Park-Clark transformation is used to transform the three-phase quantities from the three-phase reference frame to the rotating reference frame. The inverse Park-Clark transformation transforms the quantities in the rotating reference frame into three-phase quantities. The Park-Clark transformation uses two conventions:

- The rotating frame aligned with a-axis at the time *t=0*, which means at *t=0*, the d-axis is aligned with a-axis. This type of transformation is called cosine-based Park transformation.
- The rotating frame aligned 90 degrees behind a-axis at *t=0*, which means at *t=0*, the q-axis is aligned with a-axis. This type of transformation is called sine-based Park transformation [53]

Figure 11 shows the graphical representation of cosine-based Park-Clarke transformation. Since the rotating frame is aligned with a-axis, the following relations can be derived:

$$I_s = i_d + j \cdot i_q = (i_\alpha + j \cdot i_\beta) \cdot e^{-j \cdot \theta} = \frac{2}{3}(i_a + i_b \cdot e^{-j \cdot \frac{2\pi}{3}} + i_c \cdot e^{j \cdot \frac{2\pi}{3}}) \cdot e^{-j \cdot \theta} \qquad \textit{Eq. 14}$$

$$\begin{bmatrix} i_d \\ i_q \\ i_0 \end{bmatrix} = \frac{2}{3} \begin{bmatrix} cos(\theta) & cos(\theta - \frac{2\pi}{3}) & cos(\theta + \frac{2\pi}{3}) \\ -sin(\theta) & -sin(\theta - \frac{2\pi}{3}) & -sin(\theta + \frac{2\pi}{3}) \\ \frac{1}{2} & \frac{1}{2} & \frac{1}{2} \end{bmatrix} \begin{bmatrix} i_a \\ i_b \\ i_c \end{bmatrix} \qquad \textit{Eq. 15}$$

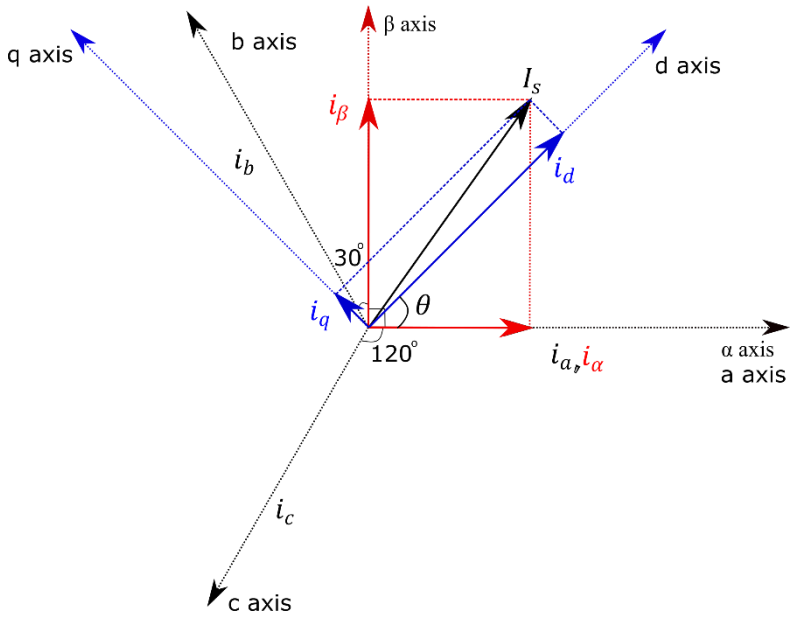

Figure 11. Park-Clarke transformation.

where i_a, i_b and i_c are the three-phase quantities, i_d and i_q are two-phase rotating reference frame quantities and θ angle between a-axis and d-axis.

The inverse Park-Clarke transformation is derived as shown in Eq. 16.

$$\begin{bmatrix} i_a \\ i_b \\ i_c \end{bmatrix} = \begin{bmatrix} cos(\theta) & -sin(\theta) & 1 \\ cos(\theta - \frac{2\pi}{3}) & -sin(\theta - \frac{2\pi}{3}) & 1 \\ cos(\theta + \frac{2\pi}{3}) & -sin(\theta + \frac{2\pi}{3}) & 1 \end{bmatrix} \begin{bmatrix} i_d \\ i_q \\ i_0 \end{bmatrix} \qquad \textit{Eq. 16}$$

3.2.2.2 Inverter

A power inverter is an electronic device that changes the direct current (DC) to alternating current (AC) [54]. A typical circuit model of three-phase voltage source inverter is shown in Figure 12. The model of the inverter has a full bridge topography with the three inverter legs. Each leg consists of two power switches. It has six power switches(S1-S6) that produce the three-phase output voltage. The power switches can be built using the power BJT, GTO, IGBT etc. The selection of the switching components depend on the desired power, required switching frequency and amount of the power loss [55]. The working principle of power inverters is simple. When the upper switch in one leg turns on, the lower switch in the same leg turns off with the help of the gate signals [56]. Then, the control of the output voltage became possible by controlling the ON and OFF states of the upper transistor S_1, S_3 and S_5.

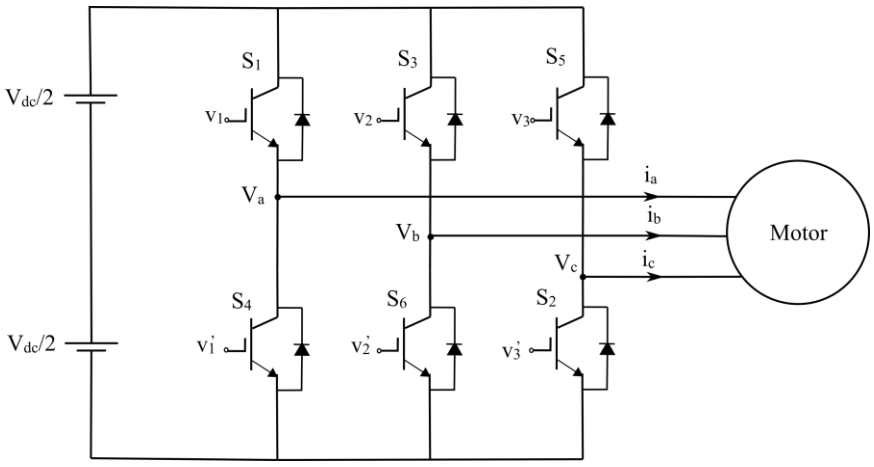

Figure 12. Three-phase voltage source inverter.

The relation between the switching variable vectors (v_1, v_2, and v_3) and phase voltage vectors (V_{an}, V_{bn} and V_{cn}) is expressed as in following Eq. 17.

$$\begin{bmatrix} V_{an} \\ V_{bn} \\ V_{cn} \end{bmatrix} = \frac{V_{dc}}{3} \begin{bmatrix} 2 & -1 & -1 \\ -1 & 2 & -1 \\ -1 & -1 & 2 \end{bmatrix} \begin{bmatrix} v_1 \\ v_2 \\ v_3 \end{bmatrix} \qquad \textit{Eq. 17}$$

3.2.2.3 Current Hysteresis PWM

The current hysteresis PWM method is instantaneous feedback current control method of PWM. The actual current continuously tracks the reference current in defined bandwidth.

In the current hysteresis controller, the desired current is subtracted from the actual current. The error is fed to the comparators having hysteresis band. When the error signal crosses the lower limit of the hysteresis band, the upper switch of the inverter turns on. When the error signal crosses the upper limit of the hysteresis band, the lower switch of the inverters turns on [57]. The following equations are used to determine the state of switching variable vector of the first leg.

$$i_e = i_{ref} - i_{act} \qquad \textit{Eq. 18}$$

$$v_1 = \begin{cases} 1 & i_e > \Delta i \\ 0 & i_e < -\Delta i \\ v_1 & -\Delta i < i_e < \Delta i \end{cases}$$
$$v_1' = \begin{cases} 0 & i_e > \Delta i \\ 1 & i_e < -\Delta i \\ v_1' & -\Delta i < i_e < \Delta i \end{cases} \qquad \textit{Eq. 19}$$

where i_{ref} is the desired current, i_{act} is the actual current, Δi is the current hysteresis band, and i_e is the error between the actual and desired current.

3.2.2.4 Space Vector Pulse Width Modulation

Space vector pulse width modulation (SVPWM) is one of the most common pulse width modulation (PWM) technique for variable-frequency drive applications due to its superior performance characteristics. The method is used for producing the alternating current waveforms.

The SVPWM was originally developed as a vector approach PWM for three-phase inverters. The method is improved to generate the sine wave with higher voltage and lower total harmonic distortion (THD). The technique aims to provide the variable output with maximum fundamental components and minimum harmonics [58].

The Voltage Source Inverter has six-active and two-zero switching states. The switching status of the active (V_1-V_6) and zero (V_0-V_7) vectors are shown in Figure 13. The vectors constitute a hexagonal where the angle between the two adjacent vectors is $\pi/2$ [59]. The zero vectors (V_0 and V_7) locate at the origin and provide zero voltage to the system, while active vectors (V_1-V_6) enables the power transfer. The methods approximate the reference voltage vector (V_{ref}) using the switching states. The reference voltage is generated as the average output of the inverter in a short period.

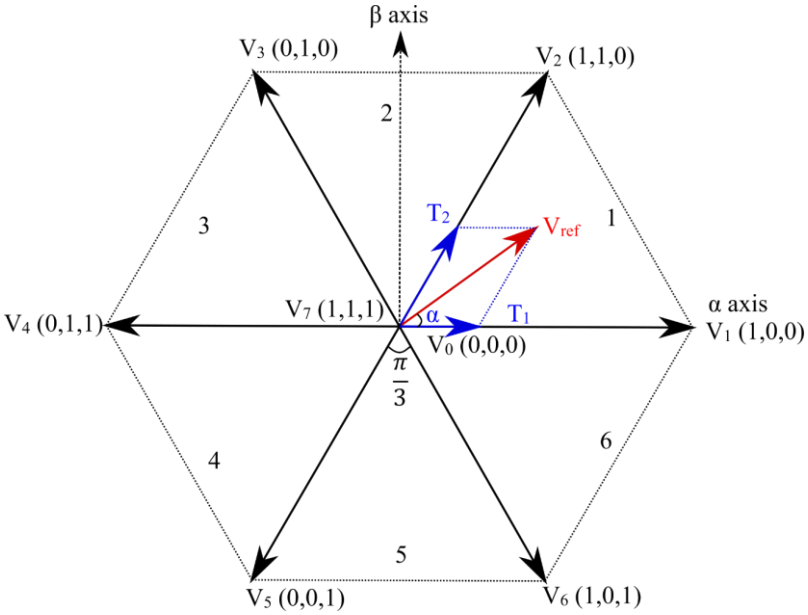

Figure 13. Active and zero vectors.

The SVPWM method is implemented as in the following steps:

- Determination of magnitude reference voltage and phase angle ($V_{ref,}$ and α)
- Determination of the time durations (T_1, T_2 and T_0)
- Determination of activation time for each switch (S_1-S_6)

The three-phase voltages are required to be transformed to the two-axis orthogonal stationary reference voltages. The Clark transformation, which is provided in Eq. 10, can be used for this transformation. V_{ref} and α are determined using V_α and V_β as in the following equations:

$$|V_{ref}| = \sqrt{V_\alpha^2 + V_\beta^2}$$
$$\alpha = tan^{-1}(\frac{V_\beta}{V_\alpha}) \quad \textit{Eq. 20}$$

α angle is used for the determination of the sector of the reference voltage. Depending on the sector, the active vectors that become adjacent to the reference voltage, and zero vectors are determined [59]. The Eq. 21-Eq. 23 determines the switching time duration in any sector.

$$T_1 = \frac{\sqrt{3}\,T_z\,|V_{ref}|}{V_{dc}}(sin\frac{n}{3}\pi\, cos\alpha - cos\frac{n}{3}\pi\, sin\,\alpha) \quad \textit{Eq. 21}$$

$$T_2 = \frac{\sqrt{3}\,T_z\,|V_{ref}|}{V_{dc}}(-cos\alpha\, sin\frac{n-1}{3}\pi + sin\alpha cos\frac{n-1}{3}\pi) \quad \textit{Eq. 22}$$

$$T_0 = T_z - T_1 - T_2 \quad \textit{Eq. 23}$$

where n is the number of sectors, T_z is the switching period, T_0 is the switching period for zero vectors, T_1 is the switching time duration for the first adjacent vector, T_2 is the switching time duration for the second adjacent vector and V_{dc} is the DC link voltage.

There are several switching patterns which is possible to use to implement the SVPWM method. In order to minimise the switching losses, only two adjacent active vectors and zero vectors are used in a sector [55]. The described goal can be achieved by starting each switching with a zero vector and ends with a zero vector during the sampling time. The discussed pattern decreases the THD in the output voltage. The corresponding switching sequence for sector 4 is indicated in Figure 14. It could be seen that the switching sequence is symmetrical during the whole period. The switching time for each sector can be determined as given in Table 2.

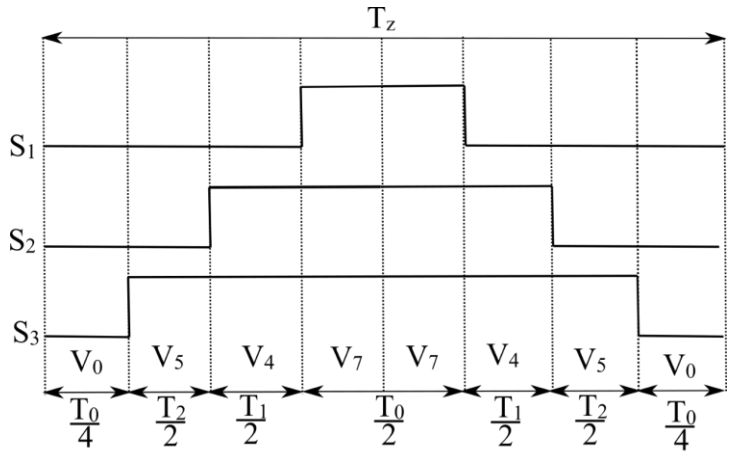

Figure 14. Switching sequence for sector 4.

Table 2: Transmission times of switches.

Sector	Upper Switches	Lower Switches
1	$S_1=T_1+T_2+T_0/2$ $S_3=T_2+T_0/2$ $S_5=T_0/2$	$S_2=T_0/2$ $S_4=T_1+T_0/2$ $S_6=T_1+T_2+T_0/2$
2	$S_1=T_1+T_0/2$ $S_3=T_1+T_2+T_0/2$ $S_5=T_0/2$	$S_2=T_2+T_0/2$ $S_4=T_0/2$ $S_6=T_1+T_2+T_0/2$
3	$S_1= T_0/2$ $S_3=T_1+T_2+T_0/2$ $S_5=T_2+T_0/2$	$S_2=T_1+T_2+T_0/2$ $S_4=T_0/2$ $S_6=T_1+T_0/2$
4	$S_1=T_0/2$ $S_3=T_1+T_0/2$ $S_5=T_1+T_2+T_0/2$	$S_2=T_1+T_2+T_0/2$ $S_4=T_2+T_0/2$ $S_6=T_0/2$
5	$S_1=T_2+T_0/2$ $S_3=T_0/2$ $S_5=T_1+T_2+T_0/2$	$S_2=T_1+T_0/2$ $S_4=T_1+T_2+T_0/2$ $S_6=T_0/2$
6	$S_1=T_1+T_2+T_0/2$ $S_3=T_0/2$ $S_5=T_1+T_0/2$	$S_2=T_0/2$ $S_4=T_1+T_2+T_0/2$ $S_6=T_2+T_0/2$

3.2.2.5 Asynchronous Motor Scalar Control (AMSC)

The scalar control is one of the common speed control strategies of the induction motor. It is also known as voltage/frequency control. The basic principle of the control strategy is keeping the voltage/frequency ratio constant to avoid variation in magnetic field strength. The speed control of the AM that is used for the experiment is provided by scalar control. The open-loop voltage/frequency control structure for the AM is illustrated in Figure 15. The AMSC block computes the magnitude of the stator voltage based on the reference frequency as expressed in Eq. 24 [60].

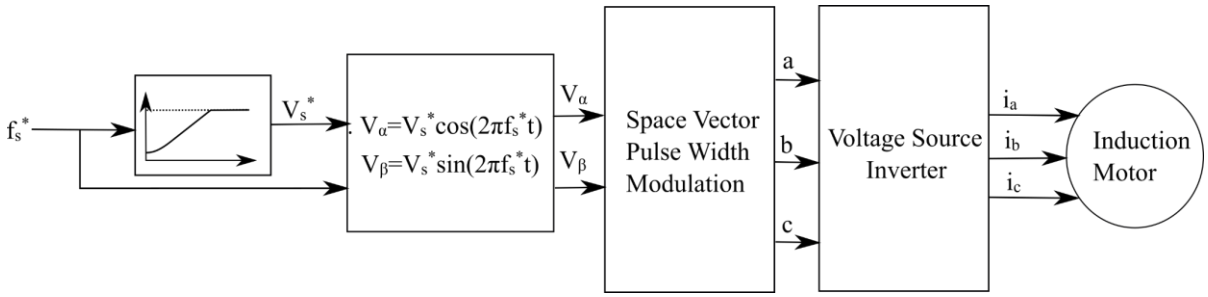

Figure 15.The structure of Open-loop Voltage/Frequency Control.

$$V_s^* = \left(\frac{V_n - V_{min}}{f_n - f_{min}}\right) f_s^* \qquad \textit{Eq. 24}$$

where f_s^* reference frequency, V_n is the rated voltage of AM, V_{min} is the minimum voltage, f_n is the rated electrical frequency of AM, and f_{min} is the minimum frequency.

The voltage components in the stationary reference frame are derived as the following equations:

$$V_\alpha = V_s^* \cos(2\pi f_s^* t)$$
$$V_\beta = V_s^* \sin(2\pi f_s^* t) \qquad \textit{Eq. 25}$$

where V_α is the α-axis voltage in the stationary reference frame and V_β is the β-axis voltage in the stationary reference frame. V_α and V_β voltages are provided to the SVPWM to generate switching variables to control the VSI.

3.2.3 Dynamic Model of Permanent Magnet Synchronous Motor

The permanent magnet synchronous motor (PMSM) is a rotating electric machine which the construction of the stator is similar to an induction motor and the conventional synchronous motor. The rotor is a permanent magnet rotor [61]. The equivalent dynamic model of the PMSM on the rotor reference frame is indicated in Figure 16.

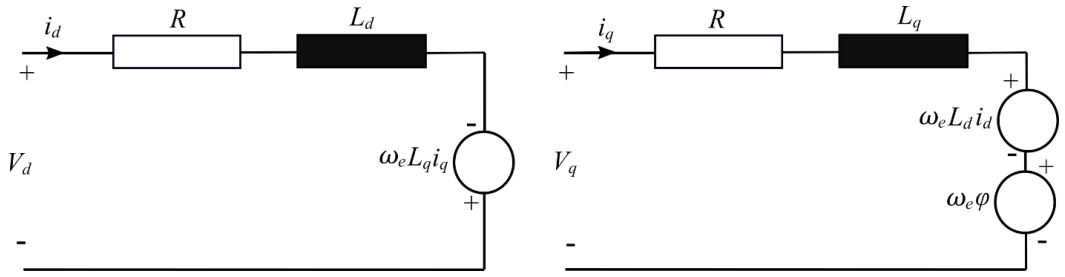

Figure 16. The equivalent dynamic model of the PMSM on the rotor reference frame.

The dynamic equations of the stator currents may be written with respect to Figure 16.

$$\frac{d}{dt} i_d = \frac{1}{L_d} V_d - \frac{R}{L_d} i_d + \frac{L_q}{L_d} \omega_e i_q \qquad \textit{Eq. 26}$$

$$\frac{d}{dt} i_q = \frac{1}{L_q} V_q - \frac{R}{L_q} i_q - \frac{L_d}{L_q} \omega_e i_d - \frac{\varphi}{L_q} \omega_e \qquad \textit{Eq. 27}$$

where V_d and V_q are d-q axis voltages on the rotating reference frame, i_d and i_q are d-q axis currents, R is the resistance of the stator windings, φ is the amplitude of the flux induced by the permanent magnet of the rotor in the stator phases, L_d and L_q are d-q axis self-inductances, and ω_e is the angular velocity of the rotor [62].

The electromagnetic torque produced by the PMSM is calculated using Eq. 28:

$$T_p = \frac{3}{2} p[\varphi i_q - (L_d - L_q) i_q i_d] \qquad \textit{Eq. 28}$$

where p is the number of pole pairs of PMSM.

The electrical speed and angular position of the rotor are calculated as given in Eq. 29 and Eq. 30:

$$\frac{d}{dt}\omega_e = \frac{p}{J_p}(T_p - T_w) \qquad \textit{Eq. 29}$$

$$\frac{d}{dt}\theta_e = \omega_e \qquad \textit{Eq. 30}$$

where ω_e is the electrical speed of the motor and θ_e is the position of the rotor.

The field-oriented control (FOC) is used to control the PMSM in the experimental test stand. For the simulations, the FOC has been replaced with the hysteresis current control. The schematic of the hysteresis current control of the PMSM is shown in Figure 17.

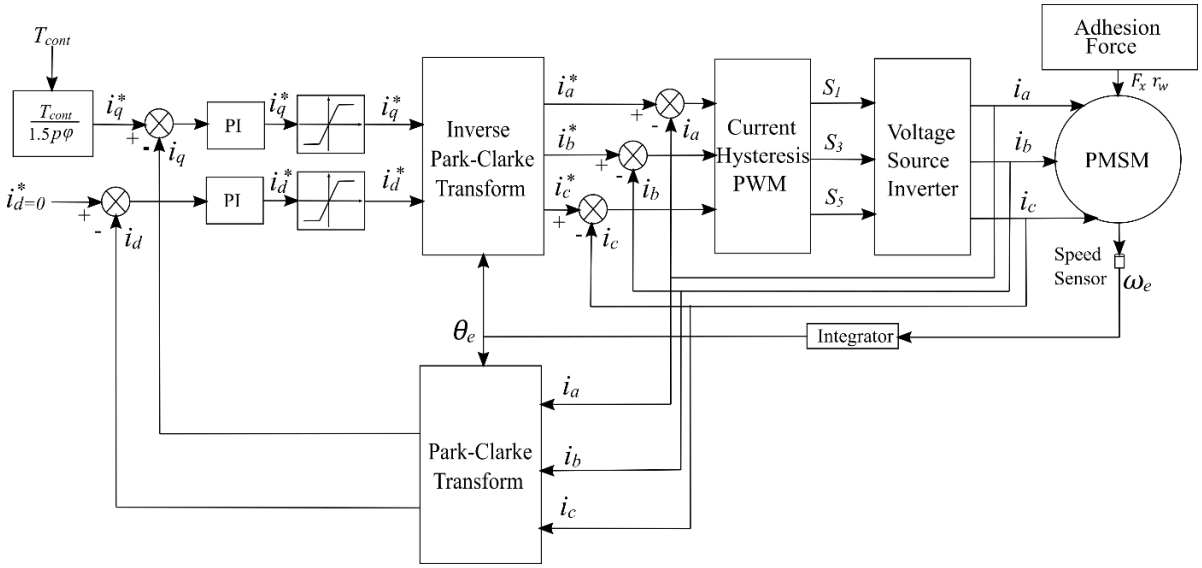

Figure 17. The hysteresis current control of the PMSM [63].

The electrical parameters of the PMSM are provided in Table 3. Details of the PMSM and its drive system are presented by Simanek et al. in [64].

Table 3: Electrical parameters of the PMSM

Power	58 kW
Current (rated)	122 A
Number of poles	44
Torque (nominal)	852 N.m
Flux	0.2 Wb
Speed (nominal)	650 rpm

3.2.4 Dynamic Model of Asynchronous Motor

The asynchronous motor (AM) used in test stand provides the opposing torque against the PMSM to keep the roller at a constant speed. Therefore, an accurate dynamic model of AM plays a vital role in the numerical model of the test stand. The model of the motor is developed based on the dynamic equivalent circuit of AM that is represented in the rotating reference frame as provided in Figure 18 [65]. All quantities are referred to the stationary reference frame side.

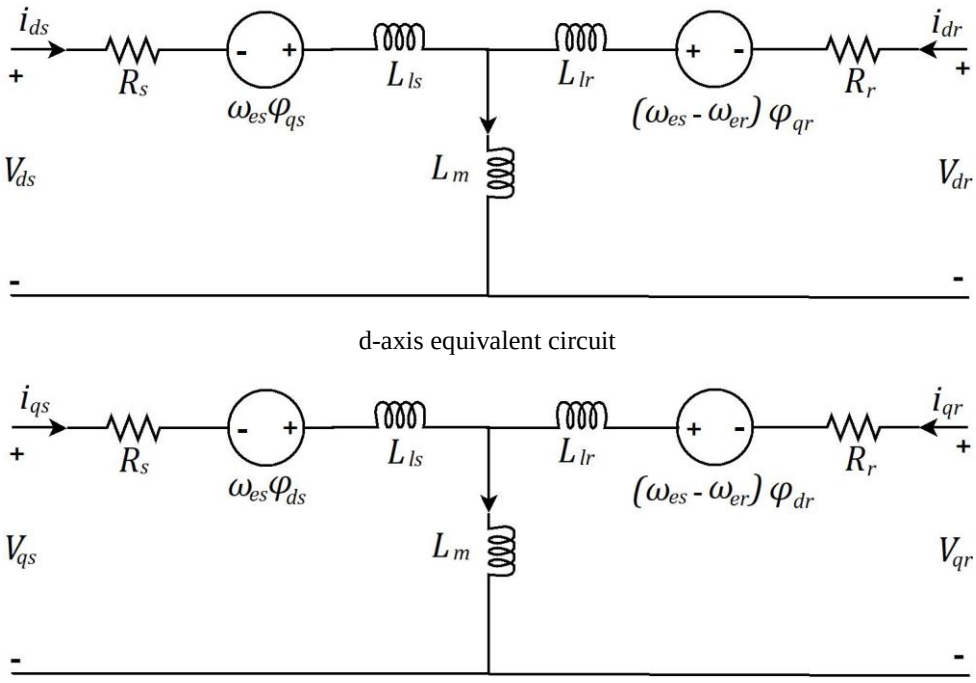

Figure 18. Dynamic equivalent circuits of AM [65].

The mathematical model of the squirrel cage motor can be derived according to Figure 18, as provided in Eq. 31-Eq. 34.

$$\frac{d\varphi_{ds}}{dt} = V_{ds} - R_s i_{ds} + \omega_{es}\varphi_{qs} \qquad \textit{Eq. 31}$$

$$\frac{d\varphi_{qs}}{dt} = V_{qs} - R_s i_{qs} - \omega_{es}\varphi_{ds} \qquad \textit{Eq. 32}$$

$$\frac{d\varphi_{dr}}{dt} = V_{dr} - R_r i_{dr} + (\omega_{es} - \omega_{er})\varphi_{qr} \qquad \textit{Eq. 33}$$

$$\frac{d\varphi_{qr}}{dt} = V_{qr} - R_r i_{qr} + (\omega_{es} - \omega_{er})\varphi_{dr} \qquad \textit{Eq. 34}$$

where d is the direct axis, q is quadrature axis, φ_{ds}, φ_{qs}, φ_{dr} and φ_{qr} are the flux linkages, V_{ds} and V_{qs} are d-q axis stator voltages, V_{dr} and V_{qr} are d-q axis rotor voltages, i_{ds} and i_{qs} are d-q axis stator currents, i_{dr} and i_{qr} are d-q axis rotor currents, R_s is the stator resistance, R_r is the rotor resistance, ω_{er} is rotor electrical speed and ω_{es} is reference frame angular speed. It should be noted that the rotor voltage (V_{dr} and V_{qr}) are zero for squirrel cage motors.

The currents in the above equations can be expressed in terms of flux linkages as given below:

$$i_{ds} = \frac{L_r}{L_s L_r - L_m^2}\varphi_{ds} - \frac{L_m}{L_s L_r - L_m^2}\varphi_{dr} \qquad \textit{Eq. 35}$$

$$i_{qs} = \frac{L_r}{L_s L_r - L_m^2}\varphi_{qs} - \frac{L_m}{L_s L_r - L_m^2}\varphi_{qr} \qquad \textit{Eq. 36}$$

$$i_{dr} = \frac{L_s}{L_s L_r - L_m^2}\varphi_{dr} - \frac{L_m}{L_s L_r - L_m^2}\varphi_{ds} \qquad \textit{Eq. 37}$$

$$i_{qr} = \frac{L_s}{L_s L_r - L_m^2}\varphi_{qr} - \frac{L_m}{L_s L_r - L_m^2}\varphi_{qs} \qquad \textit{Eq. 38}$$

where L_s is stator self-inductance, L_r is rotor self-inductance inductance, and L_m is the magnetising inductance.

The electromagnetic torque of the motor, electrical, mechanical speed of the rotor and the position of the rotor can be calculated as given in the following equations:

$$T_a = \frac{3P}{2} L_m (i_{qs} i_{dr} - i_{qr} i_{ds}) \qquad \textit{Eq. 39}$$

$$\frac{d\omega_{er}}{dt} = \frac{P}{J_a}(T_a - T_r) \qquad \omega_a = \frac{w_{er}}{P} \qquad \textit{Eq. 40}$$

$$\frac{d}{dt}\theta_{es} = \omega_{es} \qquad \textit{Eq. 41}$$

where T_a is electromagnetic torque, P is the number of pole pairs, ω_{er} is the electrical angular speed of the rotor, ω_a is the mechanical speed of the rotor, ω_{es} is the angular speed of the reference frame, and θ_{es} is the reference frame position.

The control of the AM is provided by an open loop voltage/frequency method with SVPWM technique in which the structure can be seen in Figure 15. The electrical parameters of the AM are provided in Table 4. Simanek et al. present more detailed information about the AM in his following works [64], [66].

Table 4: Electrical parameters of the AM.

Power	55 kW
Current (rated)	133 A
Number of poles	10
Torque (nominal)	891 N.m
Voltage (rated)	3x380 V/Δ
Frequency (rated)	50 Hz

3.2.5 Wheel-Roller Contact Model

The model of Polach has been implemented for simulating the tangential contact force between the wheel and roller. The Polach contact force model allows simulating various wheel-rail contact conditions using one parameter set. The parameters can be determined from experimental measurements or recommended parameters for similar wheel-rail contact condition can be used [67]. The Polach contact force model has an advantage over more detailed contact models by allowing shorter computation time. The model does not diverge significantly from more exact models when steady rolling with pure longitudinal and lateral creepage is considered.

The coefficient of the adhesion (CoA) between the wheel and the roller is modelled using the function in Eq. 42.

$$\mu = \frac{2}{\pi} f(atan(\varepsilon) + \frac{\varepsilon}{1+\varepsilon^2}) \qquad \textit{Eq. 42}$$

where μ is the coefficient of adhesion, defined as the ratio of the tangential force to the normal force in contact; f is the variable coefficient of friction and ε is scaled slip.

The scaled slip is obtained using Eq. 43:

$$\varepsilon = \frac{aK_t|s|}{p_{max}f}k_{red} \qquad \textit{Eq. 43}$$

where a represents the contact half-length, K_t is the tangential stiffness of the surface layers, p_{max} is the maximum Hertzian pressure in the contact, and k_{red} is the reduction factor of the brush contact model. The variable coefficient of friction, mentioned in the above equations, depends on the slip speed as expressed in Eq. 44. A term for the representation of dynamic phenomena has been added, as explained further.

$$f = \left|f_0 * \left((1-A) * e^{-B|w_s|} + A\right)\right| + C_1\frac{dw_s}{dt} \qquad \textit{Eq. 44}$$

where f_0 is the static coefficient of friction, C_1 is the sensitivity parameter, A is the ratio of limit friction coefficient f_∞ at infinity slip speed to maximum friction coefficient f_0, B is the coefficient of the exponential friction decrease, w_s is the wheel slip speed.

Adhesion models usually describe stationary adhesion characteristics (creep curves) only, while experimental results show that non-stationary phenomena also occur [46]. It is not within the scope of this study to propose and test hypotheses of their mechanical principles; a simple mathematical representation of a class of these phenomena ($C_1\frac{dw_s}{dt}$) has been added to the Polach creep curve following [46]. This represents the slender clockwise loops that are observed in some results. The sensitivity parameter (C_1) is set in accordance with the experimental measurement.

The typical parameters of Polach contact force model for several surface conditions are provided in Table 5. The parameters of the Polach adhesion force model are selected corresponding to the experimental setup that is outlined in section 3.1.

Table 5: Typical model parameters for different surface conditions of wheel-roller contact.

	$f_0[1]$	$A[1]$	$B[s/m]$	$k_{red}[1]$
Half-dry	0.305	0.1	0.4	0.4
Water	0.2556	0.2	0.05	0.2
Grease	0.126	0.2	0.05	0.1
Water-Grease	0.076	0.2	0.05	0.05

4 DEVELOPED WHEEL SLIP CONTROL METHODS

The wheel slip control block is one of the essential parts of traction control of the vehicle in terms of reducing wheel/rail damage and improving traction or braking performances. The wheel slip control methods have been discussed in Section 2.4. Based on the described methods, several methods have been implemented to the tram wheel roller rig to investigating the performance. The implemented control methods are introduced in detail in this section.

4.1 Wheel Slip Control Based on a Single Threshold

Wheel slip control based on a single threshold (WSCST) is one of the simplest control algorithms that is developed to prevent the severe wheel slip. The method has been introduced in Section 2.4.1. The method is based on the assumption that the maximum value of the adhesion occurs at approximately at the same wheel slip value. In order to investigate the performance of the method, it is adapted to the experimental tram wheel roller rig. Moreover, the torque increase/decrease rate is made adjustable to make the algorithm more flexible. The applied adjustment provides us with the opportunity of the determination of the optimum control parameters.

The block diagram of the WSCST is depicted in Figure 19. The actual value of the wheel slip is determined using the Eq. 9. The determined wheel slip value is compared with a constant threshold value. If actual wheel slip exceeds the threshold value, the controller regulates the applied torque according to Eq. 45. The output of the torque regulator is limited to prevent excessive torque increase, and the output torque of limiter is compared with the driver torque request. The smaller torque request is selected as control torque. The wheel slip detection and torque regulation of the control method are provided in Figure 20.

$$T_{ref}^{*} = \begin{cases} T_{cont}\,(1 - \dfrac{dt}{A_{dec}}), & s_{act} \geq s_{th} \\ T_{cont}\,(1 + \dfrac{dt}{A_{inc}}), & s_{act} < s_{th} \end{cases} \qquad \textit{Eq. 45}$$

where T_{ref}^{*} is the reference torque output of the controller, T_{cont} is the final output torque request, dt is the resolution time of speed sensor, A_{dec} is the control parameter which determines the deceleration rate of torque, A_{inc} is the control parameter which determines the increment rate of the torque, s_{th} is the slip threshold value, and s_{act} is the actual wheel slip occurs between the wheel and the roller.

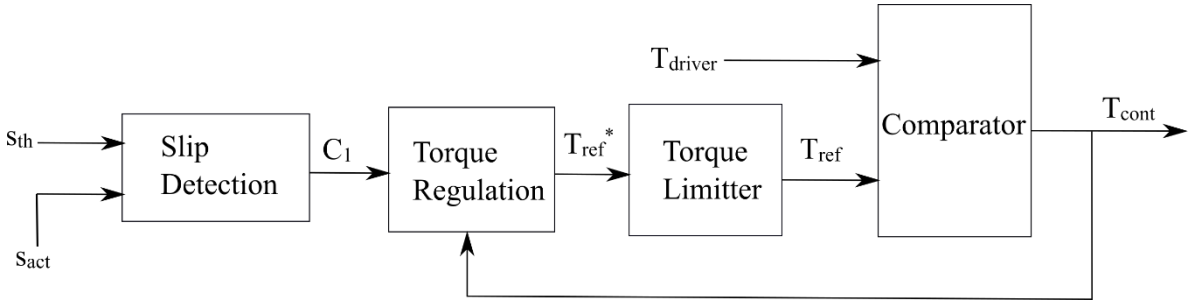

Figure 19. Block diagram of WSCST.

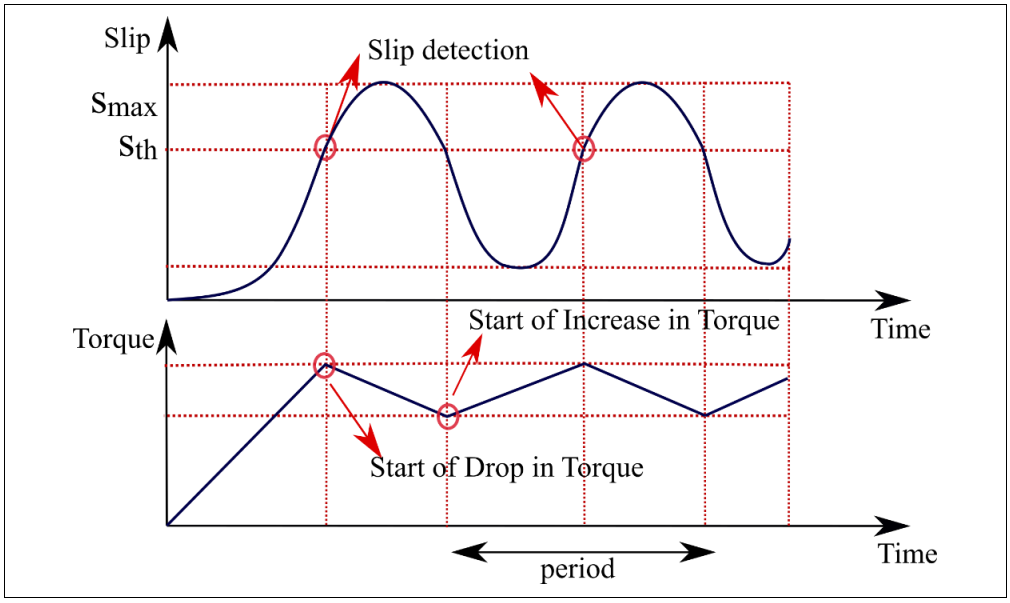

Figure 20. Wheel slip detection and torque regulation for WSCST.

The assignment of slip threshold *(s_{th})* value is very critical for the control process. The optimum amount of the threshold value ought to be slightly below the peak of the slip curve, where the maximum adhesion occurs. The determination of the optimum slip threshold value is possible via the experimental measurements. Furthermore, A_{dec} is a vital control parameter which directly affects the convergence rate of the actual wheel slip. Selecting a high value for

control parameter A_{dec} might cause an excessive drop in the motor torque. If A_{dec} is set to a low entity, the wheel slip might reach very high levels. The control parameter A_{inc} determines the torque increase rate of the controller. Adjustment a small value for A_{inc} causes a slow torque recovery; nevertheless, selecting a higher value might result in unstable wheel slip control.

4.2 Wheel Slip Control Based on Multiple Thresholds

Wheel slip control based on multiple thresholds (WSCMT) is an improved version of the abovementioned method (WSCST). In order to prevent extreme torque drop and increase, two threshold values are employed. Both of the threshold values are assigned in the stable part of the slip curve. The control action of the developed control is illustrated in Figure 21. The controller allows torque increase of motor until wheel slip reaches the first threshold value. Then, the motor torque is kept constant to decrease the rate of increase of wheel slip. When the wheel slip reaches the second threshold value, the controller starts to decrease the motor torque. The torque drop continues until wheel slip becomes lower than the second threshold value. The motor torque is kept constant in between the two slip threshold value. When the wheel slip value becomes smaller than the first threshold, the motor torque starts to rise again. The WSCMT is expected to provide less wheel slip and better adhesion utilisation than the WSCST. The block diagram of the developed control method can be seen in Figure 22.

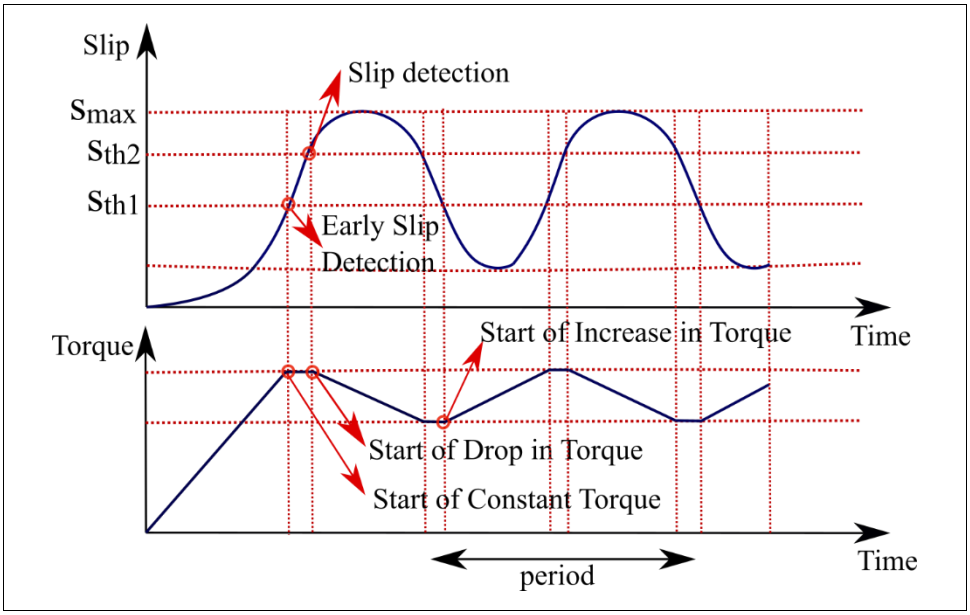

Figure 21. Wheel slip detection and torque regulation with multiple threshold values.

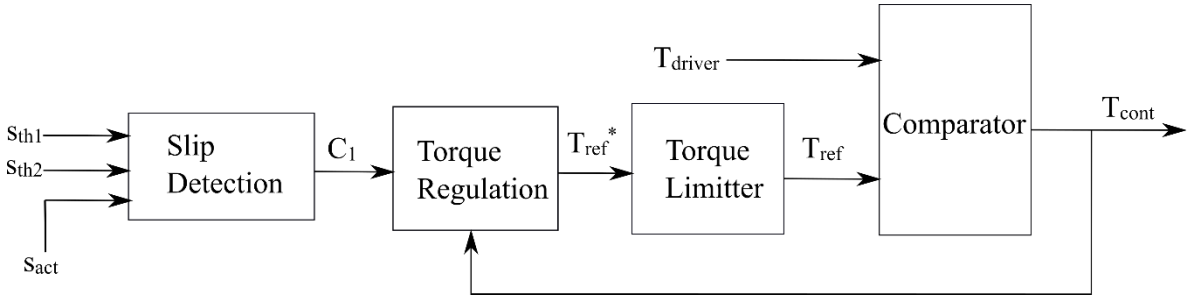

Figure 22. Block diagram of WSCMT.

The torque regulation of the motor is provided by Eq. 46.

$$T_{ref}^{*} = \begin{cases} T_{cont}\,(1 - \dfrac{dt}{A_{dec}}), & s_{act} \geq s_{th2} \\ T_{cont}\,, & s_{th1} \leq s_{act} \leq s_{th2} \\ T_{cont}\,(1 + \dfrac{dt}{A_{inc}}), & s_{act} < s_{th1} \end{cases} \qquad \textit{Eq. 46}$$

where s_{th1} is the first threshold value, and s_{th2} is the second threshold value.

The torque regulation of the WSCMT is similar to the WSCST. The difference between these two methods is the number of the threshold value, only. Both threshold value (s_{th1}-and s_{th2}) must be selected in the stable part of the slip curve and lower than the optimal wheel slip where the maximum adhesion is observed. Although the selection criteria for s_{th2} is clear (slightly less than optimal value), s_{th1} can be determined by trial and error method. Setting a high value for s_{th1} decreases its influence on the control process while the lower value of s_{th1} restricts the drive torque to reach desired levels. The impact of the other control parameters (A_{dec} and A_{dec}) on the control process is the same as the previous method. The effect of the control parameters and the threshold value on wheel slip control and adhesion utilisation is investigated by both the experimental and simulation tests in the upcoming section.

4.3 Wheel Slip Control Based on Angular Acceleration of wheel

The acceleration-based slip regulation (ASR) method is an alternative way of wheel slip control. Here, it is referred to; the wheel slip control based on the angular acceleration of wheel (WSCAA). Recently, the acceleration performance of the four in-wheel motor drive electric vehicles have been improved using the WSCAA systems [35]–[37]. Furthermore, WSCAA is

used in rail vehicles as a part of the hybrid wheel slip control method to eliminate the disadvantages of the individual control methods [24].

Most of the methods available in both literature and commercial systems employ the wheel slip information for control purposes. However, obtaining the longitudinal velocity to determine the wheel slip level is a challenging task. There are also some control methods that use the adhesion force as input to control the wheel slip and improve traction performance. Although they claim to be effective in stabilisation of the slip, measurement of the adhesion force on track is not possible. Moreover, the control system based on wheel slip and adhesion force information requires more sensor inputs, which increases the cost of the controllers. Due to its advantages that have been discussed in Section 2.4.3, the WSCAA is becoming more popular nowadays.

Acceleration wheel slip regulation is based on the principle that the angular acceleration of a vehicle wheel, provided that it rolls without slip, is equal to linear acceleration of the vehicle divided by the wheel radius. The acceleration of the vehicle is limited by the inertia of the vehicle and the traction force. If the wheel shows higher angular acceleration than what corresponds to this limit, it means that it accelerates independently of the vehicle motion – in other words, it slips.

The block diagram of WSCAA is provided in Figure 23. The wheel slip is detected through comparison of actual angular acceleration and the threshold value of the acceleration. The wheel slip detection signal is transmitted to the torque regulation block where the control torque is reduced or increased according to the developed torque regulation algorithm. The limiter that is seen in the block diagram prevents the control torque from exceeding certain minimum and maximum values or extremities.

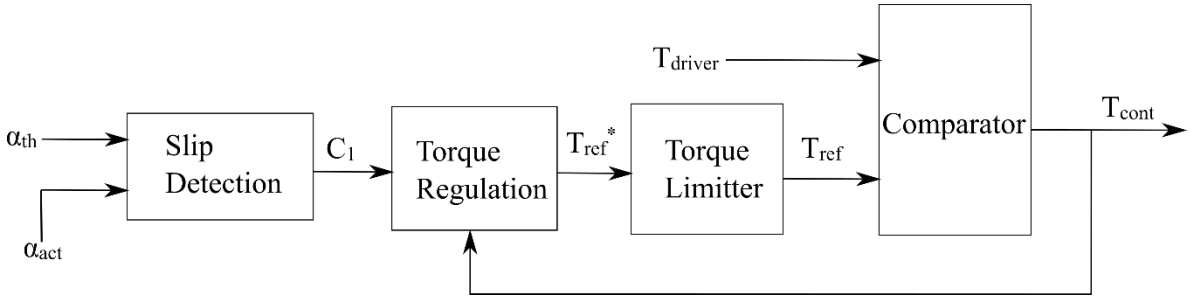

Figure 23. Block diagram for WSCAA.

The control action of the WSCAA is summarised graphically in Figure 24. Here, it should be noted that the delay due to filtering and sensors are not included. The torque regulator in Figure 23 provides the control torque according to Eq. 47.

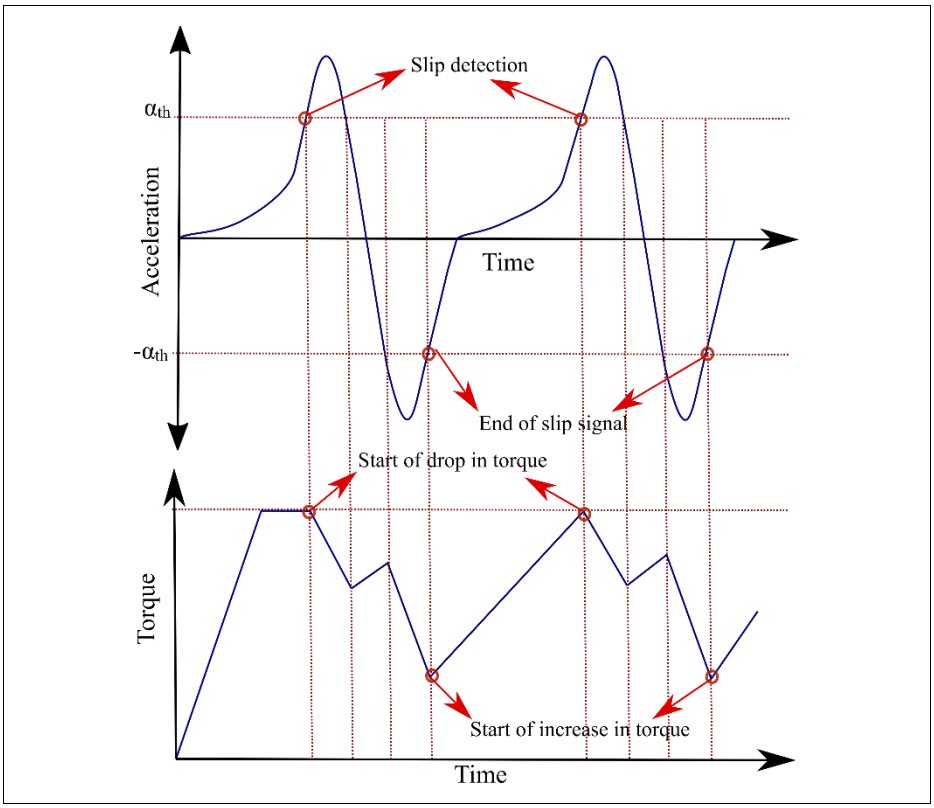

Figure 24. Wheel slip detection and torque regulation of WSCAA.

$$T_{ref}^* = \begin{cases} T_{cont}\,(1 - \dfrac{dt}{A_{dec}}), & \alpha_{act} \geq \alpha_{th} \,||\, \alpha_{act} \leq -\alpha_{th} \\ T_{cont}\,(1 + \dfrac{dt}{A_{inc}}), & \alpha_{act} < \alpha_{th} \,||\, \alpha_{act} \geq -\alpha_{th} \end{cases} \qquad \textit{Eq. 47}$$

where α_{act} is the actual angular acceleration of the wheel and α_{th} is the threshold value of angular acceleration for the wheel slip detection.

The control process of the WSCAA is similar to previous methods. The A_{inc} is the control parameter which arranges the rate of the torque increase while A_{dec} is the control parameter which determines the rate of the torque decrease. Both parameters have the physical meaning of time constants. The WSCAA uses the rotation acceleration signal for wheel slip detection. Therefore, the threshold value of the acceleration (α_{th}) is a very critical parameter for the implemented method. A small threshold value may guarantee the wheel does not slip heavily; nevertheless, the tractive force efficiency may drop drastically due to undesired frequent torque oscillations. On the other hand, a high threshold value might result in severe wheel slip due to the delay in wheel slip detection. This is why it is important to adjust α_{th} properly for optimal wheel slip control and adhesion utilisation.

4.4 PI Wheel Slip Control

PID controllers are a feedback control loop which calculates an error signal by taking the difference between the output of a system and the desired set point. In most of the process industries, PI and PID are generally used due to their simple design and tuning methods. However, the PI controllers are preferred more than the PID controllers because of being less sensitive to the noise and more simple [68]. Since the measurement from the tram wheel roller rig has electrical and mechanical noise, the PI controller is decided to be used for the wheel slip control.

The PI controller can be used for the rail vehicles to control wheel slip and improve their traction performance. For effective control, a reference slip value that is close to the peak of the slip curve can be chosen to be used as a control signal. It is also essential that the selected reference wheel slip value is on the stable side of the slip curve. However, determination of such reference is not easy since the adhesion condition that differs depending on between dry, wet and greasy rails. Therefore, the PI controllers are widely combined with adhesion prediction systems. There is no need for adhesion prediction systems for our work since the adhesion is directly measured from the tram wheel roller rig using the torque sensor that is attached to the roller shaft.

The discrete time form of a PI controller is expressed as in Eq. 48.

$$u(k) = u(k-1) + K_p\big(e(k) - e(k-1)\big) + K_i e(k) \qquad \textit{Eq. 48}$$

where u is the output torque of the controller, K_p is the proportional gain of the controller, K_i is the integral gain of the controller, k is the iterative step, e is the error between the actual wheel slip and desired wheel slip. The error is calculated as shown in Eq. 49.

$$e(k) = s_d - s_{act}(k) \qquad \textit{Eq. 49}$$

where s_d is the desired wheel slip value, and s_{act} is the actual wheel slip value.

The functionality of the control parameters of the PI (K_p and K_i) controller can be summarised as following [69].

- K_p provides an overall control action proportional to the error signal through the all-pass gain factor.
- K_i reduces the steady-state error through low-frequency compensation by an integrator.

The effects of increasing the PI gains independently on a closed-loop system are summarised in Table 6.

Table 6: Effect of increasing PI gains on a closed-loop system.

Close-loop Response	Rise Time	Overshoot	Settling Time	Steady-State Error	Stability
$\boldsymbol{K_p}$	Decrease	Increase	Slight increase	Decrease	Degrade
$\boldsymbol{K_i}$	Decrease	Increase	Increase	High increase	Degrade

The block diagram of the PI wheel slip control method (PI-WSC) is provided in Figure 25. The difference between the desired wheel slip and actual wheel slip (error) is calculated and sent to the PI torque regulator as an input signal. The PI torque controller regulates the torque applied to wheel according to the error signal. The torque limiter is used to prevent the generated

torque from exceeding maximum torque of the synchronous motor. The comparator is utilised to decide between the driver torque and regulated torque requests.

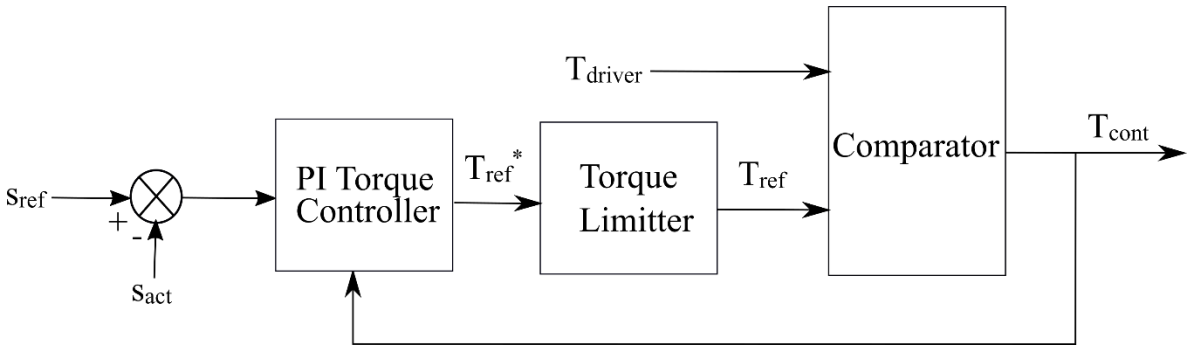

Figure 25. Block diagram for PI-WSC.

4.5 Sliding Mode Wheel Slip Control

The sliding mode controller (SMC) has been widely-studied for vehicle control systems because of certain advantages [70]–[72]. The controller is an attractive robust control method which has effective properties to stabilise nonlinear and uncertain systems. The controller keeps the systems insensitive to uncertainties on a sliding surface. Moreover, the SMC has good and rapid transient performance [73].

The conventional SMC is designed in two steps. In the first step, the sliding surface is defined to obtain specific desired characteristics along the sliding surface trajectories. Next, the controller is designed to lead the system to the desired system trajectories within a finite time.

The sliding surface *S(t)* for the design of the adaptive sliding mode torque control systems is defined as follows:

$$S(t) = s - s_d \qquad \textit{Eq. 50}$$

The main objective of Eq. 50 is to track the desired wheel slip ratio (s_d) that is given as an input to the system, based on experience from previous experimental measurements. Therefore, the sliding surface is selected as *S(t)=0* for the zero-tracking error. It is possible to keep the wheel slip in a defined trajectory by designing a correct dynamic feedback control law.

In order to satisfy the reachability conditions that direct the system trajectories toward a sliding surface where they remain, the derivative of the sliding surface is selected as Eq. 51 [74], [75]:

$$\dot{S} = -DS - K \cdot sgn(S) = -D(s - s_d) - K \cdot sgn(s - s_d) \cdot \qquad Eq.\ 51$$

where the proportional term-*DS* forces the system state to approach the sliding surface faster when the sliding surface has a significant value [70]. The parameters *D* and *K* are positive definite design parameters. *D* determines the convergence rate of the tracking error, while *K* is adjusted in compliance with the number of uncertainties and the disturbance in the system.

The determination of the reference slip value s_d is challenging in real time. Therefore, the value of s_d is pre-defined from previous experimental data where maximum adhesion is observed. The *sgn* function in Eq. 51 above results in a chattering issue because of undesired noise and delays in the actuator. For this reason, the *sgn* function is replaced with a saturation function [76]. Nevertheless, a lowpass filter is implemented to overcome the high-frequency chattering problem in the system, which is basically to stabilise the algorithm.

The sliding mode control law is designed in the following steps according to Eq. 51:

The wheel slip dynamics during acceleration is obtained by taking the time derivative of Eq. 9:

$$\dot{s} = r_w \frac{\dot{\omega_w}}{r_r |\omega_r|} - r_w \frac{\omega_w |\dot{\omega_r}|}{r_r \omega_r^2} \qquad Eq.\ 52$$

The relationship between the wheel slip dynamic and forces at the contact point can be obtained by substituting Eq. 6 into Eq. 52:

$$\dot{s} = r_w \frac{-T_w - r_w F_{adh}}{J_w r_r |\omega_r|} - r_w \frac{\omega_w |\dot{\omega_r}|}{r_r \omega_r^2} + d \qquad Eq.\ 53$$

where *d* is disturbance due to vibration in the system, driving resistances and parameter uncertainties.

By taking the time difference of the sliding surface in Eq. 50, and substituting Eq. 51 and Eq. 53, the following sliding law control torque can be achieved:

$$T_{p,con} = -r_w F_{adh} - \frac{J_w \omega_w |\dot{\omega_r}|}{|\omega_r|} - \frac{J_w r_r |\omega_r| (-D(s - s_d) - K \cdot sgn(s - s_d))}{r_w} - \frac{J_w r_r |\omega_r| \dot{s_d}}{r_w} \quad \textit{Eq. 54}$$

Since the time derivative of s_d constant is zero and the acceleration value of the roller is neglected for the tram wheel roller rig, the sliding mode control law torque is modified to the following equation [63]:

$$T_{p,con} = -r_w F_{adh} - \frac{J_w r_r |\omega_r| D(s - s_d)}{r_w} - \frac{J_w r_r |\omega_r| K \cdot sgn(s - s_d)}{r_w} \quad \textit{Eq. 55}$$

Asymptotical stability of the sliding mode control law can be proven for closed-loop control by employing a Lyapunov function [70], [76]:

$$V = \frac{1}{2} S^2 \quad \textit{Eq. 56}$$

Taking the time derivative of Eq. 56 and substituting Eq. 53:

$$\begin{gathered} S\dot{S} = S(\dot{s} - \dot{s_d}) \\ S\dot{S} = \left[r_w \frac{-T_w - r_w F_{adh}}{J_w r_r |\omega_r|} - r_w \frac{\omega_w |\dot{\omega_r}|}{r_r \omega_r^2} + d - \dot{s_d} \right] \\ S\dot{S} = S[-D(s - s_d) - K \cdot sgn(s - s_d) + d] \\ S\dot{S} \leq -DS^2 - K|S| + |d| \cdot |S| \end{gathered} \quad \textit{Eq. 57}$$

where the disturbance *d* is physically bounded. If the *K* is selected larger than |d|, then:

$$S\dot{S} \leq -DS^2 - |S| \cdot |K - d| < 0 \quad \textit{Eq. 58}$$

This guarantees the asymptotic stability of the control law for Eq. 55, since $\lim_{t \to \infty} S(t) = 0$.

The Block diagram of the sliding mode wheel slip control method (SM-WSC) is illustrated in Figure 26. The slip error (e), roller rotational speed (ω_r) and adhesion force (F_{adh}) signals are transmitted as input to the SM-WSC. Based on the input signals, the controller generates a new reference output torque request to control the wheel slip at the desired level. Here, T_{ref}^* corresponds to $T_{p,con}$.

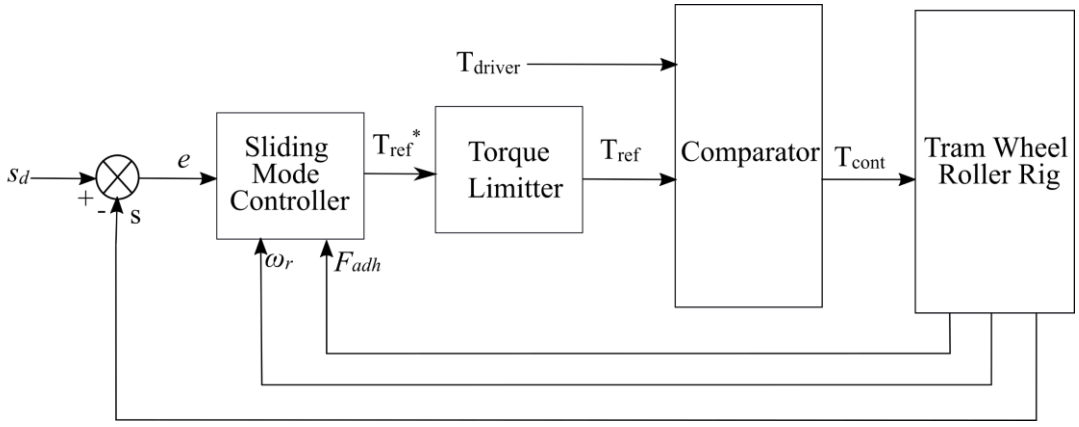

Figure 26. Block diagram for the SM-WSC.

5 RESULTS AND DISCUSSION

In this section of the work, initially, the numerical model has been validated by comparison of the simulation and experimental test results. Then, the performances of the designed wheel slip controllers are evaluated with the help of the experimental tram wheel roller rig and its numerical model. The tests are carried out for five of wheel slip control strategies. WSCST, WSCMT and WSCAA are called as re-adhesion control strategies which cannot prevent the wheel slip formation but limits it. Hence, the tests are focused on the formation and suppression of wheel slip. The SM-WSC and PI-WSC are the wheel slip control strategies that aim to stabilise the wheel slip at the desired level. Therefore, the performances of the controllers are also evaluated in terms of traction efficiency.

5.1 Validation of Numerical Model

In order to use the developed numerical model of the tram wheel roller rig for the performance evaluation of the implemented wheel slip control strategies, the validity of the model has to be proven. Hence, the numerical model is tested without any wheel slip controller. Figure 27 shows the comparison of the simulation and experimental results carried out under water contaminated test conditions. The tests are performed for the same PMSM torque request, as provided in Figure 27(a). The resultant wheel slips are illustrated in Figure 27(b). Here, it can be seen that both results are in good agreement. The slip curves (simulation and experiment) are presented in Figure 27(c). It is noticed that the slender clockwise loops that are observed in experiment results are successfully simulated with the numeric model. Furthermore, slight differences between the simulation and experimental wheel speed results are displayed in Figure 27(d).

When Figure 27 is analysed in depth, several differences between the simulation results and the experimental results are observed. The first group of factors causing mentioned differences consist in simplifications of the model which does not include all mechanical details and imperfections of the real experimental device and testing conditions. Other factors are related to the measurement procedure including parasitic signals (mainly electromagnetic noise), resolution of sensors, as well as processing the simulation results – filtering which

impacts the signals particularly when wheel slip is suddenly terminated. Despite the effects of mentioned factors, it is seen that the results obtained from the developed numerical model are consistent with the experimental results. This fact proves the validity of the developed numerical model.

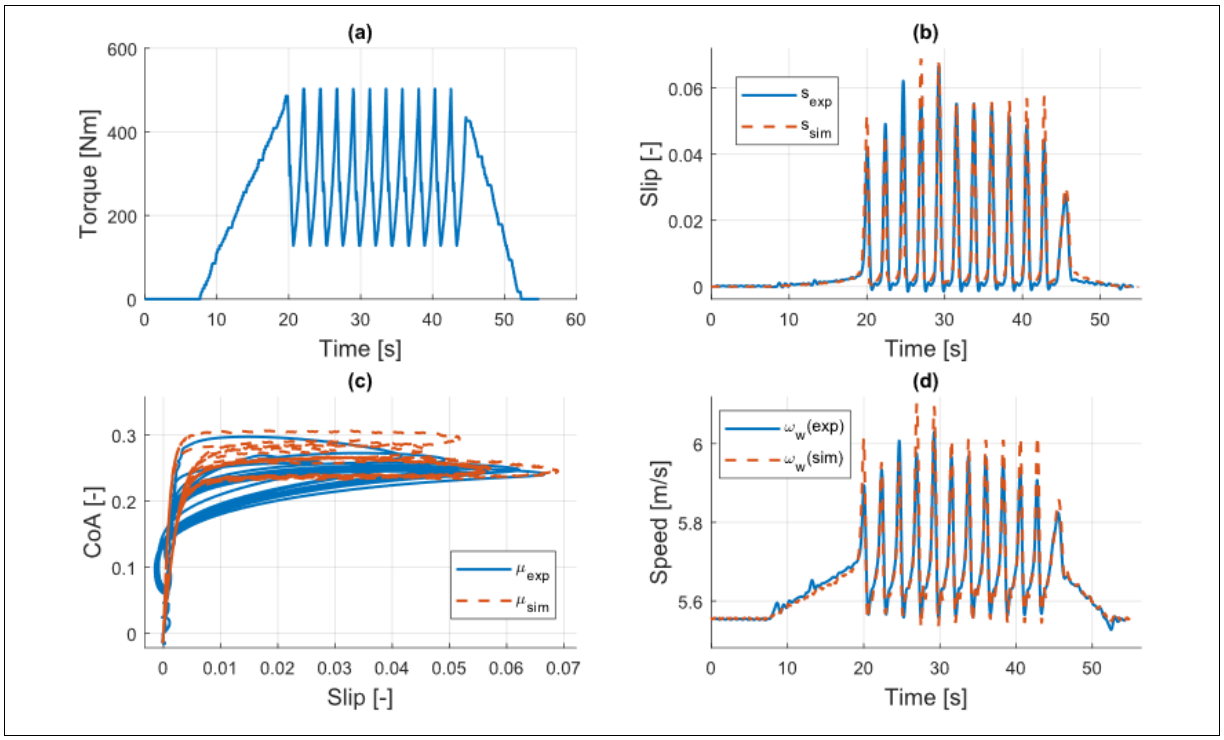

Figure 27. The comparison of the simulation and experimental results: (a) PMSM torque request; (b) Wheel slip; (c) Slip curves; (d) Wheel and roller speeds.

5.2 Simulation Results

In this step of the study, the wheel slip control performances of the algorithms are verified using the validated numerical model of the tram wheel roller rig (see section 3.2). The model, which includes nonlinear effects caused by time delay and disturbances, is generated to match the values of the experimental test setup. The model consists of five main components: the mechanical model of the torsional system, the dynamic model of the PMSM, dynamic model of the AM, the Freibauer/Polach adhesion force model, and the anti-slip control model. Polach contact parameters, which have been found by experimental measurements, are given in Table 5.

The step time of the integrations is selected as *20 μs* to guarantee the accuracy of calculations. However, the control action of the anti-slip control models is limited to the period of *0.04 ms* to simulate the control action of the controller in the real tram wheel roller rig. The initial peripheral speed of the roller is selected as *5.56 m/s*, which corresponds to *20 km/h* for a tram vehicle, in the simulations. To be able to observe wheel slip in low torque value, the normal force is assigned relatively small. Hence, the normal force is provided to the simulation as an average value of *4250 N*.

5.2.1 Wheel Slip Control Based on a Single Threshold

The first simulation is carried out using the Polach contact model parameters corresponding to the wet surface case. The control parameters are selected as following; $s_{th}=0.01$, $A_{inc}=1$ and $A_{dec}=0.5$. The minimum torque (T_{min}) generated by the WSCST controller is set as *15%* of the nominal torque of PMSM. It is assumed that the water is continuously supplied to the contact area.

Figure 28 shows the simulation results of the WSCST that is conducted under the assumption of water contaminated test condition. The driver and WSCST torque requests are shown in Figure 28(a), separately. Initially, the driver torque request is zero, after *t=4.4 s*, it is increased approximately linear up to *537 N.m*. In the time history between *t=13 s* and *t=44.2 s*, the torque request is kept as a constant value of *537 N.m*. At *t=44.2 s*, the torque request is reduced approximately linear to zero again. When driver torque request increases, the wheel and roller angular speeds increase as seen in Figure 28(b). However, the wheel speed gets higher values than the roller speed. The wheel slip (the relative difference between speeds of the wheel and the roller) is illustrated in Figure 28(c). When the wheel slip exceeds the threshold value, the controller rapidly modulates the torque request to prevent the severe slip. The torque reduction stops when the wheel slip reaches the value below the threshold. It can be seen in Figure 28(c), wheel slip is controlled cyclically. However, the amplitude and the frequency of the cycles are not constant due to the nonlinearity, and numerical errors. The response of the controller is sufficient since the maximum wheel slip ever to occur is merely *7.4 %*.

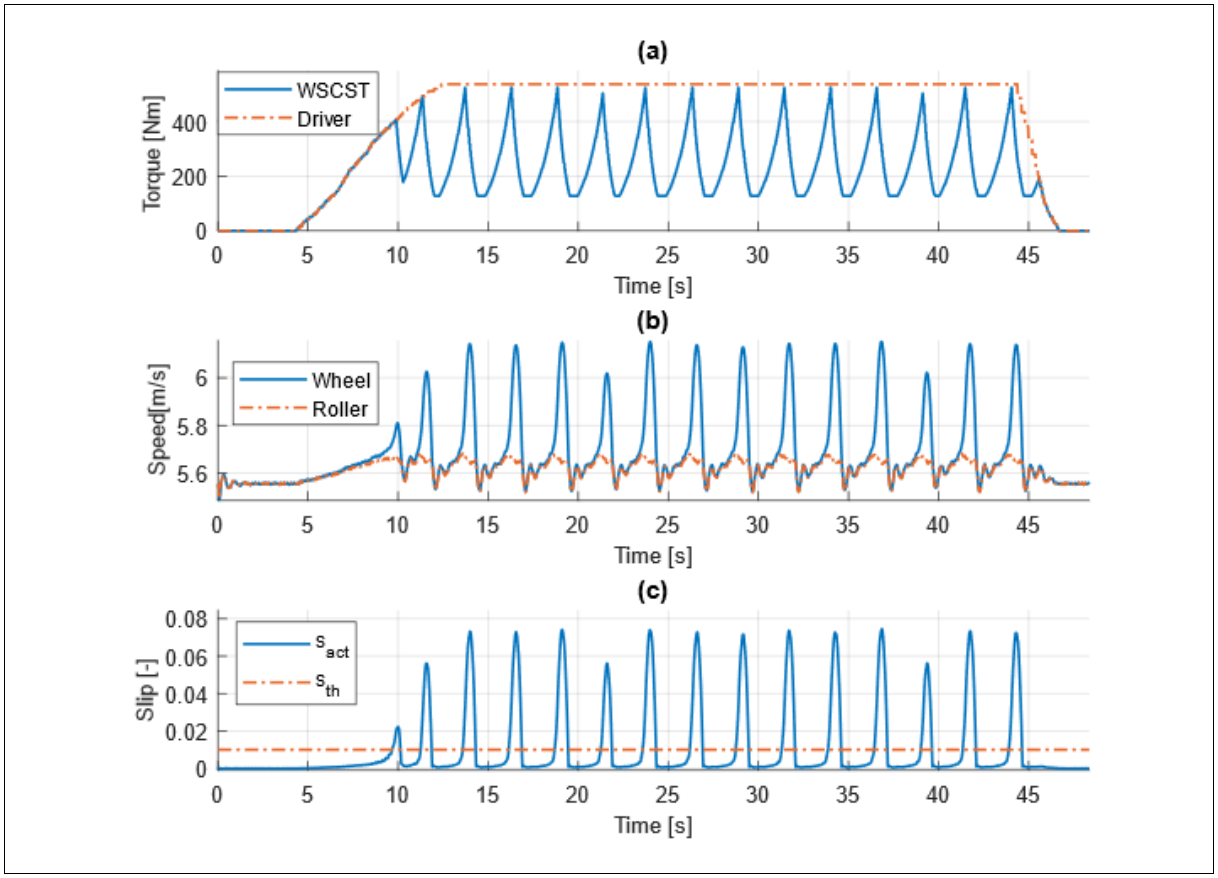

Figure 28. Simulation result of WSCST performed under the assumption of water contaminated test condition: (a) WSCST and driver torque requests; (b) Wheel and roller speeds; (c) Wheel slip.

The second simulation is carried out to investigate the performance of WSCST under the assumption of steady grease contaminated test condition. The control parameters are set as; $s_{th}=0.015$, $A_{inc}=2$ and $A_{dec}=1$. T_{min} is selected 1% of the nominal torque of PMSM.

The simulation results of the WSCST performed under the assumption of the greasy contact surface condition are presented in Figure 29. The driver torque request, which is having a trapezoid shape, and the WSCST torque requests are illustrated in Figure 29(a). The maximum driver torque request is displayed as *187 N.m*. Unlike the previous simulation, initially, WSCST torque request increases slower than the driver torque request due to T_{min} and A_{inc} limitations. The curves that show the wheel and roller speeds are exhibited in Figure 29(b). The resultant wheel slip is given in Figure 29(c). Similar to the previous simulation, the wheel slip is controlled cyclically. The dynamic behaviour (non-periodic response, irregular cycles, i.e.) of

the wheel slip observed are caused by the uncertainties and disturbances. The WSCST achieves a successful control within *4.1%* maximum wheel slip.

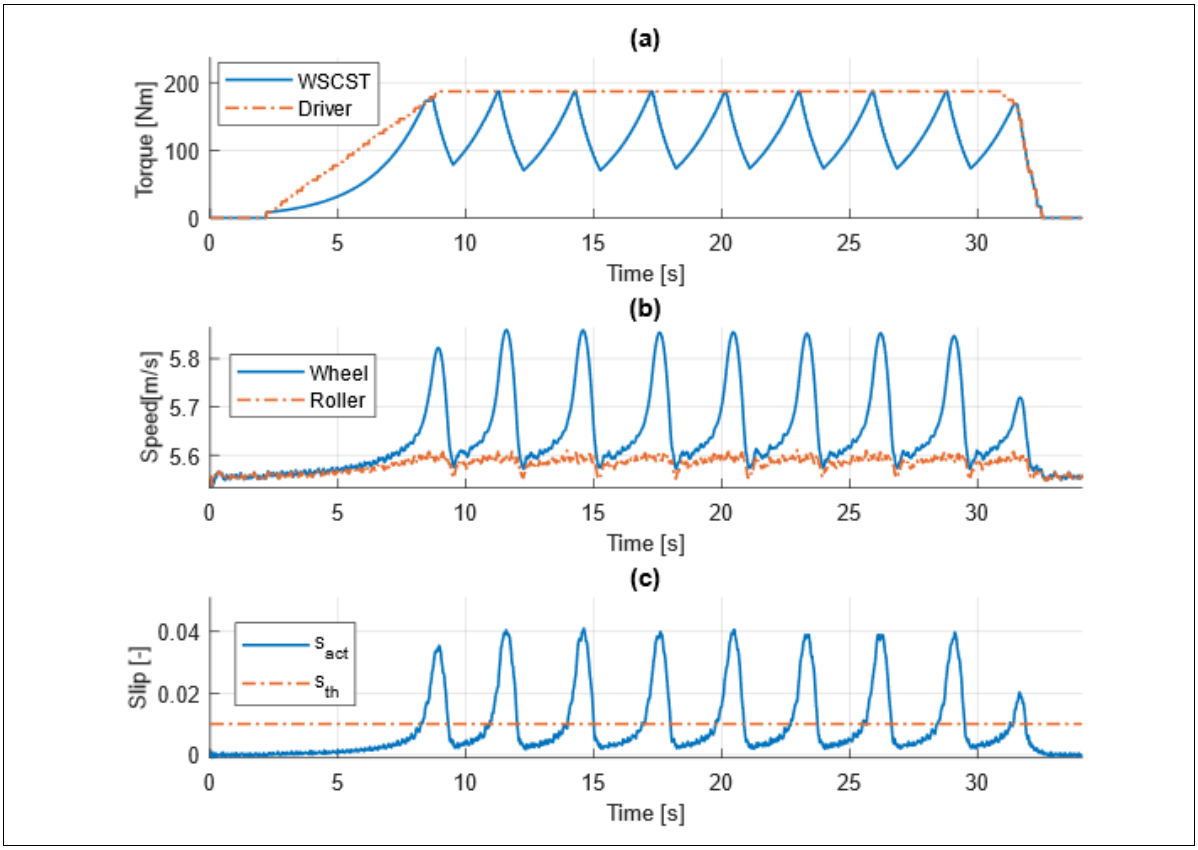

Figure 29. Simulation result of WSCST performed under the assumption of grease contaminated test condition: (a) WSCST and driver torque requests; (b) Wheel and roller speeds; (c) Wheel slip.

5.2.2 Wheel Slip Control Based on Multiple Thresholds

The wheel slip control based on multiple thresholds (WSCMT) is an improved version of WSCST. The simulations aim to point out the robustness of wheel slip control of the proposed strategy.

The performance of the controller is initially tested under the assumption of the continuous water existing between the wheel and roller. The control parameters are set as; $s_{th2}=0.006$, $s_{th1}=0.008$, $A_{inc}=4$ and $A_{dec}=1$. The minimum torque (T_{min}) generated by the WSCMT is set as *15%* of the nominal torque of PMSM.

The simulation results of the WSCMT conducted under the assumption of continuous water contaminated test condition is summarised in Figure 30. The driver torque request is increased from zero to a value which is above the maximum adhesion. The adhesion force is not depicted in Figure 30(a); however, the time course is similar to the WSCMT torque. Due to the increase in torque request, the wheel speed increases rapidly, as shown in Figure 30(b) whereas the roller speed increases slightly. Hence, a sudden wheel slip occurs. To terminate the wheel slip, WSCMT stops the torque increase when the wheel slip exceeds the first threshold value(s_{th1}). After the wheel slip exceeds the second threshold value (s_{th2}), the torque request is reduced. When Figure 30(c) is analysed, it can be seen that the maximum wheel slip of *2.3%* is observed during the simulation. Moreover, it is found in Figure 30(a) that the minimum torque the output of WSCMT is *224 N.m*. Based on the results, it is possible to claim that the controller provides an improvement in the traction characteristic of the wheel. Therefore, the functionality of the developed wheel slip controller is successfully proven for continuous water contaminant.

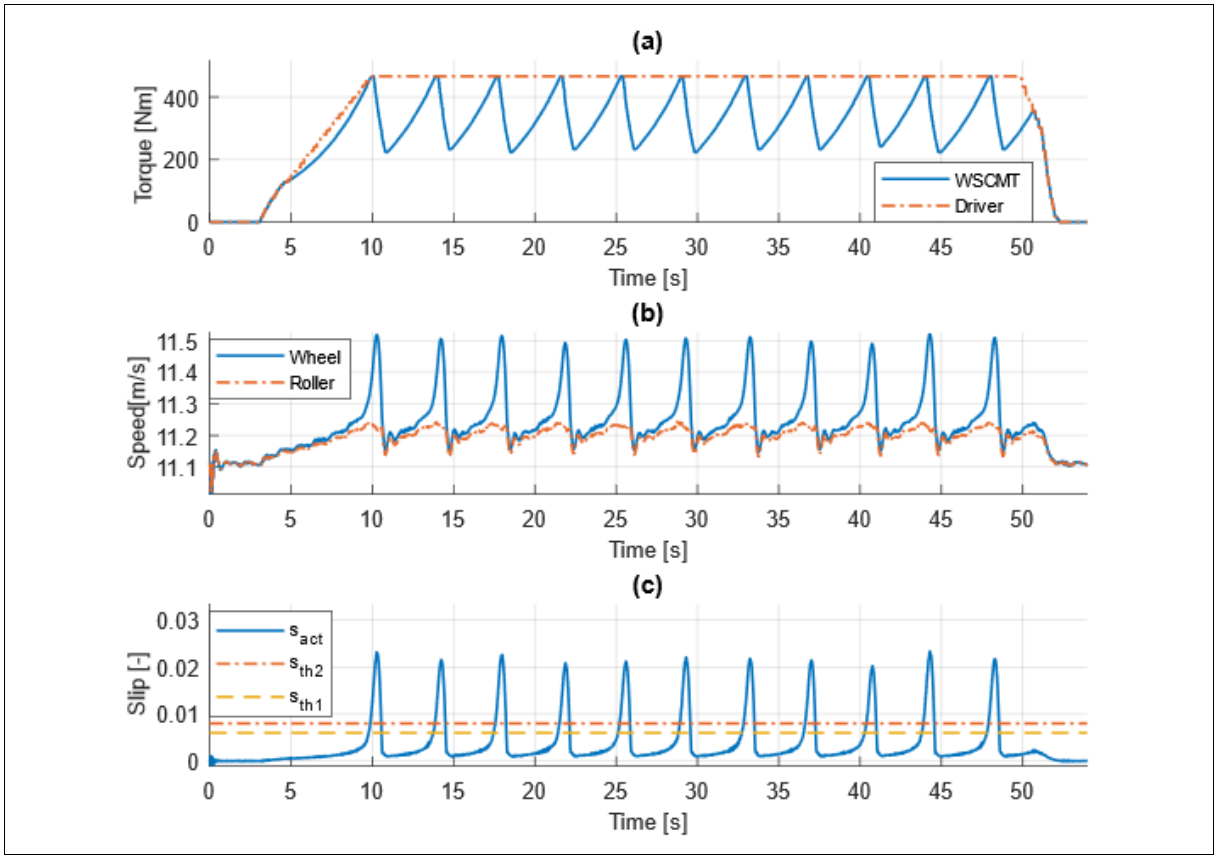

Figure 30. Simulation result of WSCMT performed under the assumption of water contaminated test condition: (a) WSCST and driver torque requests; (b) Wheel and roller speeds; (c) Wheel slip.

The second simulation has been performed for performance evaluation of WSCMT under the assumption of steady grease contaminant existing between the wheel and the roller. The control parameters are set as; $s_{th2}=0.008$, $s_{th1}=0.012$, $A_{inc}=1$ and $A_{dec}=1$. The minimum torque (T_{min}) generated by the WSCMT controller is set as *1%* of nominal torque of the PMSM.

The simulation results of the WSCMT carried out under the assumption of steady grease contaminated test condition is illustrated in Figure 31. The driver and WSCMT torque requests are presented in Figure 31(a). Similar to the previous results, it is seen in Figure 31(b) that the wheel speed increases faster than the roller speed. Hence, the wheel slip increases rapidly, as shown in Figure 31(c). It can be seen from the indicated result; maximum wheel slip of *4%* occurs. When the output of the controller is examined, it is noticed that the minimum torque is *62 N.m*. From the results, it is possible to claim that the controller prevents the wheel from the severe slip effectively. Furthermore, the controller reduces the amount of torque drop slightly.

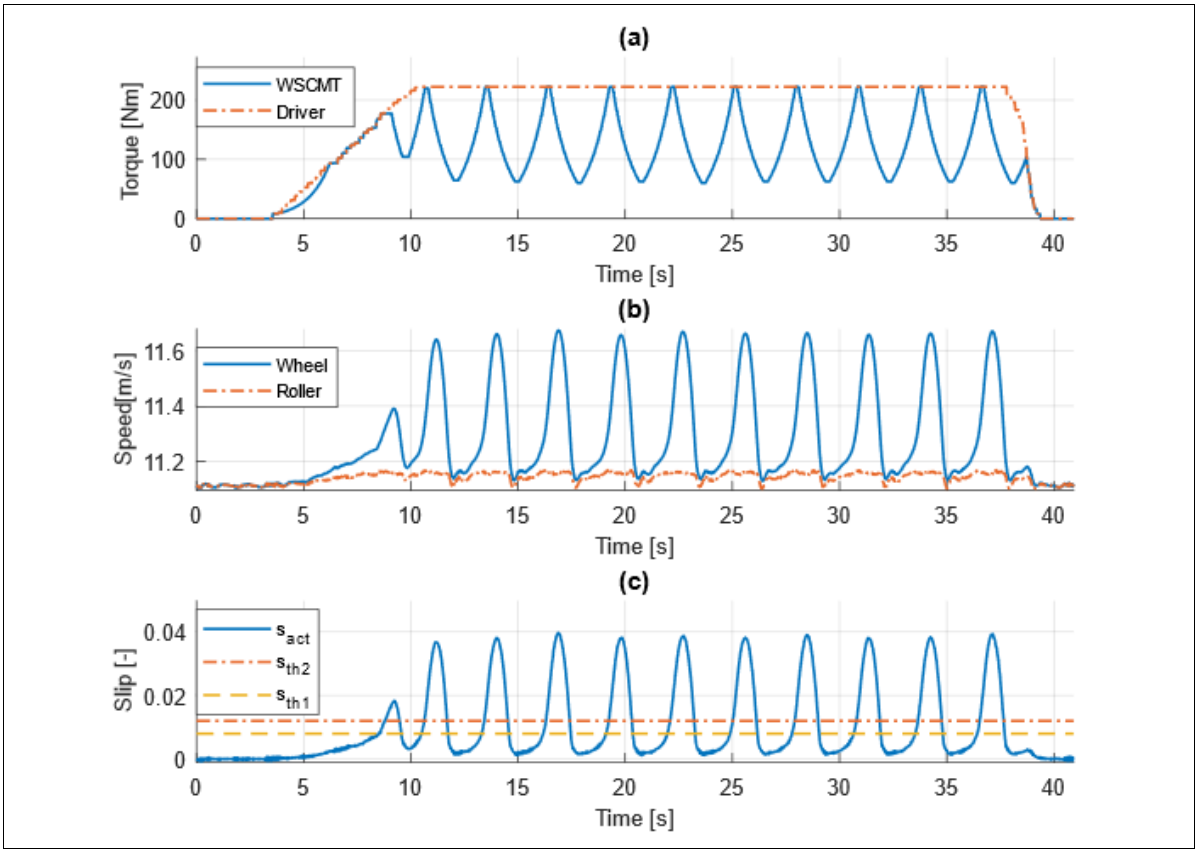

Figure 31. Simulation result of WSCMT performed under the assumption of grease contaminated test condition: (a) WSCST and driver torque requests; (b) Wheel and roller speeds; (c) Wheel slip.

5.2.3 Wheel Slip Control Based on Angular Acceleration of Wheel

To confirm the operation verification of the WSCAA method, we conduct the first simulation under the assumption of water contaminated test condition. The control parameters are selected as; $\alpha_{th}=1$, $A_{inc}=1$ and $A_{dec}=0.5$. The simulation is conducted for two cases of wheel-roller surface conditions which are half-dry and wet. Initially, the contact area is assumed to be half-dry without supplying the additional water. Then, at $t=19.8\ s$, the water is assumed to be continuously sprayed to the contact area.

Figure 32 shows the response of WSCAA performed under the assumption of the continuous water contaminated test condition. The slip curves corresponding to both cases of wheel roller surface conditions are provided in Figure 32(d). It is seen that the CoA reduce from *0.3* to *0.2556*. The driver and WSCAA torque requests are shown in Figure 32(a). Due to the increase in driver torque request and sudden decrease of the adhesion between wheel and roller, the wheel starts to accelerate instantaneously after $t=19.8\ s$ as illustrated in Figure 32(c). When the acceleration of the wheel exceeds the pre-defined threshold value, the torque request of PMSM is lowered to restore adhesion as presented in Figure 32(a). Following this, the wheel slip reaches a peak and deceleration starts. The process repeats until the driver reduces the torque request. The resultant wheel slip is depicted in Figure 32(b). It is observed that during the first cycle, the wheel slip raises to *8.6%*. However, in the next cycles, the peaks of the wheel slip are noticed around *5.9%*. The results have proved that WSCAA can avoid severe wheel slip when the sudden changes occur in adhesion condition.

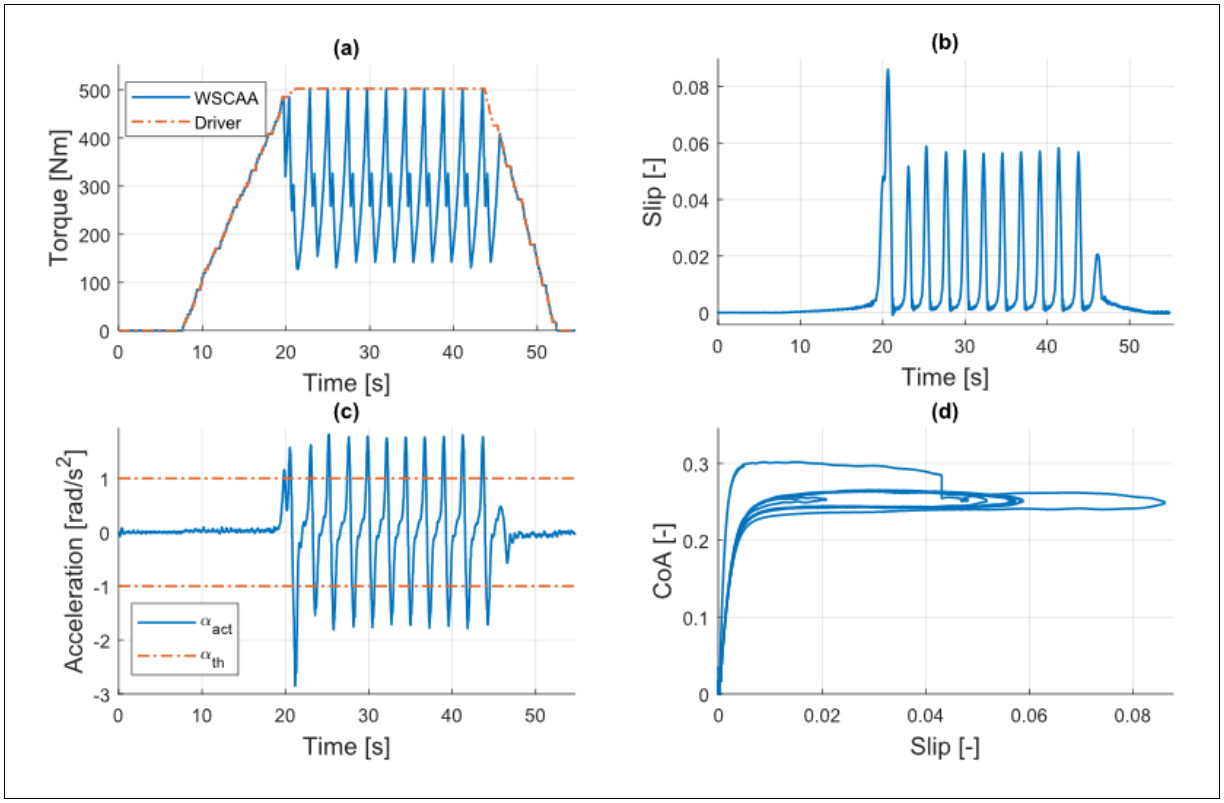

Figure 32. Simulation result of WSCAA performed under the assumption of water contaminated test condition: (a) WSCAA and driver torque requests; (b) Wheel slip; (c) Angular acceleration of wheel and the threshold value; (d) Slip curve.

The second simulation is carried out under the assumption of grease contaminated test condition. The following values of the control parameters are employed; $\alpha_{th}=0.75$, $A_{inc}=1$ and $A_{dec}=0.5$. It is assumed that the contact surface is contaminated with steady grease contaminant (without cleaning effect).

The simulation results of WSCAA performed under the assumption of grease contaminated test condition are illustrated in Figure 33. The driver and WSCAA torque requests are depicted in Figure 33(a). Initially, the driver torque request is zero. At *t=11.8 s*, the driver torque is increased gradually up to *202 N.m* and kept constant at that point. The angular acceleration of the wheel increases proportionally with the torque increment as it is given in Figure 33(c). When the wheel acceleration signal exceeds the threshold value, the WSCAA decreases the torque, as shown in Figure 33(a) to restore the adhesion. The corresponding wheel slip is depicted in Figure 33(b). It is noticed that during the first cycle; the wheel slip raises to

9.9%. In the next cycles, the peaks are observed around *7%*. It is seen that the WSCAA provides a successful wheel slip control during the low adhesion condition.

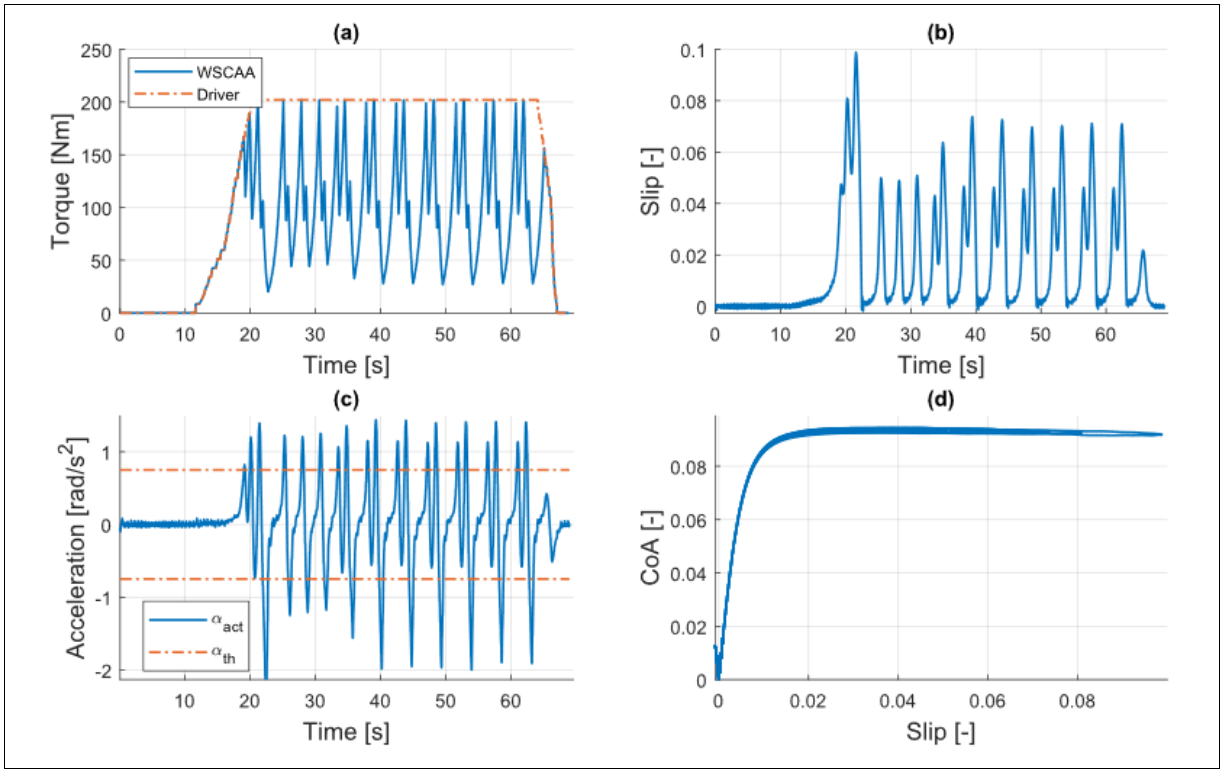

Figure 33. Simulation result of WSCAA performed under the assumption of grease contaminated test condition: (a) WSCAA and driver torque requests; (b) Wheel slip; (c) Angular acceleration of wheel and the threshold value; (d) Slip curve.

5.2.4 PI Wheel Slip Control

The dynamic response of the PI-WSC is tested under half-dry, wet and grease contaminated wheel-roller surface conditions. The friction condition between the wheel and the roller is set relatively high for the performance tests of PI-WSC.

The initial test is conducted under the assumption of the continuous water contaminant existing between the wheel and roller. The control parameters are set as; $s_d=0.01$, $K_p=500$ and $K_i=2000$. The response of the controller is presented in Figure 34. At $t=5.6$ *s*, the driver torque request is increased gradually up to *600 N.m* and kept constant at that level (see Figure 34a). However, the PI-WSC torque request increases up to *524 N.m* since the desired wheel slip ($s_d=0.01$) is reached as illustrated in Figure 34(b). The desired wheel slip corresponds to the peak of the slip curve, as depicted in Figure 34(c). When the path of the wheel slip is analysed,

no significant overshoot is observed. Hence, it is possible to claim that the PI-WSC stabilises the wheel slip at the peak of the slip curve effectively.

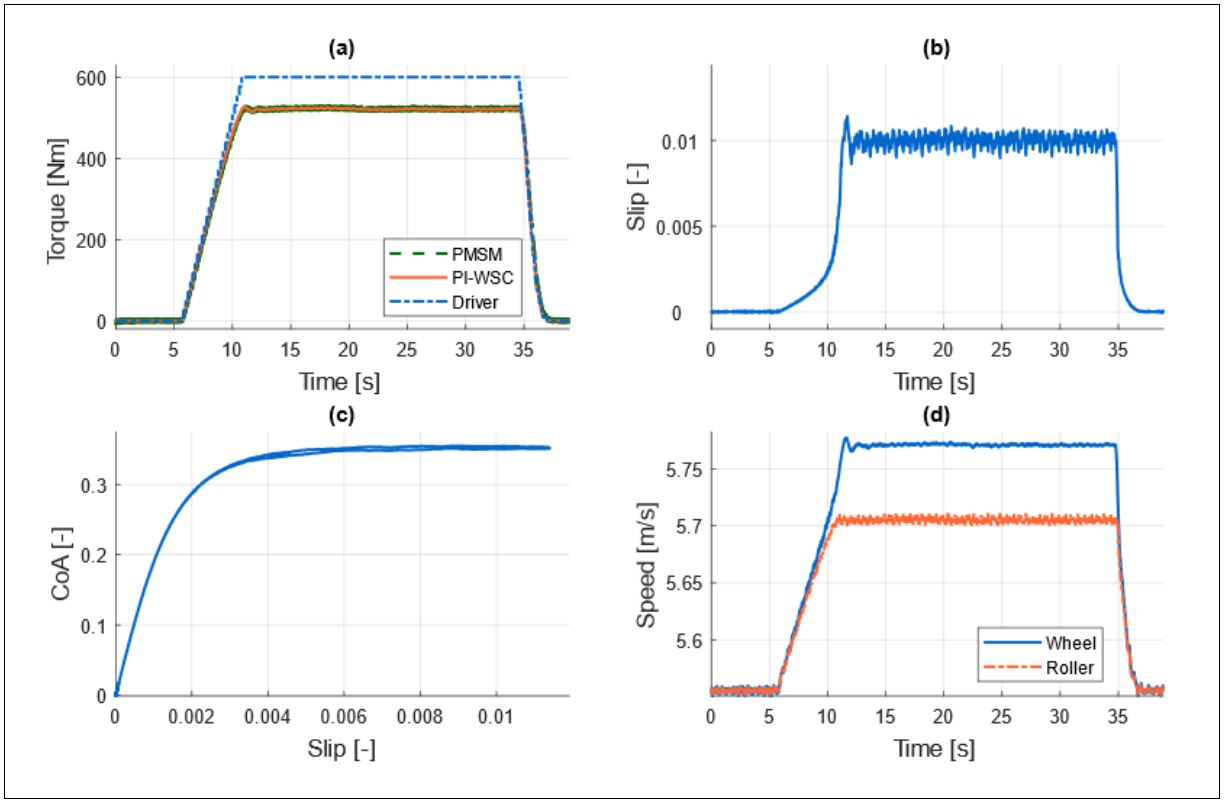

Figure 34. Simulation results of PI-WSC performed under the assumption of water contaminated test condition: (a) PMSM output torque, PI-WSC torque request and driver torque request; (b) Wheel slip; (c) Slip curve; (d) Wheel and roller speeds.

The second test is carried out to test the reaction of the PI-WSC method toward the sudden change of the friction condition. The control parameters are set as; $s_d=0.01$, $K_p=100$ and $K_i=1000$. The simulation results are summarised in Figure 35. Initially, it is assumed that the wheel and roller surfaces are half dry. At $t=4.4$ *s*, the driver torque request is increased gradually up to *620 N.m*. However, the PI-WSC controller permits torque increase up to *570 N.m* due to the desired wheel slip is reached. Then at $t=26.6$ *s*, the water is assumed to be continuously sprayed to the contact area. Because of the sudden change of the friction condition, the wheel slip increases up to *11.5%* as illustrated in Figure 35(b). To prevent the severe wheel slip, PI-WSC generates a new torque request and stabilises the wheel slip at *1%* in a short time. When Figure 35(c) is analysed, it is seen that the controller operates at the peak of the slip curves

successfully for both half-dry and wet surface cases. Furthermore, the controller shows a robust dynamic response to the sudden change in friction conditions.

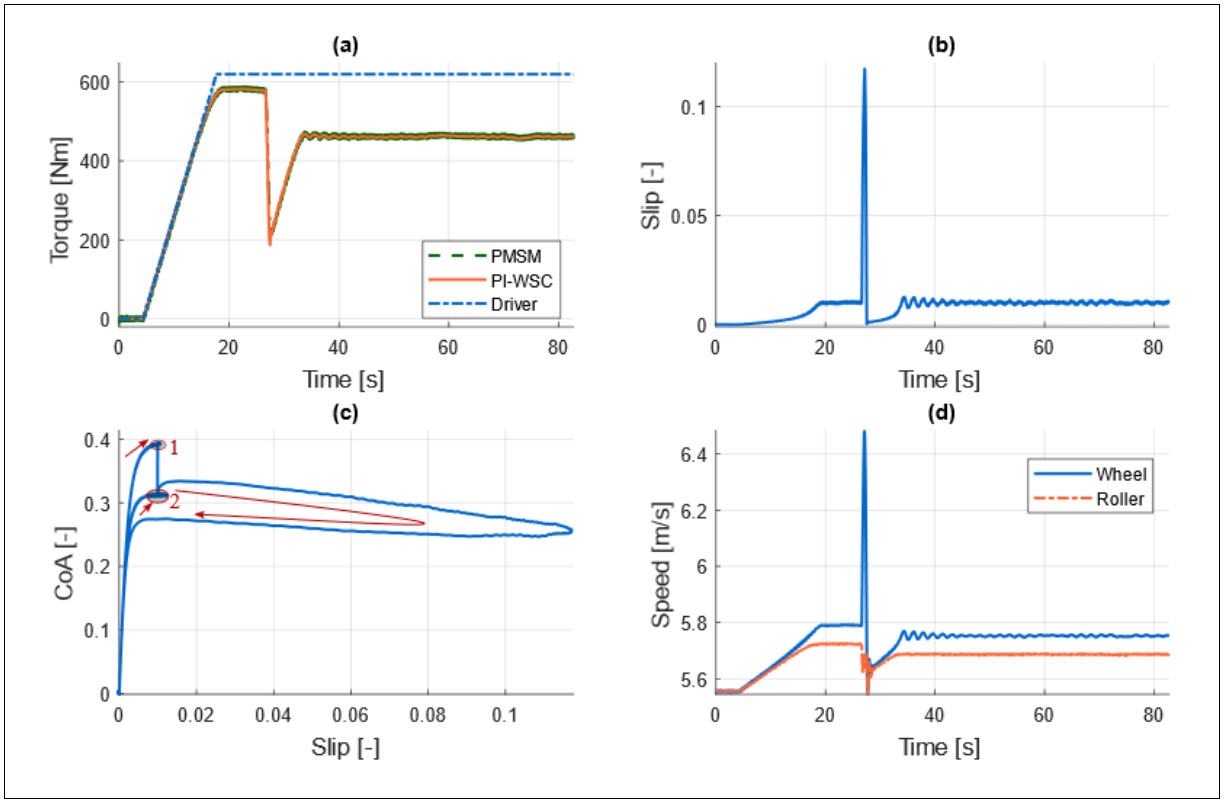

Figure 35. Simulation results of PI-WSC performed under the assumption of half-dry and water contaminated test condition: (a) PMSM output torque, PI-WSC torque request and driver torque request; (b) Wheel slip; (c) Slip curve; (d) Wheel and roller speeds.

The last simulation is conducted with the assumption of the steady grease contaminated test conditions. The control parameters are set as; $s_d=0.02$, $K_p=200$ and $K_i=1000$. The simulation results are presented in Figure 36. The driver torque request, PI-WSC torque request and PMSM torque response are shown in Figure 36(a). The speed responses of the wheel and roller are illustrated in Figure 36(d). It is observed that the controller effectively stabilises the wheel slip at the desired level with a slight overshoot (see Figure 36b). Furthermore, the desired level corresponds to the peak of the slip curve (see Figure 36c). Considering results, we can claim that the controller has an effective dynamic response.

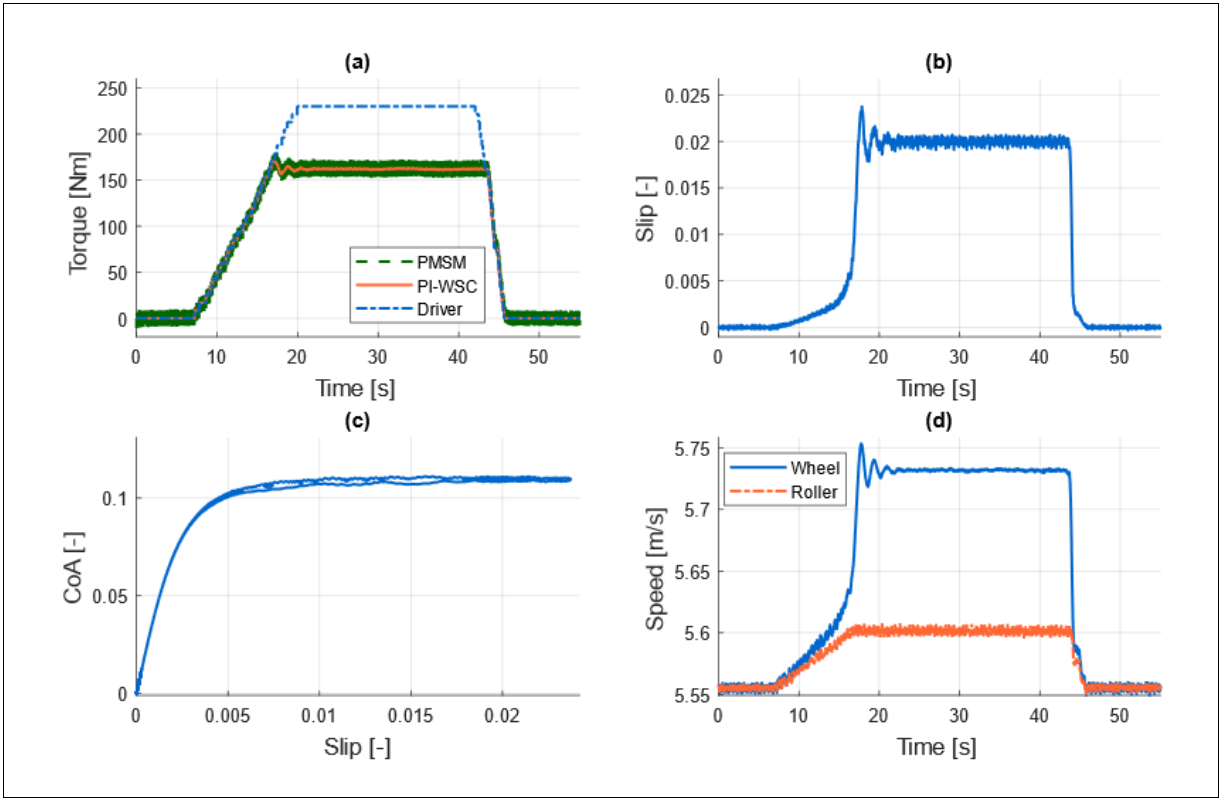

Figure 36. Simulation results of PI-WSC performed under the assumption of steady grease contaminated test condition: (a) PMSM output torque, PI-WSC torque request and driver torque request; (b) Wheel slip; (c) Slip curve; (d) Wheel and roller speeds.

5.2.5 Sliding Mode Wheel Slip Control

To verify the effectiveness of the developed control method, we performed the initial tests using the validated numeric model. The following values are selected for the control parameters; *D=10, K=1 and* s_d*=0.02.*

The simulation results of SM-WSC performed under the assumption of water contaminated test condition can be seen in Figure 37. Two phases of the adhesion scenario are selected for the simulation of water contamination. In the first phase, it is assumed that the contact zone is wet, without spraying additional water onto the contact. In the second phase, the water is continuously sprayed onto the contact area. The driver torque request is increased up to a point and kept constant, as presented in Figure 37(a). At *t=29 s*, the adhesion between the wheel and the roller drops from *0.28* to *0.22*, as shown in Figure 37(c) due to the addition of water. The sudden drop in adhesion conditions results in a sudden increase in the wheel speed, while the increase in the roller speed is relatively low, as depicted in Figure 37(d). In other

words, the wheel starts to slide. The SM-WSC contributes to a reduction in the driver torque request, as depicted in Figure 37(a) and stabilises the wheel slip at *2%*, which can be seen in Figure 37(b). The maximum overshoot displayed in the wheel slip is about *5.1%*, which is a relatively low value. The indicated results demonstrate the functionality of the proposed strategy.

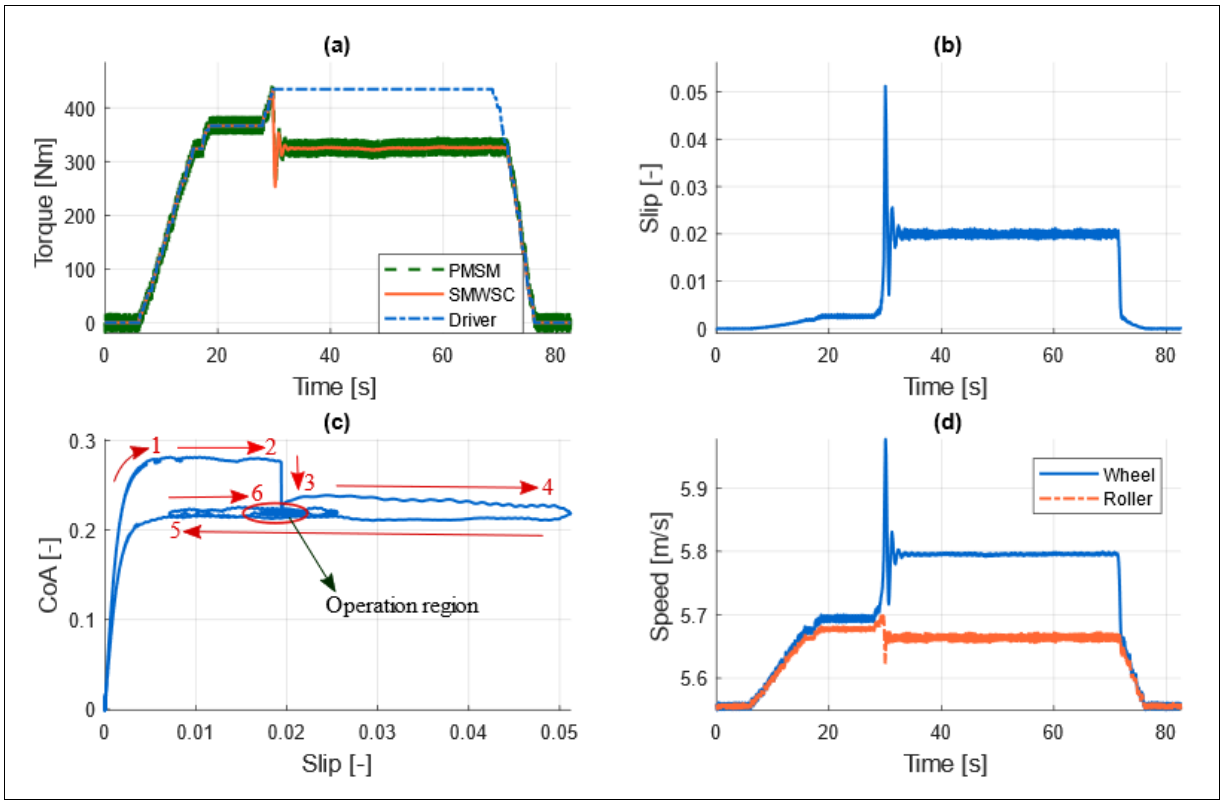

Figure 37. Simulation results of SM-WSC performed under the assumption of water contaminated test condition: (a) PMSM output torque, SM-WSC torque request and driver torque request; (b) Wheel slip; (c) Slip curve; (d) Wheel and roller speeds.

Next, Figure 38 illustrates the response of the developed algorithm when the adhesion condition between wheel and roller is selected for grease contaminated case. In this case, it is assumed that the grease on the contact surface is steady, as illustrated in Figure 38(c). The driver torque request is gradually increased after *t=5 s*, and kept constant after a point, as seen in Figure 38(a). From Figure 38(d), it can be seen that the wheel speed increases, the roller speed increases proportionally, as well. At *t=25 s*, the wheel slip increases beyond the desired value. After this point, the controller begins to step in by reducing the driving torque. It is noticed that the actual

wheel slip well tracks the desired wheel slip (*2%*) without any noticeable tracking error, as presented in Figure 38(b). The noise displayed in the results is due to the PWM inverter.

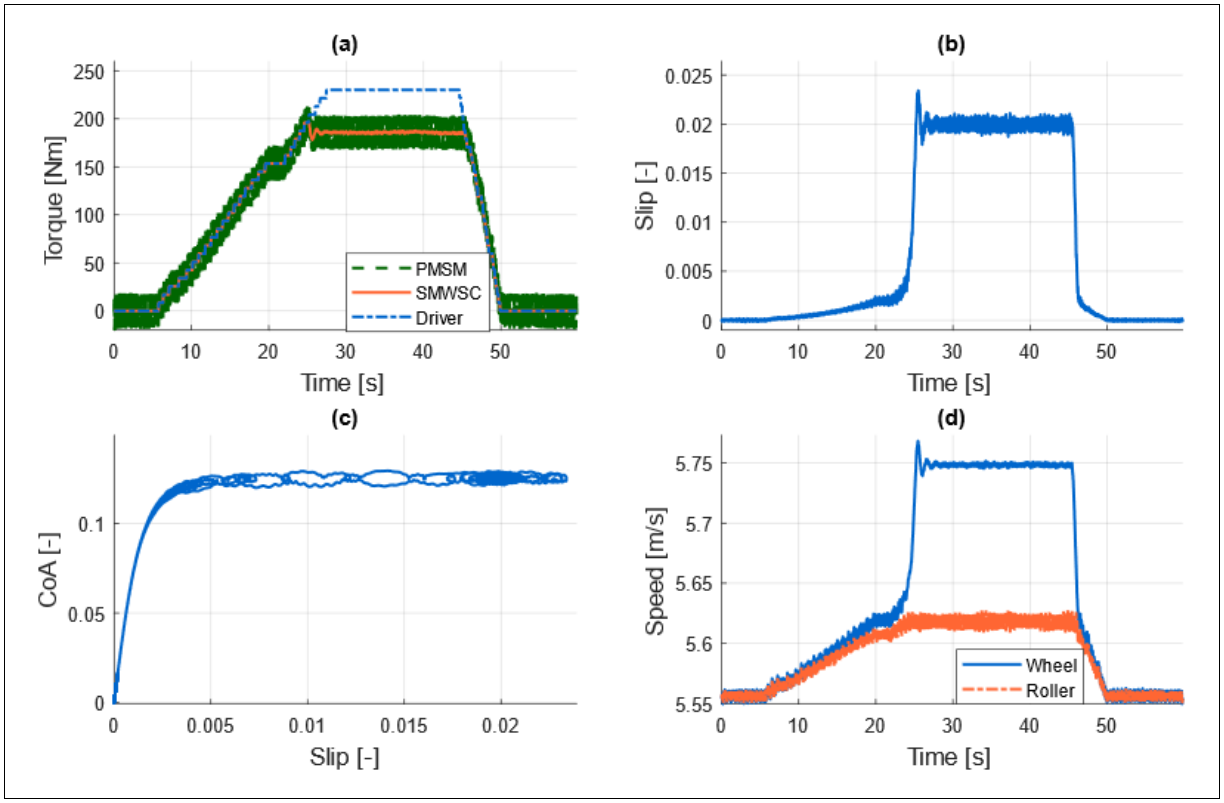

Figure 38. Simulation results of SM-WSC performed under the assumption of steady grease contaminated test condition: (a) PMSM output torque, SM-WSC torque request and driver torque request; (b) Wheel slip; (c) Slip curve; (d) Wheel and roller speeds.

5.3 Experimental Results

In the previous section, the performances of the control algorithms are verified via numerical simulations. In this section, tests are carried out with the experimental tram wheel roller rig (see section 3.1) to investigate the response of the algorithm under real operating conditions. The control parameters of the algorithms are set identical with ones used in numerical tests. Experiments are performed under four wheel-roller contact conditions, which are half-dry, wet, greasy and grease&water. During the trials with the water contaminant, water is sprayed to the contact zone continuously. Whereas, grease is placed on the contact area manually and renewed whenever cleaning effect is monitored.

The sampling rate of data logger that is connected to the test stand is *200 Hz*. However, the control action of the anti-slip algorithm is limited with *25 Hz* to gain time for data processing. The initial peripheral speed of the roller is selected as *5.56 m/s*, which corresponds to *20 km/h* for a tram vehicle. The air spring provides no air pressure to obtain the higher wheel slip with lower traction torque. Whereas, the average of the normal force is measured as *4250 N*, due to weights of the wheel, air spring and swinging arm.

5.3.1 Wheel Slip Control Based on a Single Threshold

Figure 39 shows the experimental results of WSCST performed under water contaminated test condition. The driver torque request, which can be seen in Figure 39(a), is identical to the driver torque request in the simulation (see Figure 28a). The wheel and roller speeds are illustrated in Figure 39(b). The resultant wheel slip is provided in Figure 39(c). The controller reduces the torque request whenever the wheel slip exceeds the defined threshold value. Hence, the cyclic wheel slip control is displayed. It is noticed that the magnitude of the wheel slip cycles varies due to uncertainties and disturbances. We can claim that the controller prevents the severe wheel slip effectively where maximum wheel slip of *8.1%* is seen. Additionally, the findings substantiate the simulation results that are presented in section 5.2.1 (see Figure 28).

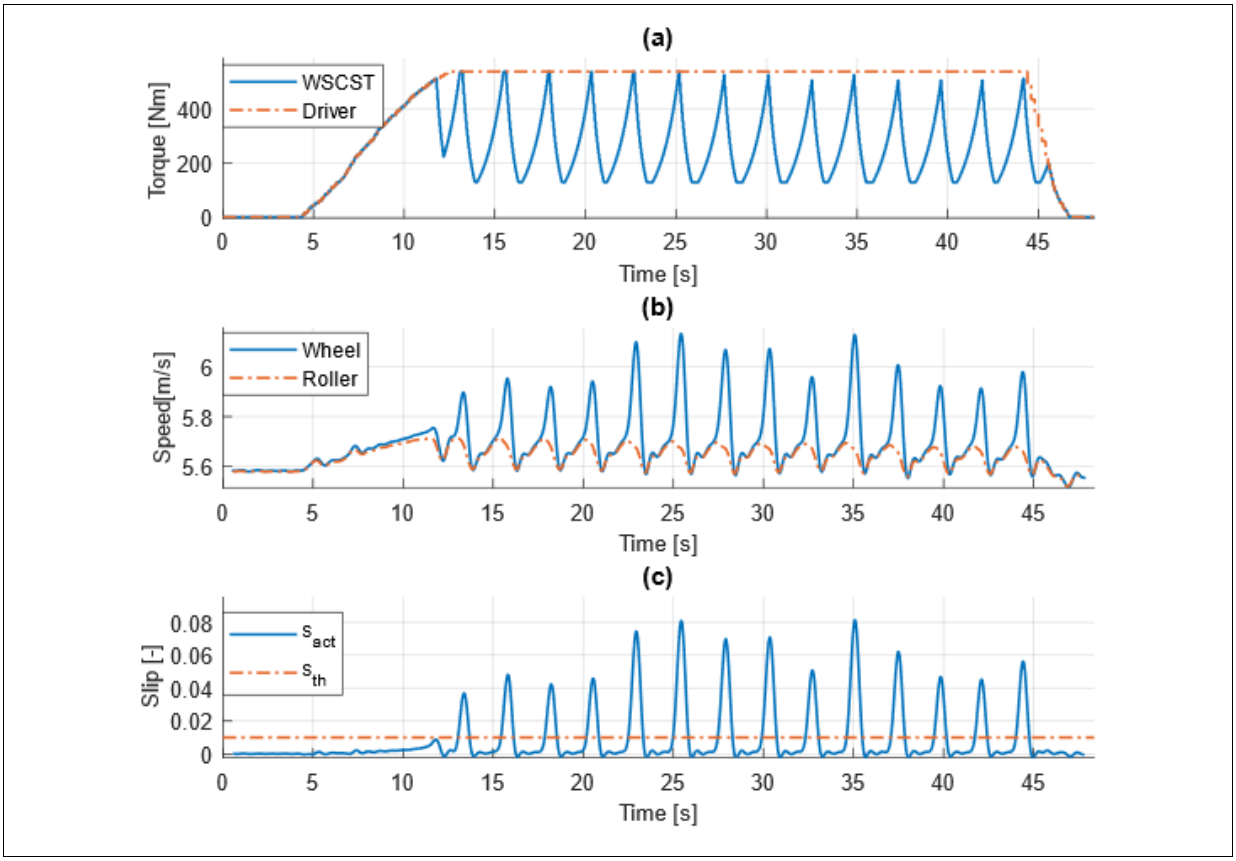

Figure 39. Experimental result of WSCST performed under water contaminated test condition: (a) WSCST and driver torque requests; (b) Wheel and roller speeds; (c) Wheel slip.

The experimental test results of WSCST under the steady grease contaminated test condition are shown in Figure 40. The driver torque requests used in experiment and simulation (see Figure 29a) are identical. The torque regulation of the controller is illustrated in Figure 40(a). Similar to the simulation result; initially, the WSCST control torque increases slower than the driver torque request due to the setting of T_{min} (*1%* of nominal PMSM torque) and A_{inc}. The speed response of the wheel and the roller are presented in Figure 40(b). The resultant wheel slip is provided in Figure 40(c). The results obtained under the grease contaminant is quite similar to findings under the water contaminant. The wheel slip is suppressed successfully with a maximum of *4%*. Hence, it can be claimed that the controller provides an effective performance. Furthermore, the experimental results match reasonably well with the simulation results that are presented in section 5.2.1.

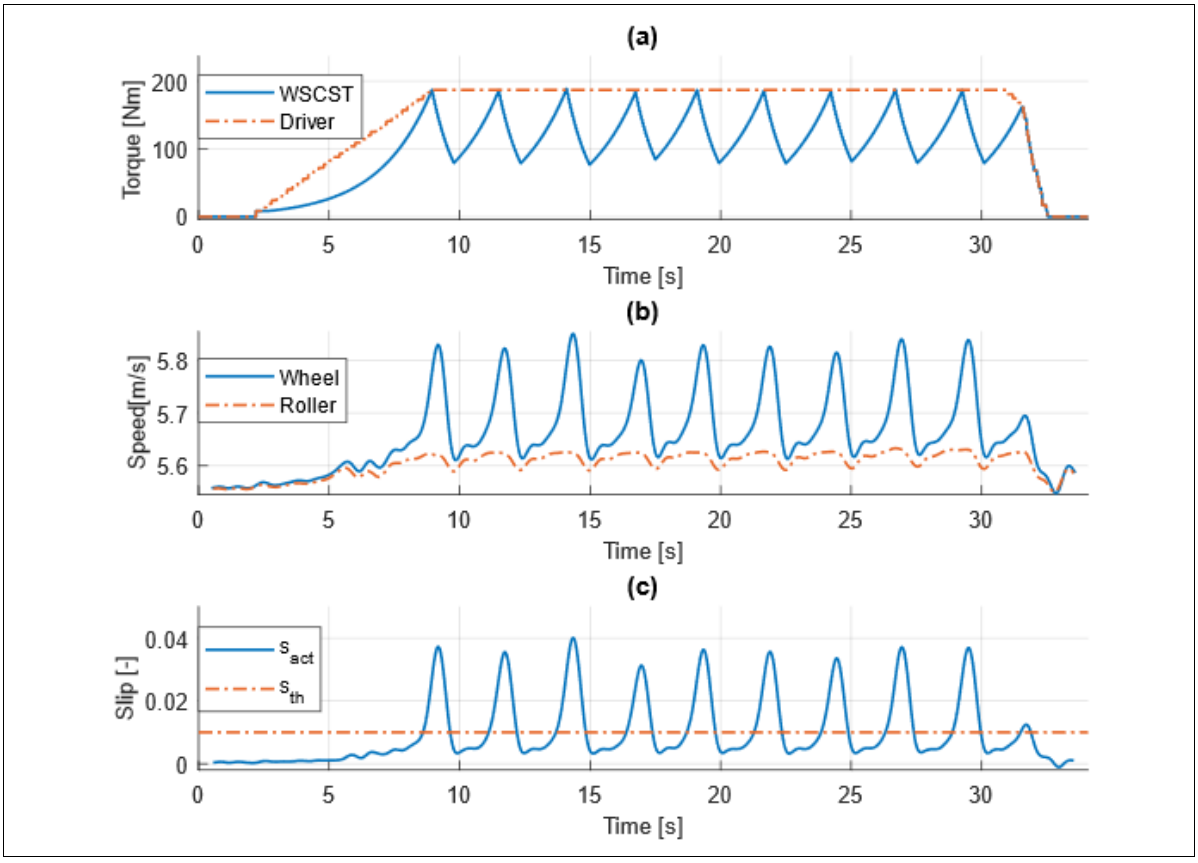

Figure 40. Experimental result of WSCST performed under grease contaminated test condition: (a) WSCST and driver torque requests; (b) Wheel and roller speeds; (c) Wheel slip.

5.3.2 Wheel Slip Control Based on Multiple Thresholds

The performance of the WSCMT is verified with the help of the experimental tram wheel roller rig. The initial roller speed is set as *11.2 m/s* that approximately corresponds to *40 km/h* for a tram vehicle.

Here, Figure 41 shows the response of the WSCMT carried out under the continuous water contaminated test condition. When the driver torque increases, correspondingly, WSCMT torque increases, as shown in Figure 41(a). Whereas, closer inspection of the figure shows WSCMT torque request increases slightly slower due to the selection of A_{inc} control parameter. The speed responses of the wheel and the roller is illustrated in Figure 41(b). As it is expected, the wheel speed increases much faster when the tractive effort exceeds the adhesion limits. Hence, the sudden wheel slip is seen as presented in Figure 41(c). The proposed algorithm appears to deliver a satisfactory performance since the strategy provides a cyclic control of

wheel slip where the peaks are noticed between *1.3-2%*. Besides, the controller prevents the wheel from the excessive torque drops, which reduce traction performance.

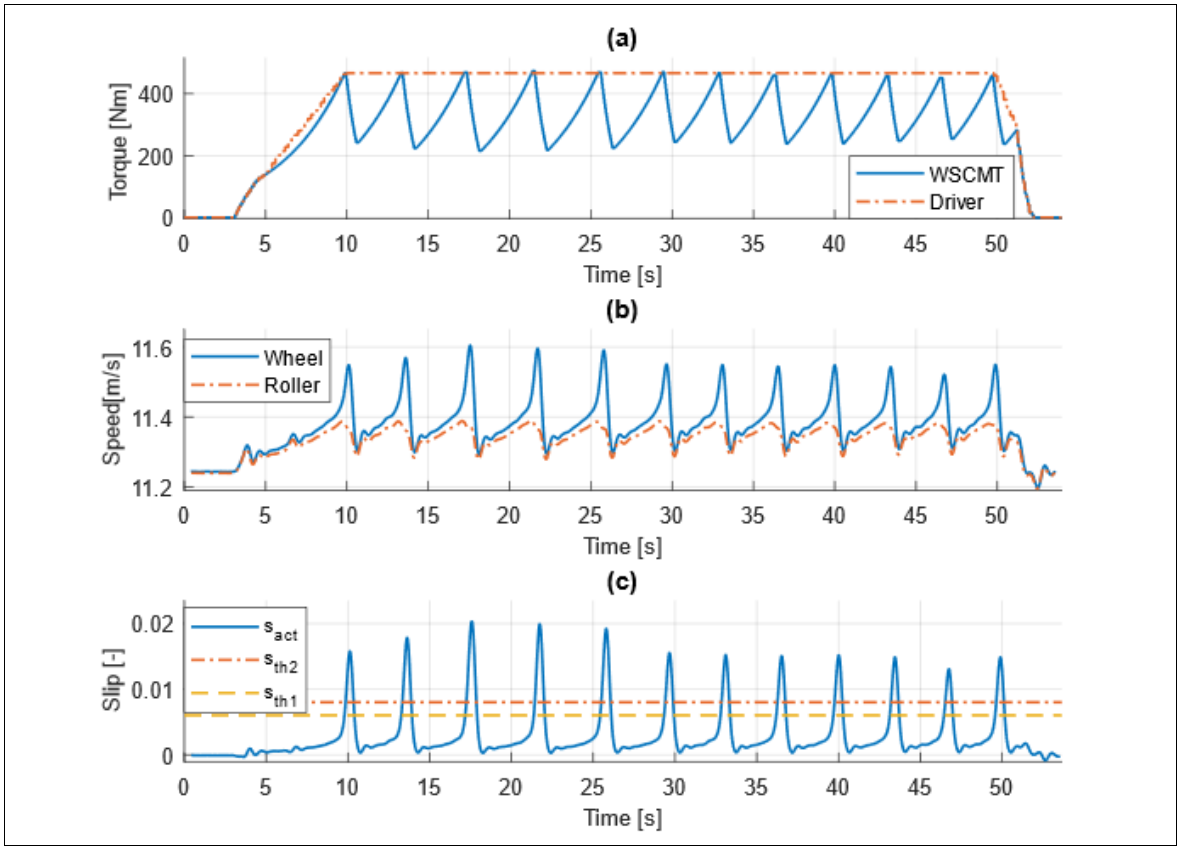

Figure 41. The experiment result of WSCMT performed under water contaminated test condition: (a) WSCMT and driver torque requests; (b) Wheel and roller speeds; (c) Wheel slip.

The second experiment is conducted under the steady grease contaminated test condition. The test is aimed to investigate the performance of the controller under the deficient adhesion condition. The details of the test results are provided in Figure 42. In Figure 42(a), the driver and controller torque requests are shown. It is apparent from the figure that initially, WSCMT torque request increases slower. The speed responses of the wheel and the roller are illustrated in Figure 42(b). The resultant wheel slip is indicated in Figure 42(c). When the results are analysed, one can figure out that the controller suppresses the wheel slip effectively where the peak of the cycles are found to be around *4.4%*.

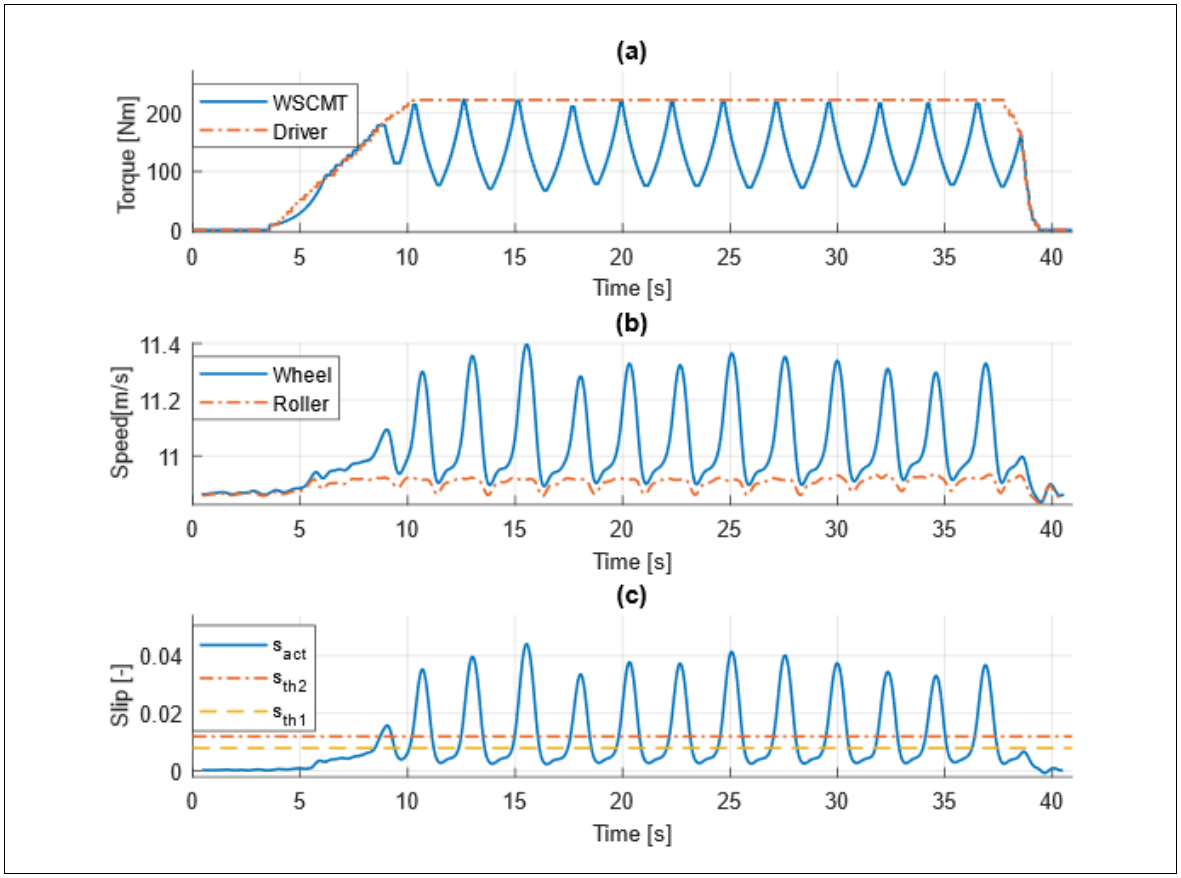

Figure 42. Experimental results of WSCMT performed under grease contaminated test condition: (a) WSCMT and driver torque requests; (b) Wheel and roller speeds; (b) Wheel slip.

5.3.3 Wheel Slip Control Based on Angular Acceleration of Wheel

To confirm the operation of the WSCAA, we conducted the first experimental test under water contaminated test condition. Initially, the wheel-roller contact zone is wet; however, no additional water is supplied. At time *t=19.8 s*, the water is sprayed to the contact area continuously. The application of additional water reduces the adhesion, as depicted in Figure 43(d). Figure 43 summarises test results performed on the experimental test stand. The driver torque request is increased progressively up to *503 N.m*, as provided in Figure 43(a). Due to the torque increase and fall in adhesion, the wheel starts to accelerate, as illustrated in Figure 43(c). When the angular acceleration of the wheel exceeds the threshold value, the WSCAA reduces the torque, as shown in Figure 43(a). The wheel slip control performance of WSCAA is depicted in Figure 43(b). During the first five cycles of the control process, the magnitude of the peak of the wheel slip tends to increase while in the next cycles, the magnitude of the peak of wheel slip

reduces gradually. A maximum wheel slip of *6.7%* is observed during the test. It is found that the controller has an effective wheel slip control performance in the given experimental results. Furthermore, the experiment results are consistent with the simulation results presented in Figure 32.

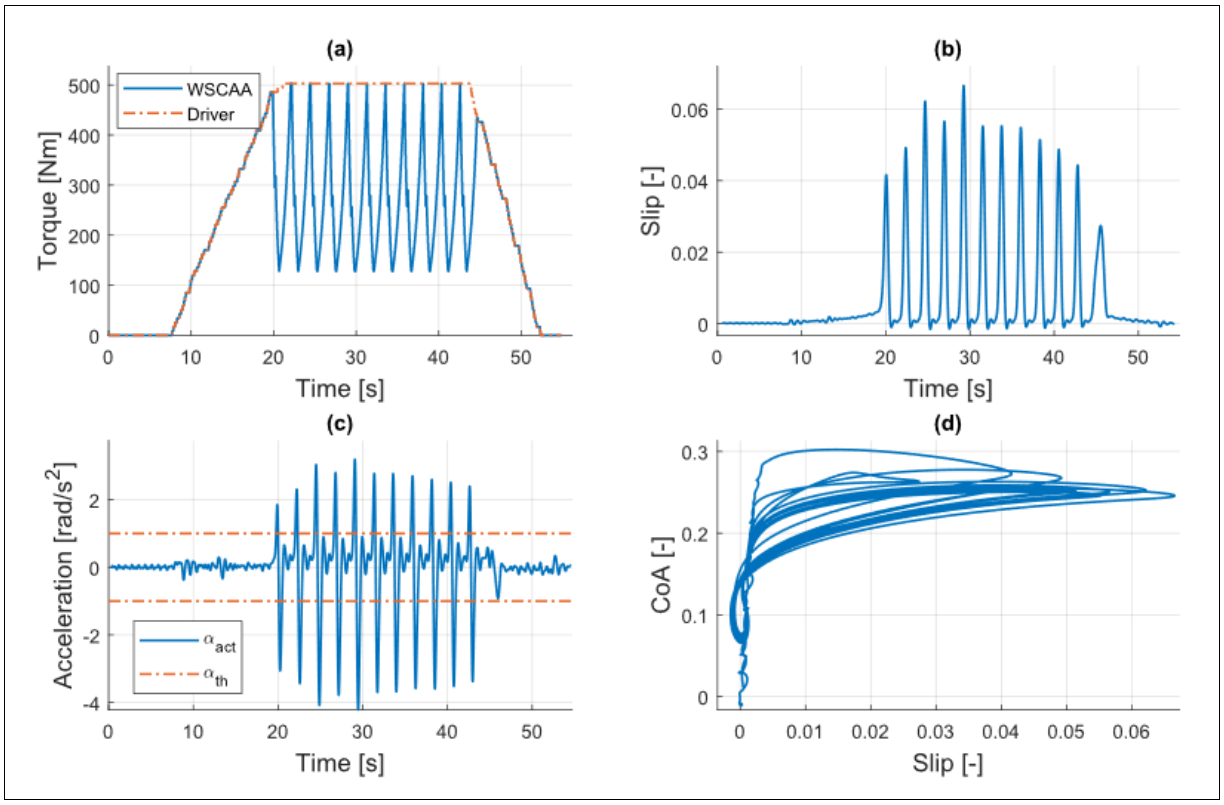

Figure 43. Experimental result of WSCAA performed under water contaminated test condition: (a) WSCAA and driver torque requests; (b) Wheel slip; (c) Angular acceleration of wheel and the threshold value; (d) Slip curve.

Next, Figure 44 shows the responses of the WSCAA performed under water contaminated test condition and the different value of threshold (α_{th}). By analysing the path of wheel slip, it can be seen that the larger α_{th} causes in higher wheel slip. Moreover, the low value of α_{th} causes the frequent drop of the drive torque, due to the noise component existing in the acceleration signal. Thus, for practical applications, the threshold value must be selected carefully for optimal control performance.

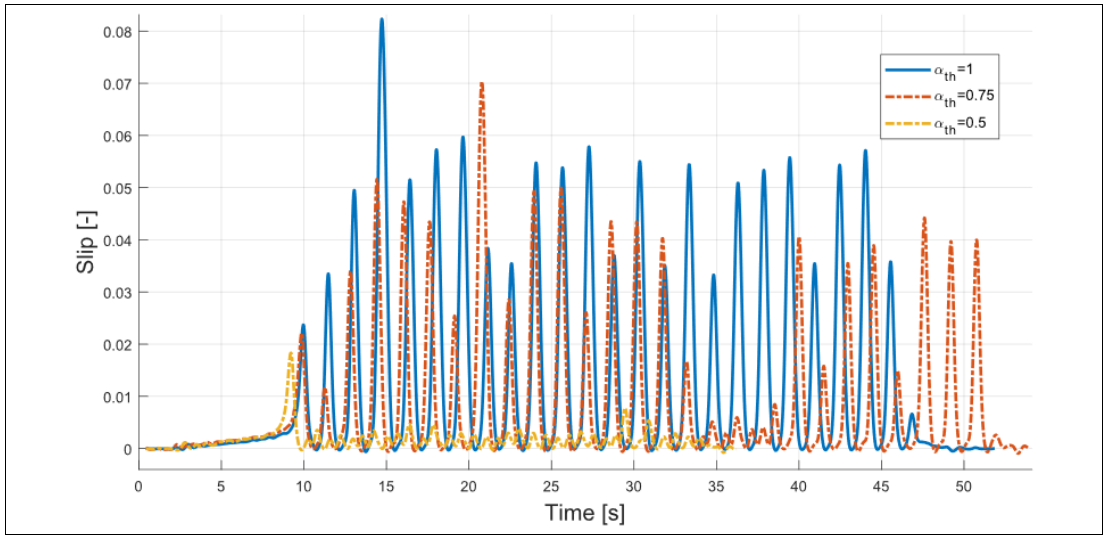

Figure 44. The effect of the threshold value (α_{th}) on wheel slip under water contaminated test condition.

A comparison of different deceleration rate control parameter (A_{dec}) is carried out under the same conditions is illustrated in Figure 45. It is seen when the value of A_{dec} is increased, the magnitude of the peak point of the wheel slip is increased. Moreover, when A_{dec} is selected even higher, it is noticed that the WSCAA is not able to avoid the severe wheel slip. Besides, setting the A_{dec} to lower values reduce the traction performance due to the excessive torque drops. Hence, optimum parameters of A_{dec} is required for an efficient wheel slip control and better adhesion utilisation.

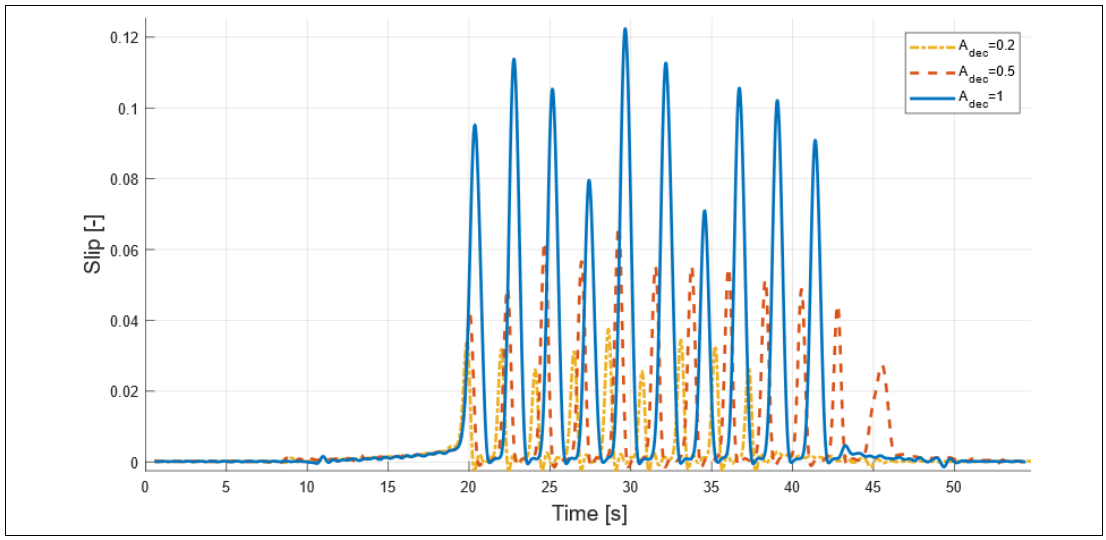

Figure 45. The effect of deceleration rate (A_{dec}) on wheel slip under water contaminated test condition.

The experimental results of WSCAA conducted under the steady grease contaminated wheel-roller surface conditions are presented in Figure 46. The WSCAA gives a similar response to that of traction under the water contaminant. The presence of the grease reduces the adhesion to a deficient value, as depicted in Figure 46(d). The driver and WSCAA torque request are given in Figure 46(a), respectively. The torque regulation is provided with the help of the wheel slip detection signal that is obtained from Figure 46(c). The corresponding wheel slip control performance under grease contaminant is indicated in Figure 46(b). Due to the system delay, a sudden wheel slip occurs at the first cycle, and then, the controller reduces the wheel slip to lower values in the next cycles. The peaks of the wheel slip cycles are observed around *5.9%*. These findings validate the usefulness of WSCAA as a wheel slip control strategy. Moreover, the experimental results are in good agreement with the simulation results.

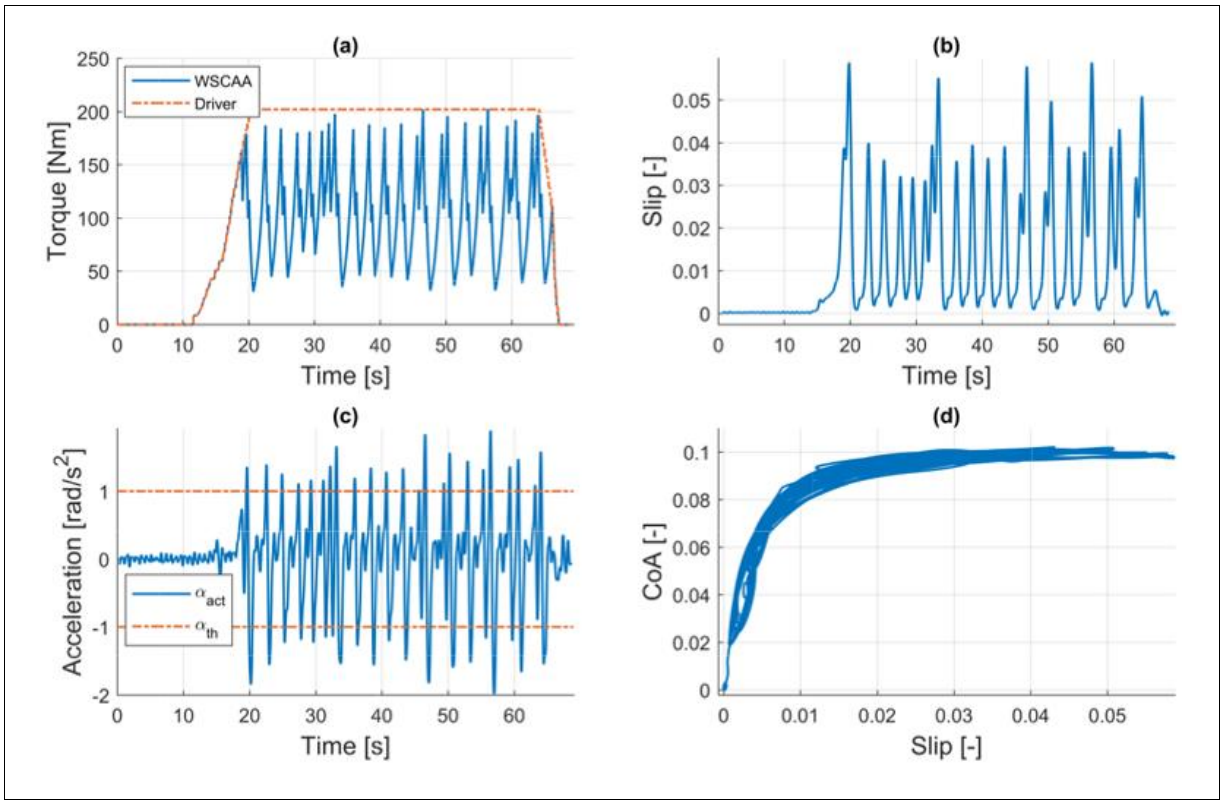

Figure 46. Experimental result of WSCAA performed under grease contaminated test condition: (a) WSCAA and driver torque requests; (b) Wheel slip; (c) Angular acceleration of wheel and the threshold value; (d) Slip curve.

5.3.4 PI Wheel Slip Control

The operation of the PI-WSC is verified initially under the continuous water contaminated test conditions. Figure 47 illustrates the response of the controller. The driver torque request is increased gradually from zero to *600 N.m* at *t=5.6 s*, as shown in Figure 47(a). However, PI-WSC permits the torque increase until *554.7 N.m* since the desired wheel slip is reached as given in Figure 47(b). Closer inspection to Figure 47(c) shows that the controller operates at the peak of the slip curve. Surprisingly, a constant difference between the wheel and roller speeds is observed in Figure 47(d), even at free rolling. This difference causes an offset in the calculated wheel slip value. However, the action of the controller is not affected. Hence, the results confirm the effectiveness of the controller under the continuous water contaminated surface condition.

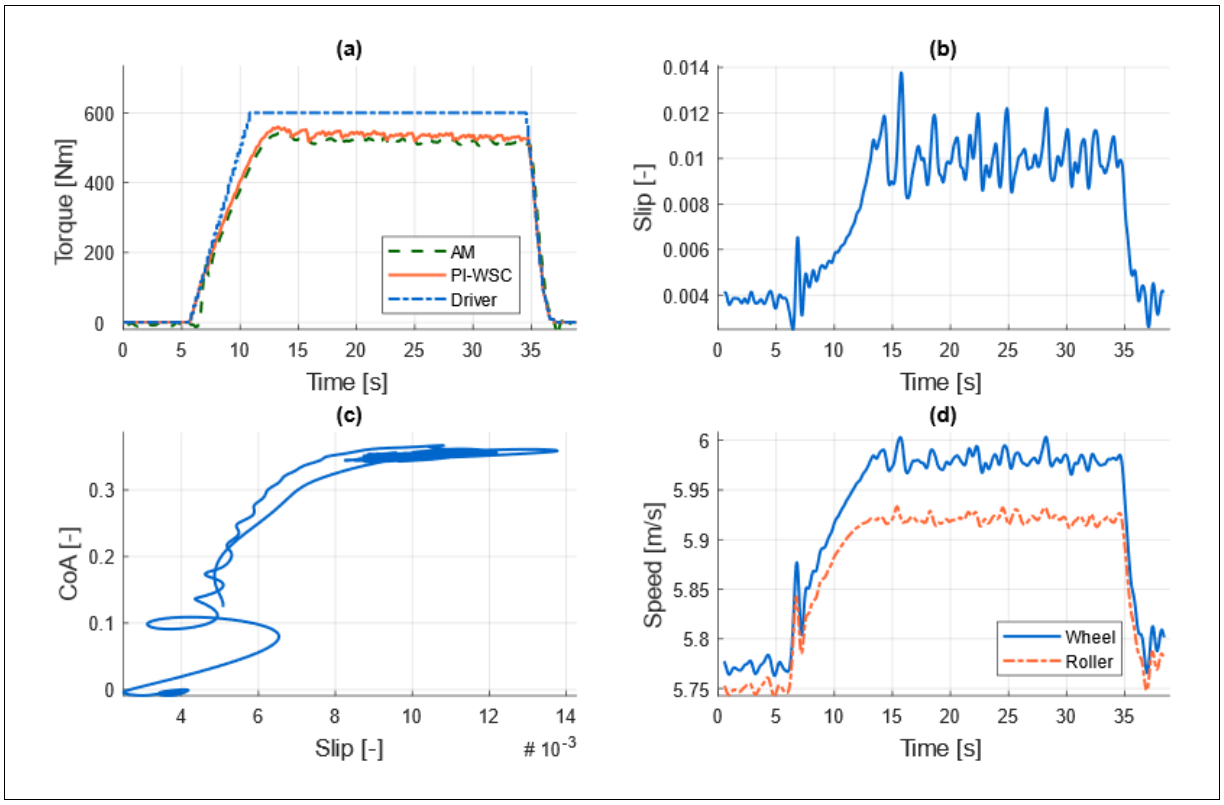

Figure 47. Experimental results of PI-WSC performed under water contaminated test condition: (a) AM output torque, PI-WSC torque request and driver torque request; (b) Wheel slip; (c) Slip curve; (d) Wheel and roller speeds.

The second experimental test is carried out to examine the dynamic response of the controller to the sudden decrease in the friction condition. Hence, initially the controller is

operated under half dry test condition, then continuous water is sprayed to contact area to reduce the friction condition. The results are presented in Figure 48. It is seen in Figure 48(b); the controller stabilises the wheel slip effectively at the desired level for the half-dry case. The first operating point of the controller, which correspond to the peak of the slip curve, is shown in Figure 48(c). When the water is sprayed, the friction condition drops and *11.7%* of wheel slip is observed. The controller provides a successful control since the recovery from the unstable side of the slip curve to the stable side of the slip curve takes in an instant. The PI-WSC stabilises the wheel slip at *1%* (second operating point) which corresponds to the peak of the slip curve for the water contaminated test condition. Similar to the previous experiment, a constant offset is seen in speed measurements, as depicted in Figure 48(d).

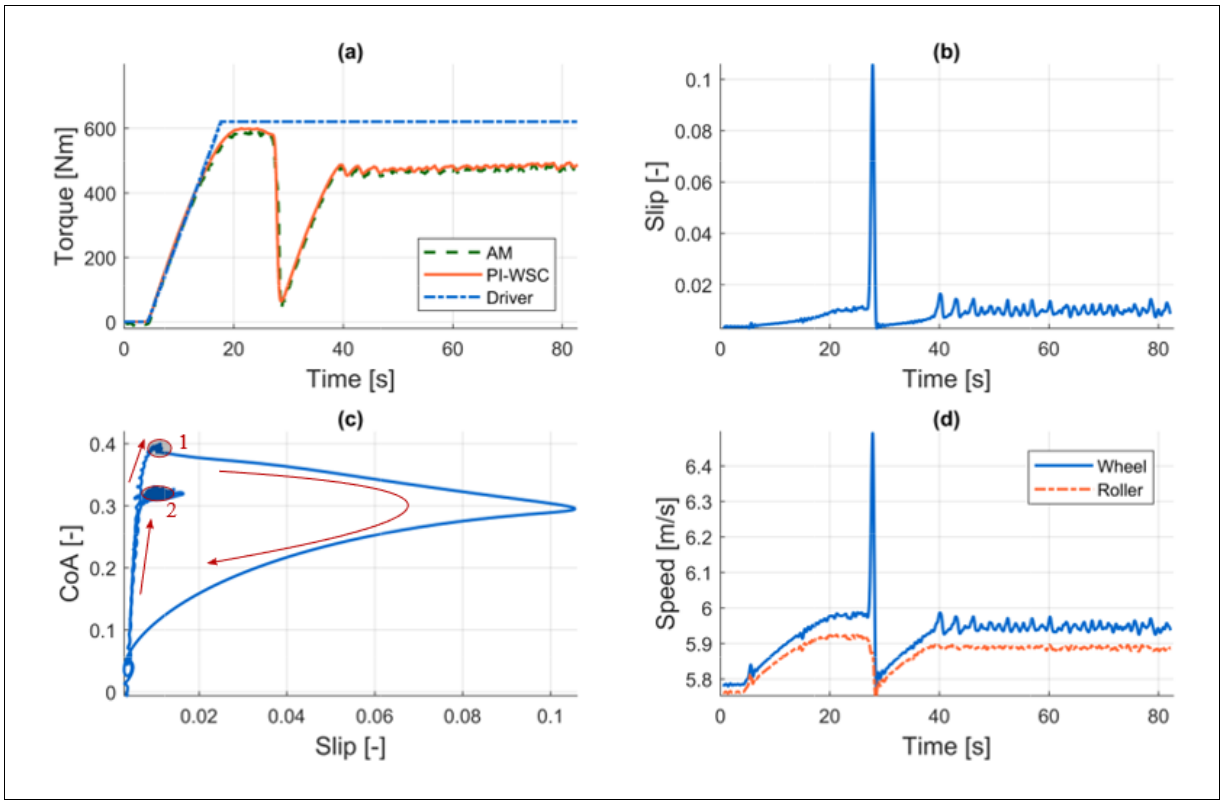

Figure 48. Experimental results of PI-WSC performed under the half-dry and water contaminated test condition: (a) AM output torque, PI-WSC torque request and driver torque request; (b) Wheel slip; (c) Slip curve; (d) Wheel and roller speeds.

5.3.5 Sliding Mode Wheel Slip Control

The control parameters and initial speed for the SM-WSC are selected as in the numerical model. Experimental tests are conducted for several cases of wheel-roller surface conditions.

The experimental results of the proposed algorithm performed under water contaminated wheel-roller surface conditions are presented in depth in Figure 49. The results of the experimental test are similar to the results obtained from the simulation in Figure 37. The available adhesion between wheel and roller is high until *t=29 s* as illustrated in Figure 49(c) since the wheel and roller contact surface is half dry. The driver torque request is increased gradually up to *434 N.m*, as shown in Figure 49(a). After *t=29 s*, water is sprayed onto the contact area. The maximum available adhesion decreases from *0.275* to *0.22*. This rapid drop in adhesion conditions results in a sudden increase in wheel speed while roller speed increases slower, relatively, as depicted in Figure 49(d). The resultant wheel slip is provided in Figure 49(b). The SM-WSC is activated right after the wheel slip value reaches beyond the desired amount (*2%*). The controller reduces the motor torque, as indicated in Figure 49(a), and the wheel slip is stabilised at *2%*. A maximum wheel slip of *7%* is observed during this test. Based on the obtained results, it is possible to claim that the controller has a robust response to the sudden change in adhesion conditions. Furthermore, when Figure 49(c) is analysed, it can be seen that the CoA is controlled slightly below the maximum value. This behaviour is due to the selection of the reference wheel slip value.

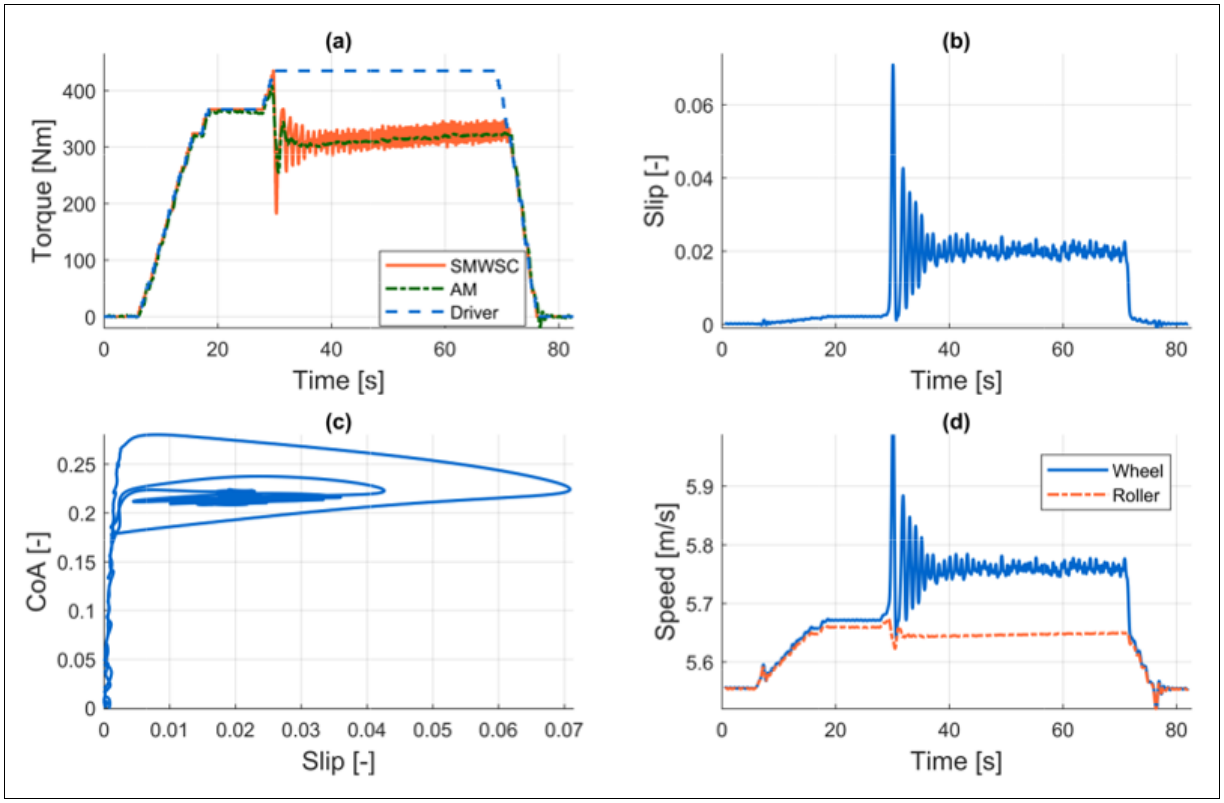

Figure 49. Experimental results of SM-WSC performed under water contaminated test condition: (a) SM-WSC torque request, AM output torque and driver torque request; (b) Wheel slip; (c) Slip curve; (d) Wheel and roller speeds.

Figure 50 shows the experimental results of the proposed algorithm performed under the steady grease contaminated test condition. The available adhesion is relatively low due to the presence of the grease contaminant in the environment (see Figure 50(c)). Figure 50(a) shows the SM-WSC torque request, the output torque response of AM and the driver torque request, respectively. The wheel speed and roller speeds are illustrated in Figure 50(d). It should be noted that both responses begin from *5.56 m/s*, and after *t=5 s*, a divergence between these two responses appears. The reason for this divergence is the desired wheel slip introduced to the controller. At *t=25 s*, stabilisation of the wheel slip on the *2%* level is established, as indicated in Figure 50(b). The response of the controller is effective for a low level of the adhesion since the value of the wheel slip is successfully stabilised at *2%*. Moreover, when the slip curve in Figure 50(c) is analysed, it can be seen that *2%* of wheel slip corresponds to a point where the maximum adhesion is seen. The observed fluctuations in output torque response of the controller are similar to the previous experiment.

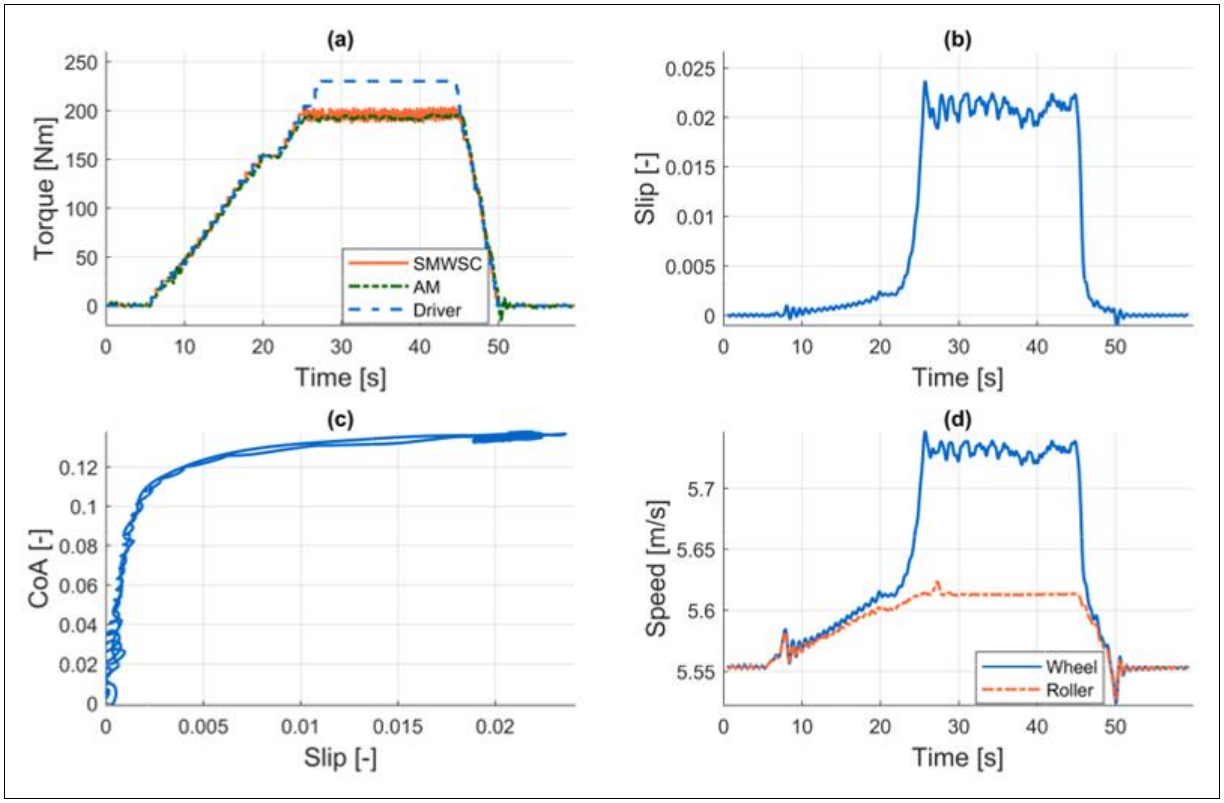

Figure 50. Experimental results of SM-WSC performed under the steady greasy contaminated test condition: (a) SM-WSC torque request, AM output torque and driver torque request; (b) Wheel slip; (c) Slip curve; (d) Wheel and roller speeds.

Figure 51 shows the experimental results of the proposed control algorithm carried out under grease and water&grease contaminated test conditions. The test aims to point out the dynamic response of the controller to the sudden change of the adhesion condition. The experimental conditions are similar to the water contaminated case, except that the wheel-roller contact zone is contaminated with steady grease. Figure 51(a) corresponds to the SM-WSC torque request, the AM torque response and the driver torque request. The wheel and roller speeds increase with an increase in driver torque request, as depicted in Figure 51(d). The SM-WSC regulates the motor torque at a *230 N.m* mean value when the reference wheel slip (*2%*) is achieved. It can be seen in Figure 51(c) that the maximum available adhesion at the operating point is *0.16*. When the water is sprayed onto the contact area (*t=38 s*), the available maximum adhesion drops dramatically, which increases the wheel slip, as can be seen in Figure 51(b). The SM-WSC reduces the motor torque to a *110 N.m* mean value, as seen in Figure 51(a) and stabilises wheel slip at *2%*. After *t=56 s*, the water flow is stopped. Because of the motion of the wheel and the roller, a cleaning effect (removal of water) is seen in the contact area. Due to

the cleaning effect, the adhesion between the wheel and the roller increases up to slightly below the previous operating point under steady grease conditions. The SM-WSC stabilises the wheel slip at *2%*. Here, it must be noted that *2%* of the wheel slip corresponds to the point where the peak of the slip curve (see Figure 51(c)) is observed. Hence, the controller achieved the maximum utilisation of the adhesion in all cases.

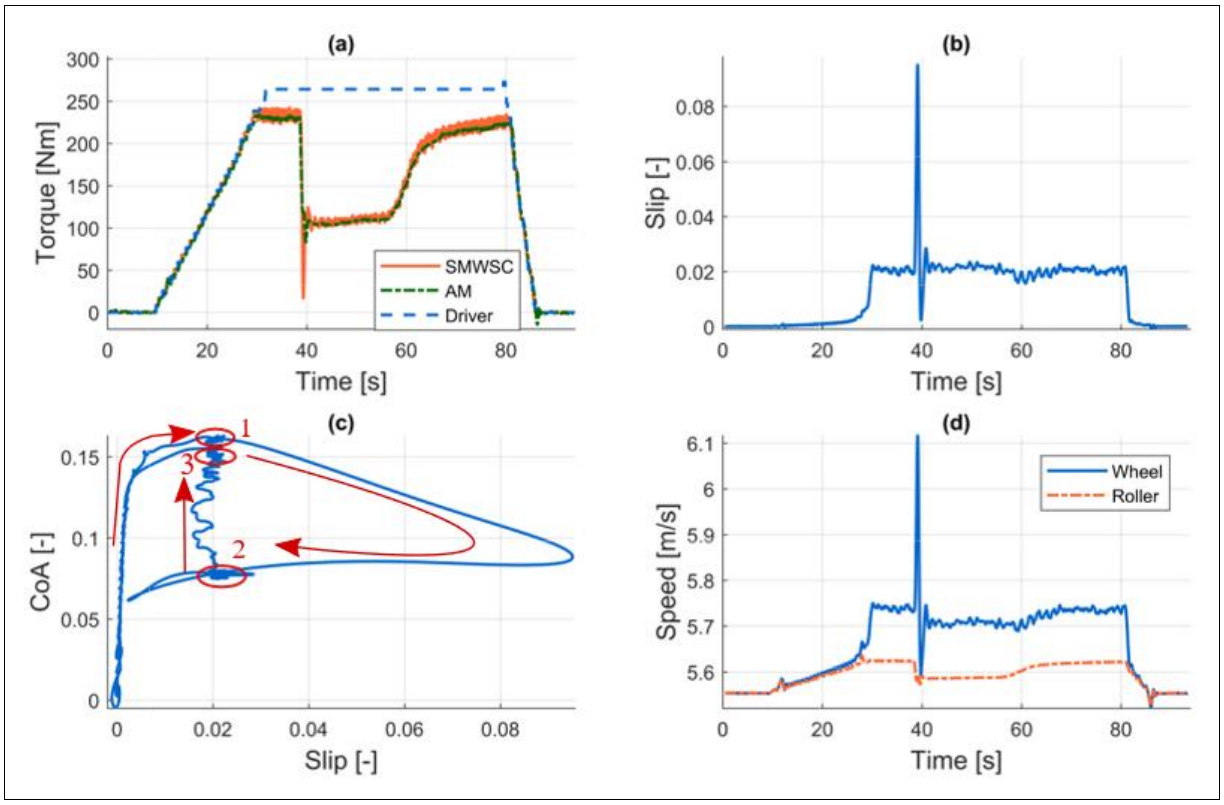

Figure 51. Experimental results SM-WSC performed under grease and water&grease contaminated test condition: (a) SM-WSC torque request, AM output torque and driver torque request; (b) Wheel slip; (c) Slip curve; (d) Wheel and roller speeds.

5.4 Analysis of Results

In this study, five wheel slip control strategies - wheel slip control based on single threshold (WSCST), wheel slip control based on multiple thresholds (WSCMT), wheel slip control based on angular acceleration of wheel (WSCAA), PI wheel slip control (PI-WSC), and sliding mode wheel slip control (SM-WSC) - have been implemented. The performances of the control methods are evaluated via experiments on a roller rig and simulations on its numerical

model. The conditions of the simulations and the experiments are employed identical to provide a comparative discussion.

The WSCST is the most straightforward wheel slip control strategy, which uses only a single threshold value for the control purpose. Whenever the actual wheel slip value exceeds the threshold value, the PMSM torque request is reduced to prevent the wheel from the severe slip. Figure 28 and Figure 39 show the simulation and experimental results conducted under the continuous water contaminated test condition, respectively. As it is expected, the wheel slip is controlled cyclically. A maximum wheel slip of *7.4%* is seen in simulation, while the maximum wheel slip of *8.1%* is seen in the experimental test. When the results for the steady grease in Figure 29 and Figure 40 are analysed, similar responses are found. A maximum wheel slip of *4.1%* is seen in the simulation, and *4%* is seen in the experiment. Based on the findings of the above simulations and experimental analysis, it is possible to claim that the WSCST strategy suppresses severe the wheel slip successfully. One of the interesting results is observed in the tests under grease contaminated surface condition (Figure 29(a) and Figure 40(a)). Initially, the WSCST controller torque request rises slower than the driver torque request. The slow torque recovery can be attributed to the setting of T_{min} and A_{inc} to low values. T_{min} is set as *1%* of the nominal torque of PMSM during the tests under grease contamination. The rise of the WSCST torque from T_{min} is slower due to the nature of the torque regulation algorithm. The faster torque increase is noticed during the test under the water contaminant since T_{min} is set as *15%* the nominal torque of PMSM. Furthermore, the increment rate parameter (A_{inc}) is another reason for the slow torque increase.

The performance evaluation of WSCST with various roller speeds, threshold values, deceleration rates and increment rates are conducted through the validated numerical model. The effects of the variation of the parameters on results are indicated in Appendix-A of the thesis. Findings from the validated numerical model can be summarised (independent from surface conditions) as follows:

- Lower wheel slip is noticed at higher roller speeds.
- The lower value of slip threshold value has a negative influence on the utilisation of adhesion, while high threshold value causes severe wheel slip.

- Setting the deceleration rate parameter (A_{dec}) lower results in excessive torque drops, whereas severe wheel slip is seen when it is set higher.
- The higher value of the increment rate (A_{inc}) causes slow torque recovery of the electric motor; on the other hand, lower values result in severe wheel slip.

The tests reveal that the WSCST prevents the severe wheel slip effectively. However, the traction performance of the motor suffers from repeating torque oscillation. Hence, it can be claimed that WSCST is a re-adhesion controller which primarily aims to suppress the excessive wheel slip. Thus, it is appropriate to use the WSCST on Electric Multiple Units (EMUs) which do not requires the maximum utilisation of the adhesion.

Wheel slip control based on multiple thresholds (WSCMT) is an improved version of the method mentioned above. In order to prevent excessive torque drop and increase, two threshold values are introduced. Both threshold values are selected on the stable part of the slip curve. Figure 30 and Figure 41 depict the simulation and experimental results of WSCMT method performed under the continuous water contaminated test condition, respectively. The severe wheel slip is prevented effectively in both tests. Similar responses are observed in simulation and experimental tests under the steady grease contaminated surface conditions (see Figure 31 and Figure 42). For profound research, the performance of the controller with various roller speeds, threshold values, deceleration rates and increment rates are conducted through the validated numerical model. The effect of each parameter on the control behaviour is illustrated in Appendix-B of the thesis. The obtained results are summarised as follows:

- The peak of wheel slip cycles decreases when the roller speed increases.
- Higher threshold values result in higher wheel slip
- Setting the deceleration rate parameter (A_{dec}) lower causes extreme torque drop, while higher values result in high wheel slip.
- Setting the increment rate parameter (A_{inc}) higher results in slow torque recovery after the suppression of wheel slip, while lower values cause a sudden wheel slip.

The findings are similar to the results of the WSCST due to the nature of the control strategy. It is concluded from the analysis that the controller can suppress severe wheel slip effectively. Furthermore, the controller reduces the excessive torque increase, and it is assured

that the torque drop becomes small. WSCMT method provides cyclic control of the wheel slip. Thus, the application of WSCMT method is recommended for use on EMUs since the maximum utilisation of the adhesion is not the primary consideration.

A wheel slip control based on the angular acceleration of wheel (WSCAA) is an alternative way of wheel slip control strategy. The method is developed to control the wheel slip via the angular acceleration signal. The simulation and experimental results of WSCAA performed under water contaminated test condition are given in Figure 32 and Figure 43, respectively. The resultant wheel slip is indicated in Figure 32(b) and Figure 43(b). A maximum wheel slip of *8.6%* is observed in the simulation, while the maximum wheel slip of *6.7%* is observed in the experiment. Based on the results, it is possible to claim that the WSCAA provides effective wheel slip control performance in both simulation and experiment under water contamination. Figure 33 and Figure 46 are the simulation and experimental results carried out under the steady grease contaminant, respectively. A maximum wheel slip of *9.9%* is seen in the simulation results, while the maximum wheel slip of *5.9%* is seen in the experiment results. The provided results confirm that the WSCAA controller is capable of preventing the wheel from the severe slip during deficient adhesion condition.

For more detailed analyses, the effect of roller speeds, threshold values, deceleration rates and increment rates variations on the performance of the controller are investigated through the validated numerical model. The impact of each parameter on the control behaviour is given in the Appendix-C of the thesis. The obtained results are concluded as follows:

- The peaks of the wheel slip cycles reduce with the increase in the roller speed.
- Improper setting of the threshold value to a lower or a higher value cause the failure.
- Setting the deceleration rate parameter (A_{dec}) lower causes excessive torque drop; nevertheless, higher values result in severe wheel slip (failure).
- Setting the increment rate parameter (A_{inc}) high causes slow torque recovery after the suppression of wheel slip, while lower values cause a sudden wheel slip.

The indicated results have a number of similarities with previous work of Yamashita and Soeda [38] in terms of wheel slip control characteristics. Moreover, high torque fluctuation

is also observed in their presented work. The method prevents excessive the wheel slip similar to the previous two strategies. Therefore, it is appropriate to use the WSCAA on EMUs.

Abovementioned strategies suppress the wheel slip in the same manner. Thus, to provide a comparative discussion, the responses of the control strategies are tested on the experimental test stand with the same control parameters (A_{dec}, A_{inc} *and* T_{min}) and surface conditions. Table 7 summarises the experimental results that are carried with the mentioned methods. Here, s_{max} is the mean value of the peak of the wheel slip cycles, ΔT is the mean value of generated torque request fluctuations, and t_p is the mean value of the time duration of wheel slip cycles. The WSCST and WSCMT suppress the wheel slip better than the WSCAA. On the other hand, the fluctuation of the generated torque request and time duration of wheel slip cycles is lower for the WSCAA. Hence, the WSCAA improves traction performance better than the WSCST and WSCMT. Consequently, small differences are observed between the performances of abovementioned methods. Based on this fact, the WSCAA strategy is primarily recommended to be used on EMUs due to its advantages (see section 2.4.3) over the other methods.

Table 7: Performance comparison of the wheel slip controllers based on the threshold value (under grease contaminated test condition and identical control parameters).

Method	s_{max} **[%]**	**ΔT [N.m]**	t_p **[s]**
WSCST	2.81	155.22	2.88
WSCMT	2.82	139.87	2.81
WSCAA	4.05	125.1	2.46

The PI controllers are widely used in industrial application because of their simplicity, low cost and robustness [77]. In this study, it is used to stabilise the wheel slip at the desired level. The simulation and experimental tests of the controller under continuous water contaminated surface conditions are summarised in Figure 34 and Figure 47, respectively. In both trials, the controller stabilises the wheel slip at the desired level without significant overshoot as provided in Figure 34(b) and Figure 47(b). Moreover, the maximum utilisation of the adhesion is realised since the controller operates at the peak of the slip curves, as shown in Figure 34(c) and Figure 47(c). Thus, the results confirm the effectiveness of the PI-WSC under the continuous water contaminated test condition. The second test is conducted to see the

dynamic reaction of the controller to the sudden change of the adhesion condition. Figure 35 and Figure 48 present the simulation and experimental results of the controller under half-dry&water contaminated test conditions, respectively. In Figure 35(c) and Figure 48(c), it is seen the controller has a robust dynamic response to the sudden change of the adhesion condition since the operation point recover from the unstable side to the stable side in a short time. In both cases of the adhesion condition, the controller operates at the peak of the slip curves. Therefore, it is possible to claim that the controller has a robust reaction to sudden changes. Surprisingly, a constant difference between the speeds of wheel and roller is noticed in experimental results, even at free rolling. This difference results in *0.4%* of offset in the calculated wheel slip. The reasons for the offset is not investigated since the action of the controller is not interrupted. Another interesting observation from the tests is the high level of the adhesion condition. It is seen that the maximum CoA adhesion is to *0.4* for the half-dry case and *0.32* for the continuous water contaminated case. It is believed the decent cleaning of the wheel and roller surfaces provides such high adhesion.

Further tests with various roller speeds, desired wheel slip ratios, proportional gain parameters (K_p) and integral gain parameters (K_i) are performed through the verified numerical model. The performed simulations, which are depicted in Appendix-D, allow formulating the following conclusion:

- The controller exhibits good wheel slip tracking performance with all roller speeds and all contact conditions. However, low amplitude vibrations are noticed at lower roller speeds.
- The controller provides successful performance under the water and grease contaminated test conditions when the desired wheel slip is set on the stable part of the slip curve. On the other hand, adjustment of the desired wheel slip to the unstable part of the slip curve brings the risk of control quality deterioration.
- Higher overshoot is observed with the lower proportional gain parameter (K_p) independent from the contact conditions. Additionally, it is noted that the controller is not able to stabilise the wheel slip under grease contaminated case when K_p sets lower.

- The integral gain parameter (K_i) influences the rise time to the desired set point. When K_i sets to a lower value, the higher rise time is seen.

Based on the observed results, it can be claimed that PI-WSC can be used to control the wheel slip and improve the traction performance of the electric locomotives. However, the tunning of the control parameters is very critical for a robust response. Moreover, the desired wheel slip has a significant influence on the stability of the controller and utilisation of the adhesion. Hence, the implementation of the PI-WSC with optimal wheel slip ratio tracking algorithms [22], [78] is adviced for stable control process and optimum traction performance. Thus, the provided method is advised to be implemented on the electric locomotive.

The sliding mode wheel slip control (SM-WSC) is an attractive robust control method which has useful properties to stabilise nonlinear and uncertain systems. The controller keeps the systems insensitive to uncertainties on a sliding surface. Moreover, SM-WSC has good and rapid transient performance [73]. The experimental and numerical results of the SM-WSC performed under water contaminated test condition are given in Figure 37 and Figure 49, respectively. In Figure 37(b) and Figure 49(b), it is noted that the wheel slip with the SM-WSC converged with the reference value (*2%*) accurately in a short time when a sudden drop in adhesion is applied. Furthermore, when Figure 37(c) and Figure 49(c) are analysed, it can be seen the *2%* of wheel slip corresponds to the slightly below the peak of the slip curve. Figure 38 and Figure 50 show the numeric results and the experimental results conducted under the steady grease contaminant, respectively. The test results in Figure 38(b) and Figure 50(b) reveal that SM-WSC has a robust performance in the stabilisation of the wheel slip. Moreover, Figure 38(c) and Figure 50(c) prove that the controller provides optimal utilisation of the adhesion. One of the most significant results of the study is noticed in the experimental test carried out under grease&water contaminated surface condition. During the experiment, it is found that the adhesion between the wheel-roller at the steady grease condition drops drastically with the presence of water in the contact area, as illustrated in Figure 51(c). Using this fact, the response of SM-WSC is tested experimentally by spraying water on a steady grease contaminated surface. Figure 51 shows the experimental results of the test. The test result presented in Figure 51(b) confirms the controller is reasonably effective in the stabilisation of wheel slip under quite low

adhesion conditions. Furthermore, the traction performance of the wheel is improved when an improvement in adhesion is seen, as indicated in Figure 51(a).

The performance of SM-WSC with various roller speeds, desired wheel slip ratios, convergence rate parameters (D) and uncertainties parameters (K) are carried out through the verified numerical model. The effect of each parameter on the control behaviour is given in Appendix-E of the thesis. The results of the analysis are summarised as follows.

- The wheel slip overshoot increases slightly at higher roller speeds; however, the amplitude of vibrations reduces.
- The controller is able to stabilize wheel slip even on the unstable part of the slip curve.
- The convergence rate parameter (D) influences the damping of the wheel slip. The higher value of the convergence rate parameter causes higher overshoot and longer settling time.
- The uncertainties parameter (K) has no significant influence on the results.

The presented results have several similarities with the findings of Kim et al. [74]. Moreover, both the experimental and simulation results are consistent with the previous work of Nam et al. [70] in terms of stabilisation of the wheel slip and improvement of traction ability. Kabzinski [79] claims that the proposed method is useful in the stabilisation of wheel slip, even in the presence of all the unavoidable measurement noises and errors caused by the digital implementation of the control algorithm. The findings of the tests support the presented claim since there have been successful results even in the presence of high amplitude noise in the measurements. It is known that the proposed method has certain limitations for the running of real vehicles, such as determination of adhesion force and longitudinal velocity. However, these limitations can be cleared by several means using estimation methods [80]–[82]. Moreover, the optimal point of the wheel slip where the maximum adhesion is observed is one of the challenging parameters. In this study, the optimum wheel slip is determined using the results of previous experiments, while Huang et al. [78] offer an optimal wheel slip ratio searching algorithm. Consequently, SM-WSC is highly recommended for use on electric locomotives since the optimum utilisation of the adhesion is the main consideration.

6 CONCLUSION

The work presented in the thesis is aimed to determine effective and viable solutions to wheel slip problem. To fulfil our purpose; first, the general background information about the adhesion, the wheel slip, and the wheel slip control strategies have been studied based upon the literature sources. Then, the wheel slip control methods available in the literature are investigated with their pros and cons. After that, to evaluate the performance of the developed wheel slip controllers, a numerical model representing the tram wheel roller rig is created in the MATLAB environment. The numerical model consists of five main components: the mechanical model of the torsional system, the dynamic model of the PMSM, dynamic model of the AM, the Freibauer/Polach adhesion force model, and the anti-slip control model. Afterwards, Five wheel slip control strategies -wheel slip control based on single threshold (WSCST), wheel slip control based on multiple thresholds (WSCMT), wheel slip control based on angular acceleration of wheel (WSCAA), PI wheel slip control (PI-WSC), and sliding mode wheel slip control (SM-WSC)- are suggested.

The validity of the developed numerical model is proven through the comparison of the numerical and experimental results. Then, the performances of the control methods are evaluated through experiments on a roller rig and simulation tests on the validated numerical model. Moreover, the influence of different roller speeds and control parameters are investigated through the validated numerical model since it provides an advantage by allowing us to set the identical test condition for each case. It is observed wheel slip control strategies based on the threshold value (WSCST, WSCMT and WSCAA) suppress the severe wheel slip effectively. Due to its advantages over the other methods, the WSCAA strategy is primarily recommended to be used on EMUs. The PI-WSC and SM-WSC successfully stabilise the wheel slip at a defined reference slip value. Furthermore, the PI-WSC and SM-WSC algorithms do not only stabilise the wheel slip but also help to establish optimum utilisation of the adhesion characteristic regardless of the severity of contaminants between the wheel and the roller when the optimal reference wheel slip is introduced. The SM-WSC has an advantage over the PI-WSC due to its useful properties in the stabilisation of nonlinear and uncertain systems. Hence, it is appropriate to use the SM-WSC on electric locomotives.

6.1 Completed Objectives of Doctoral Thesis

The completed objectives of the thesis are as follows:

(i) **Summarising a large number of published studies on the wheel slip, adhesion and slip control methods:** In section 2, initially, the gathered information about the adhesion and slip mechanism are explained to give the reader a general picture of the research covered in the thesis. Then the wheel slip detection methods and wheel slip control methods based on the literature review are introduced with their pros and cons.

(ii) **Reproducing a numerical model of the tram wheel roller rig in MATLAB environment that can be used for performance evaluation of the wheel slip control strategies:** In section 3.2, the numerical model of tram wheel roller rig, that is introduced in section 3.1, is reproduced in MATLAB environment. The developed model includes nonlinear effects caused by time delay and disturbances to match the values of the experimental test setup.

(iii) **Proposing algorithms to control the wheel slip mechanism and establishing optimum utilisation of adhesion**: In section 4, the developed wheel slip control strategies are introduced. Strategies in sections 4.1, 4.2 and 4.3 are designed to be used on EMU while strategies in sections 4.4 and 4.5 are designed to be used on electric locomotives.

(iv) **Validation of reproduced numeric model:** In section 5.1, the validity of the developed numerical model (see section 3.2) is proven by comparing simulation results with experimental results.

(v) **Verifying the functionality of proposed wheel slip control algorithms by either the validated numerical model or experimentally obtained results from the tram wheel roller rig:** In section 5.2, the functionality of the proposed wheel slip control algorithms is verified by the validated numerical model (under the assumption of several surface conditions). In 5.3, the functionality of the controllers is proven with the experimental setup under several test conditions.

(vi) **Performance evaluation of the proposed wheel slip control algorithms with different speeds and control parameters:** The validated numerical model is used

for the further performance evaluation of the wheel slip control algorithms with different speeds and control parameters. The simulation results are presented in the Appendices of the thesis. The summaries of the simulations are presented in section 5.4.

6.2 Scientific Contributions of Doctoral Thesis

An advanced numerical model of a tram wheel roller rig that includes nonlinear effects caused by time delay and disturbances to match the values of the experimental test setup is developed so that other researchers can easily simulate the dynamic responses of wheel slip and electric motor control strategies.

Three different re-adhesion (WSCST, WSCMT and WSCAA) are suggested for the use on the EMUs. The WSCST and WSCAA are conventional re-adhesion strategies. Employing WSCMT on wheel slip control is unique and proposed by the author. It aims to provide an improvement to the utilisation of the adhesion.

Two more different strategies (PI-WSC and SM-WSC) for the use of electric locomotive are also proposed in this thesis. It is known that the PI-WSC method is widely used for industrial applications. However, the wheel slip control stability cannot be guaranteed with the PI controllers due to their linear characteristics [22]. On the other hand, SM-WSC is an attractive robust control method which has effective properties to stabilise the nonlinear and uncertain systems. The author has modified and applied a control strategy which is presented for a personal electric vehicle in the previous literature [70]. According to the author's knowledge, SM-WSC is an original control strategy in the related literature which aims to stabilise the wheel slip for a roller rig.

The dynamic responses of the implemented anti-slip control strategies are evaluated under different surface conditions (half-dry, wet, greasy and wet&greasy) on both experimental tram wheel roller rig and its numeric model. Furthermore, the performance of the control strategies with different speeds, threshold values, deceleration and increment rates are evaluated on the validated numerical model. The carried-out simulations and experiments bring considerable knowledge in the related scientific field.

6.3 Future Works

The purpose of the slip control methods is to prevent the wheel from severe slip and improve the traction effort of the vehicle. Furthermore, the development of such systems is very critical for the safety of the vehicles. Hence, we have presented five of the wheel slip control strategies. The presented strategies are validated by tests on the experimental roller rig and its numerical model. The further verification of the developed strategies can be carried on the real locomotive in future. Another future work can be the development of optimal reference slip ratio seeking algorithm. In this work, the reference value of the wheel slip is obtained from the experimental measurements (predefined reference value). However, it is possible to obtain the reference using the characteristic slip curve. Hence it is planned to adopt recursive least square with the steepest gradient method (RLS-SGM) to determine the optimal wheel slip ratio online for the presented control strategies.

REFERENCES

[1] M. Inan and M. Demir, “DEMİRYOLU ULAŞIMI VE TÜRKİYE’DE HIZLI TREN YATIRIMLARININ ETKİLERİ: ESKİŞEHİR-KONYA ÖRNEĞİ,” *Fırat Üniversitesi Sos. Bilim. Derg.*, Jan. 2017.

[2] P. Pichlík, “Strategy of Railway Traction Vehicles Wheel Slip Control,” CZECH TECHNICAL UNIVERSITY, Prague, 2018.

[3] H. Chen, T. Ban, M. Ishida, and T. Nakahara, “Experimental investigation of influential factors on adhesion between wheel and rail under wet conditions,” *Wear*, vol. 265, no. 9–10, pp. 1504–1511, Oct. 2008.

[4] C. W. Jenks, “Improved Methods for Increasing Wheel/Rail Adhesion in the Presence of Natural Contaminants,” Transit Co-operative Research Program, Research Results Diges, 17, 1997.

[5] J. Yu, “Re-adhesion control for railway traction systems,” The University of Leeds, Leeds, 2007.

[6] Z. Soomro, “Computation of Slip analysis to detect adhesion for protection of rail vehicle and derailment,” *J. Appl. Comput. Mech.*, no. 3, Jul. 2015.

[7] Y. Zhu, “Adhesion in the wheel-rail contact,” KTH Royal Institute of Technology, Stockholm, 2013.

[8] M.-S. KIM, “Analysis of the Wheel/rail Adhesion Characteristic using the Scaled Adhesion Tester,” *Enviroment*, vol. 4, pp. 194–197, 2014.

[9] D. I. Fletcher and S. Lewis, “Creep curve measurement to support wear and adhesion modelling, using a continuously variable creep twin disc machine,” *Wear*, vol. 298–299, pp. 57–65, Feb. 2013.

[10] Y. Zhu, U. Olofsson, and K. Persson, “Investigation of factors influencing wheel–rail adhesion using a mini-traction machine,” *Wear*, vol. 292–293, pp. 218–231, Jul. 2012.

[11] W. Zhang, J. Chen, X. Wu, and X. Jin, “Wheel/rail adhesion and analysis by using full scale roller rig,” *Wear*, vol. 253, no. 1–2, pp. 82–88, Jul. 2002.

[12] W. J. Wang, H. F. Zhang, H. Y. Wang, Q. Y. Liu, and M. H. Zhu, “Study on the adhesion behavior of wheel/rail under oil, water and sanding conditions,” *Wear*, vol. 271, no. 9–10, pp. 2693–2698, Jul. 2011.

[13] E. Niccolini and Y. Berthier, “Wheel–rail adhesion: laboratory study of ‘natural’ third body role on locomotives wheels and rails,” *Wear*, vol. 258, no. 7–8, pp. 1172–1178, Mar. 2005.

[14] P. M. Cann, “The ‘leaves on the line’ problem—a study of leaf residue film formation and lubricity under laboratory test conditions,” *Tribol. Lett.*, vol. 24, no. 2, pp. 151–158, Nov. 2006.

[15] M. Spiryagin, K. S. Lee, H. H. Yoo, O. Kashura, and O. Kostyukevich, “Modeling of Adhesion for Railway Vehicles,” *J. Adhes. Sci. Technol.*, vol. 22, no. 10–11, pp. 1017–1034, Jan. 2008.

[16] H. Chen, T. Ban, M. Ishida, and T. Nakahara, “Adhesion between rail/wheel under water lubricated contact,” *Wear*, vol. 253, no. 1–2, pp. 75–81, Jul. 2002.

[17] E. A. Gallardo-Hernandez and R. Lewis, “Twin disc assessment of wheel/rail adhesion,” *Wear*, vol. 265, no. 9–10, pp. 1309–1316, Oct. 2008.

[18] R. Lewis, R. S. Dwyer-Joyce, S. R. Lewis, C. Hardwick, and E. A. Gallardo-Hernandez, “Tribology of the Wheel-Rail Contact: The Effect of Third Body Materials,” *Int. J. Railw. Technol.*, vol. 1, no. 1, pp. 167–194, Apr. 2012.

[19] Z. Li, O. Arias-Cuevas, R. Lewis, and E. A. Gallardo-Hernández, “Rolling–Sliding Laboratory Tests of Friction Modifiers in Leaf Contaminated Wheel–Rail Contacts,” *Tribol. Lett.*, vol. 33, no. 2, pp. 97–109, Feb. 2009.

[20] A. Zirek, “Anti-slip protection and control of the traction motor of a rail vehicle,” University of Pardubice, Pardubice, 2015.

[21] M. Malvezzi, L. Pugi, S. Papini, A. Rindi, and P. Toni, “Identification of a wheel–rail adhesion coefficient from experimental data during braking tests,” *Proc. Inst. Mech. Eng. Part F J. Rail Rapid Transit*, vol. 227, no. 2, pp. 128–139, Mar. 2013.

[22] D. Frylmark and S. Johnsson, “Automatic Slip Control for Railway Vehicles,” Linköpings Universitet, Linköpings, 2003.

[23] Z. Zhu, K. Yuan, W. Zou, and H. Hu, “Current-based wheel slip detection of all-wheel driving vehicle,” in *2009 International Conference on Information and Automation*, Zhuhai, Macau, China, 2009, pp. 495–499.

[24] P. Pichlík, “Overview of Slip Control Methods Used in Locomotives,” *Trans. Electr. Eng.*, vol. 3, no. 2, pp. 38–43, 2014.

[25] J. Huang, J. Xiao, D. Zhao, and S. Wang, “A wheel slip detection method of electric locomotive based on time-frequency analysis,” in *International Conference on Intelligent Transportation Systems*, Qingdao, China, 2014, pp. 1221–1225.

[26] M. Amiri and B. Moaveni, “Vehicle velocity estimation based on data fusion by Kalman filtering for ABS,” in *20th Iranian Conference on Electrical Engineering (ICEE2012)*, Tehran, Iran, 2012, pp. 1495–1500.

[27] B. Moaveni, M. Khosravi Roqaye Abad, and S. Nasiri, "Vehicle longitudinal velocity estimation during the braking process using unknown input Kalman filter," *Veh. Syst. Dyn.*, vol. 53, no. 10, pp. 1373–1392, Oct. 2015.

[28] L. Imsland, T. A. Johansen, T. I. Fossen, H. Fjær Grip, J. C. Kalkkuhl, and A. Suissa, "Vehicle velocity estimation using nonlinear observers," *Automatica*, vol. 42, no. 12, pp. 2091–2103, Dec. 2006.

[29] L. Imsland, T. A. Johansen, T. I. Fossen, J. C. Kalkkuhl, and A. Suissa, "Vehicle Velocity Estimation using Modular Nonlinear Observers," in *Proceedings of the 44th IEEE Conference on Decision and Control*, Seville, Spain, 2005, pp. 6728–6733.

[30] D. M. Bevly, J. C. Gerdes, and C. Wilson, "The Use of GPS Based Velocity Measurements for Measurement of Sideslip and Wheel Slip," *Veh. Syst. Dyn.*, vol. 38, no. 2, pp. 127–147, Feb. 2003.

[31] M. Joos, J. Ziegler, and C. Stiller, "Low-cost sensors for image based measurement of 2D velocity and yaw rate," in *IEEE Intelligent Vehicles Symposium*, San Diego, CA, USA, 2010, pp. 658–662.

[32] K. Kondo, "Anti-slip control technologies for the railway vehicle traction," in *2012 IEEE Vehicle Power and Propulsion Conference*, Seoul, South Korea, 2012, pp. 1306–1311.

[33] D.-Y. Park, M.-S. Kim, D.-H. Hwang, J.-H. Lee, and Y.-J. Kim, "Hybrid re-adhesion control method for traction system of high-speed railway," in *ICEMS'2001. Proceedings of the Fifth International Conference on Electrical Machines and Systems (IEEE Cat. No.01EX501)*, Shenyang, China, 2001, vol. 2, pp. 739–742.

[34] M. Yamashita and T. Watanabe, "Readhesion Control Method without Speed Sensors for Electric Railway Vehicles," *Q. Rep. RTRI*, vol. 46, no. 2, pp. 85–89, 2005.

[35] G. Yin, S. Wang, and X. Jin, "Optimal Slip Ratio Based Fuzzy Control of Acceleration Slip Regulation for Four-Wheel Independent Driving Electric Vehicles," *Math. Probl. Eng.*, vol. 2013, 2013.

[36] J. Gou, B. Zhang, L. Wang, and J. Zhang, "Acceleration Slip Regulation of Electric Vehicle," in *2010 International Conference on Logistics Engineering and Intelligent Transportation Systems*, Wuhan, China, 2010, pp. 1–3.

[37] H. He, J. Peng, R. Xiong, and H. Fan, "An Acceleration Slip Regulation Strategy for Four-Wheel Drive Electric Vehicles Based on Sliding Mode Control," *Energies*, vol. 7, no. 12, pp. 3748–3763, Jun. 2014.

[38] M. Yamashita and T. Soeda, "Anti-slip re-adhesion control method for increasing the tractive force of locomotives through the early detection of wheel slip convergence," in *2015 17th European Conference on Power Electronics and Applications (EPE'15 ECCE-Europe)*, Geneva, Switzerland, 2015, pp. 1–10.

[39] T. Gajdar, I. Rudas, and Y. Suda, "Neural network based estimation of friction coefficient of wheel and rail," in *Proceedings of IEEE International Conference on Intelligent Engineering Systems*, Budapest, Hungary, 1997, pp. 315–318.

[40] V. Ćirović, D. Aleksendrić, and D. Smiljanić, "Longitudinal wheel slip control using dynamic neural networks," *Mechatronics*, vol. 23, no. 1, pp. 135–146, Feb. 2013.

[41] A. D. Cheok and S. Shiomi, "Combined heuristic knowledge and limited measurement based fuzzy logic antiskid control for railway applications," *IEEE Trans. Syst. Man Cybern. Part C Appl. Rev.*, vol. 30, no. 4, pp. 557–568, Nov. 2000.

[42] M. Garcia-Rivera, R. Sanz, and J. A. Perez-Rodriguez, "An antislipping fuzzy logic controller for a railway traction system," in *Proceedings of 6th International Fuzzy Systems Conference*, Barcelona, Spain, 1997, pp. 119–124.

[43] P. Naderi, A. Farhadi, M. Mirsalim, and T. Mohammadi, "Anti-Lock and Anti-Slip Braking System, using fuzzy logic and sliding mode controllers," in *2010 IEEE Vehicle Power and Propulsion Conference*, Lille, France, 2010, pp. 1–6.

[44] M. Bauer and M. Tomizuka, "Fuzzy Logic Traction Controllers and their Effect on Longitudinal Vehicle Platoon Systems," *Veh. Syst. Dyn.*, vol. 25, no. 4, pp. 277–303, Apr. 1996.

[45] V. R. Aparow, F. Ahmad, K. Hudha, and H. Jamaluddin, "Modelling and PID control of antilock braking system with wheel slip reduction to improve braking performance," *Int. J. Veh. Saf.*, vol. 6, no. 3, pp. 265–296, 2013.

[46] P. Voltr and M. Lata, "Transient wheel–rail adhesion characteristics under the cleaning effect of sliding," *Veh. Syst. Dyn.*, vol. 53, no. 5, pp. 605–618, May 2015.

[47] P. Voltr, "Simulation of wheel-rail contact conditions on experimental equipment," *Railw. Transp. Logist.*, vol. 11, pp. 77–82, 2015.

[48] J. Gerlici, M. Gorbunov, K. Kravchenko, O. Nozhenko, and T. Lack, "Experimental rigs for wheel/rail contact research," *Manuf. Technol.*, vol. 16, no. 5, pp. 909–916, 2016.

[49] P. Voltr, M. Lata, and O. Cerny, "Measuring of wheel-rail adhesion characteristics at a test stand," in *18th International Conference Engineering Mechanics*, Svratka, Czech Republic, 2012, pp. 1543–1553.

[50] A. Onat, P. Voltr, and M. Lata, "An unscented Kalman filter-based rolling radius estimation methodology for railway vehicles with traction," *Proc. Inst. Mech. Eng. Part F J. Rail Rapid Transit*, vol. 232, no. 6, pp. 1686–1702, 2017.

[51] A. Onat, A. Zirek, and P. Voltr, "Dynamic Modelling and Numerical Simulation of a Tram Wheel Test Stand," in *3rd International Symposium on Electrical Railway Transportation Systems, ERUSIS 2017, Eskisehir, Turkey*, 2017.

[52] "Park, Inverse Park and Clarke, Inverse Clarke Transformations MSS Software Implementations User Guide." Microsemi Corporation, 2013.

[53] The MathWorks Inc., "abc to dq0, dq0 to abc," *Matlab Documentation,* 2013. [Online]. Available: https://www.mathworks.com.

[54] "The Authoritative Dictionary of IEEE Standards Terms." IEEE Press, p. 588, 2000.

[55] P. H. Tran, "MATLAB/Simulink Implementation and Analysis of Three Pulse-Width-Modulation (PWM) Techniques," Boise State University, Boise, Idaho, 2012.

[56] J.-W. JUNG, "SPACE VECTOR PWM INVERTER," The Ohio State University, Mechatronic Systems Laboratory, Dept. of Electrical and Computer Engg, 2005.

[57] R. Aparnathi and V. V. Dwivedi, "Modelling, Simulation of Permanent Magnet Synchronous Machine Drive using FOC Technique," *Glob. J. Res. Eng. Mech. Mech. Eng.*, vol. 13, no. 9, pp. 21–28, 2013.

[58] K. V. Kumar, P. A. Michael, J. P. John, and D. S. S. Kumar, "Simulation and comparison of SPWM and SVPWM control for three phase inverter," *ARPN J. Eng. Appl. Sci.*, vol. 5, no. 7, pp. 61–74, 2010.

[59] F. Sevilmis and H. Karaca, "Simulation and analysis of SVPWM based VSI for wind energy systems," in *Proceedings of the 2014 6th International Conference on Electronics, Computers and Artificial Intelligence (ECAI)*, Bucharest, Romania, 2014, pp. 73–78.

[60] The MathWorks Inc., "Induction Machine Scalar Control," *Matlab Documentation*, 2017. [Online]. Available: https://www.mathworks.com.

[61] A. Apte, R. Walambe, V. Joshi, K. Rathod, and J. Kolhe, "Simulation of a permanent magnet synchronous motor using matlab-simulink," in *2014 Annual IEEE India Conference (INDICON)*, Pune, India, 2014, pp. 1–5.

[62] The MathWorks Inc., "Permanent Magnet Synchronous Machine," *Matlab Documentation*, 2006. [Online]. Available: https://www.mathworks.com.

[63] A. Zirek, P. Voltr, M. Lata, and J. Novák, "An adaptive sliding mode control to stabilize wheel slip and improve traction performance," *Proc. Inst. Mech. Eng. Part F J. Rail Rapid Transit*, vol. 232, no. 10, pp. 2392–2405, May 2018.

[64] J. Simanek, J. Novak, O. Cerny, and R. Dolecek, "FOC and flux weakening for traction drive with permanent magnet synchronous motor," in *2008 IEEE International Symposium on Industrial Electronics*, Cambridge, UK, 2008, pp. 753–758.

[65] A. W. Leedy, "Simulink/MATLAB dynamic induction motor model for use as a teaching and research tool," *Int. J. Soft Comput. Eng.*, vol. 3, no. 4, pp. 102–107, 2013.

[66] J. Simanek, J. Novak, R. Dolecek, and O. Cerny, "Control Algorithms for Permanent Magnet Synchronous Traction Motor," in *The International Conference on "Computer as a Tool,"* Warsaw, Poland, 2007, pp. 1839–1844.

[67] O. Polach, "Creep forces in simulations of traction vehicles running on adhesion limit," *Wear*, vol. 258, no. 7–8, pp. 992–1000, Mar. 2005.

[68] R. K. Mudi, C. Dey, and T.-T. Lee, "An improved auto-tuning scheme for PI controllers," *ISA Trans.*, vol. 47, no. 1, pp. 45–52, Jan. 2008.

[69] Kiam Heong Ang, G. Chong, and Yun Li, "PID control system analysis, design, and technology," *IEEE Trans. Control Syst. Technol.*, vol. 13, no. 4, pp. 559–576, Jul. 2005.

[70] K. Nam, Y. Hori, and C. Lee, "Wheel Slip Control for Improving Traction-Ability and Energy Efficiency of a Personal Electric Vehicle," *Energies*, vol. 8, no. 7, pp. 6820–6840, Jul. 2015.

[71] D. Caporale, P. Colaneri, and A. Astolfi, "Adaptive nonlinear control of braking in railway vehicles," in *52nd IEEE Conference on Decision and Control*, Florence, Italy, 2013, pp. 6892–6897.

[72] L. Jin and Y. Liu, "Study on Adaptive Slid Mode Controller for Improving Handling Stability of Motorized Electric Vehicles," *Math. Probl. Eng.*, vol. 2014, pp. 1–10, 2014.

[73] J. J. E. Slotine and W. Li, *Applied Nonlinear Control*. NJ, USA,: Prentice-Hall: Englewood Cliffs, 1991.

[74] J. S. Kim, S. H. Park, J. J. Choi, and H. Yamazaki, "Adaptive Sliding Mode Control of Adhesion Force in Railway Rolling Stocks," in *Sliding Mode Control*, Rijeka, Croatia: InTech, 2011, pp. 385–408.

[75] W. Gao and J. C. Hung, "Variable structure control of nonlinear systems: A new approach," *IEEE Trans. Ind. Electron.*, vol. 40, no. 1, pp. 45–55, 1993.

[76] K. Nam, H. Fujimoto, and Y. Hori, "Design of an adaptive sliding mode controller for robust yaw stabilisation of in–wheel–motor–driven electric vehicles," *Int. J. Veh. Des.*, vol. 67, no. 1, pp. 98–113, 2014.

[77] S. Chowdhuri, S. Biswas, and A. Mukherjee, "Performance Studies of Fuzzy Logic Based PI-like Controller Designed for Speed Control of Switched Reluctance Motor," in *2006 1ST IEEE Conference on Industrial Electronics and Applications*, Singapore, 2006, pp. 1–5.

[78] Z. Huang, Z. Xu, B. Chen, R. Zhang, Y. Chen, and Q. Peng, "Sliding mode control for urban railway anti-slip system based on optimal slip ratio estimation with forgetting factor recursive least-squares," in *2017 36th Chinese Control Conference (CCC)*, Dalian, China, 2017, pp. 9502–9507.

[79] J. Kabzinski, “Adaptive, compensating control of wheel slip in railway vehicles,” *Bull. Pol. Acad. Sci.*, vol. 63, no. 4, pp. 955–963, 2015.

[80] K. Ohishi, K. Nakano, I. Miyashita, and S. Yasukawa, “Anti-slip control of electric motor coach based on disturbance observer,” in *AMC’98 - Coimbra. 1998 5th International Workshop on Advanced Motion Control. Proceedings (Cat. No.98TH8354)*, Coimbra, Portugal, 1998, pp. 580–585.

[81] T. Ishrat, G. Ledwich, M. Vilathgamuwa, and P. Borghesani, “Wheel slip control based on traction force estimaton of electric locomotives,” in *2016 Australasian Universities Power Engineering Conference (AUPEC)*, Brisbane, QLD, Australia, 2016, pp. 1–6.

[82] L. Chu, Y. Zhang, Y. Shi, M. Xu, and M. Liu, “Vehicle lateral and longitudinal velocity estimation based on Unscented Kalman Filter,” in *2010 3rd International Conference on Advanced Computer Theory and Engineering(ICACTE)*, Chengdu, China, 2010, vol. 3, pp. V3-325.

PUBLICATIONS OF STUDENT

A. Zirek, P. Voltr, M. Lata, and J. Novák, "An adaptive sliding mode control to stabilize wheel slip and improve traction performance," *Proceedings of the Institution of Mechanical Engineers, Part F: Journal of Rail and Rapid Transit*, vol. 232, no. 10, pp. 2392–2405, May 2018.

A. Onat, **A. Zirek**, and P. Voltr, "Dynamic Modelling and Numerical Simulation of a Tram Wheel Test Stand," in *3rd International Symposium on Electrical Railway Transportation Systems, ERUSIS 2017*, Eskisehir, Turkey, 2017.

P. Voltr, **A. Zirek**, and B. T. Kayaalp, "New Experience and Results from Experimental Measurement of Adhesion on a Roller Rig," in *23rd International Conference on Current Problems in Rail Vehicles*, Ceska Trebova, Czech Republic, 2017, pp. 423-432

A. Zirek and B. T. Kayaalp, "The Slip Control of a Tram-Wheel Test Stand Model with Single Neuron PID Control Method," in *VII. International Scientific Conference of the Faculty of Transport Engineering*, Pardubice, Czech Republic, 2018, pp. 268-275

APPENDICES

A-Wheel Slip Control Based on a Single Threshold

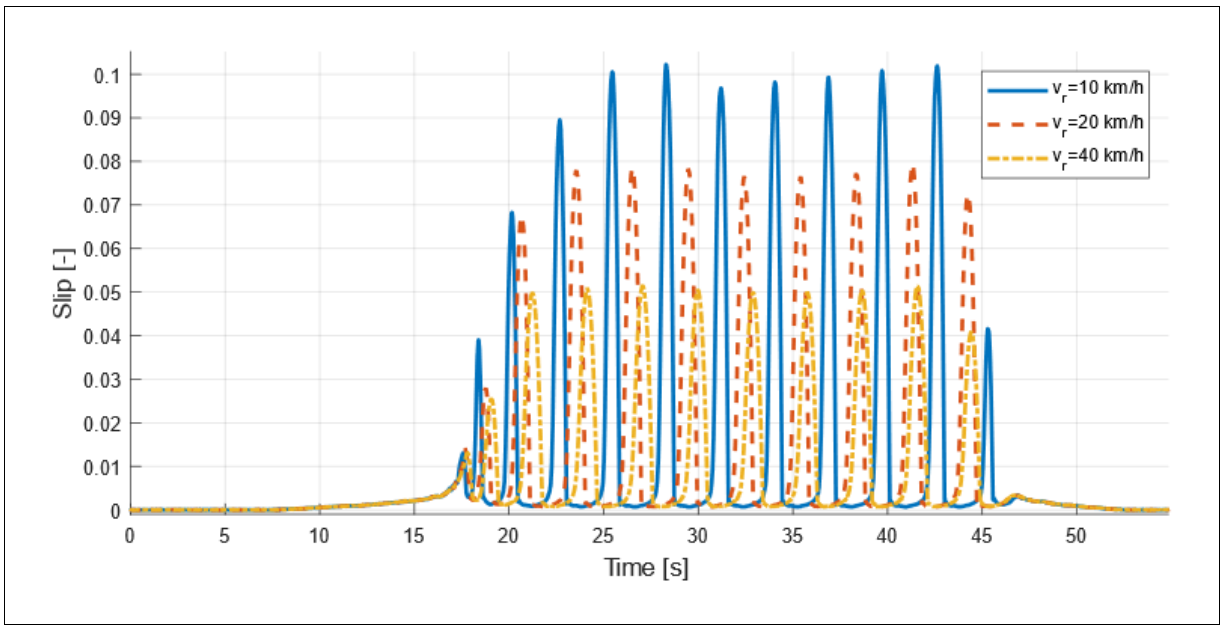

Simulation result of WSCST performed under water contaminated test condition and different roller speeds (s_{th}=0.008, A_{dec}=1, A_{inc}=1 and T_{min}=15%).

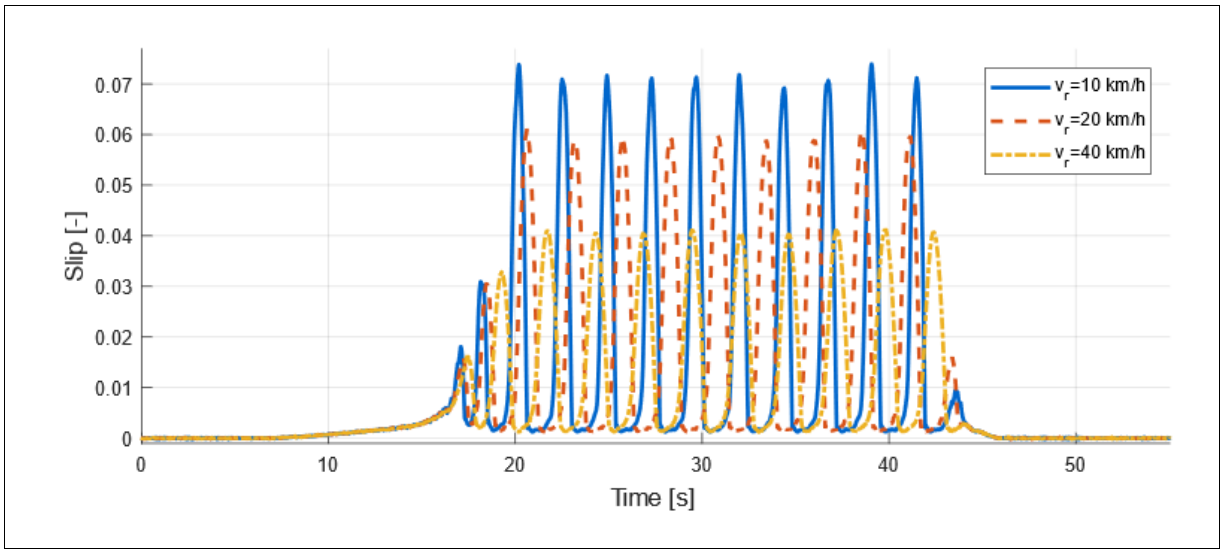

Simulation results of WSCST performed under grease contaminated test condition and different roller speeds (s_{th}=0.01, A_{dec}=1, A_{inc}=1 and T_{min}=1%).

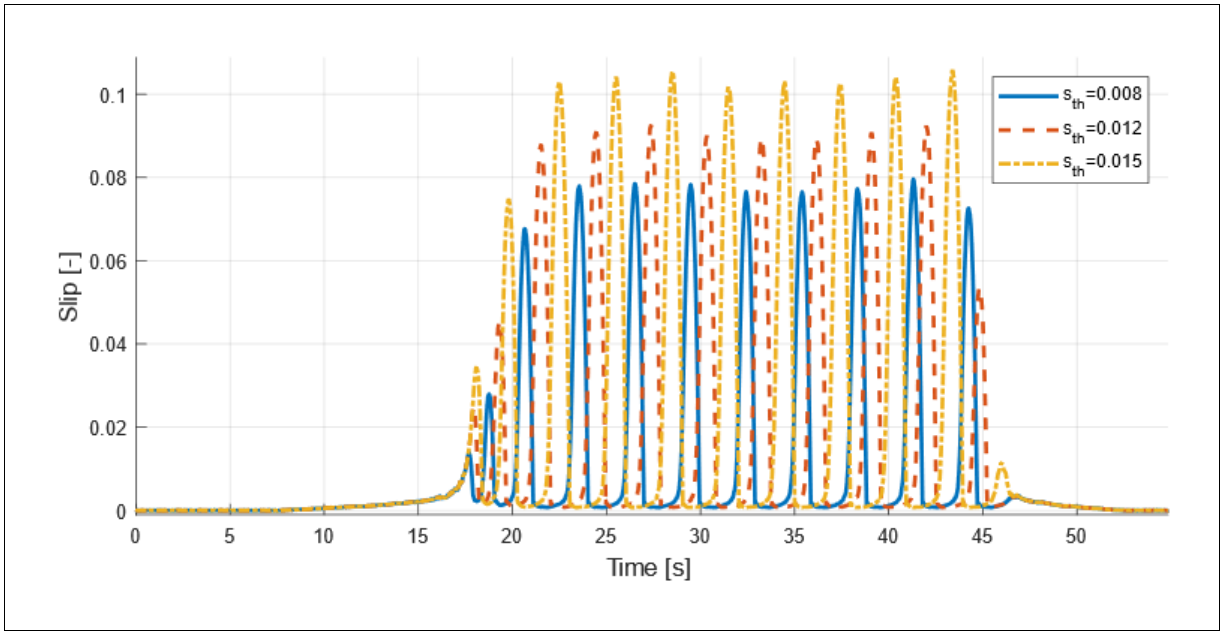

Simulation results of WSCST performed under water contaminated test condition and different threshold values (v_r=20 km/h, A_{dec}=1, A_{inc}=1 and T_{min}=15%).

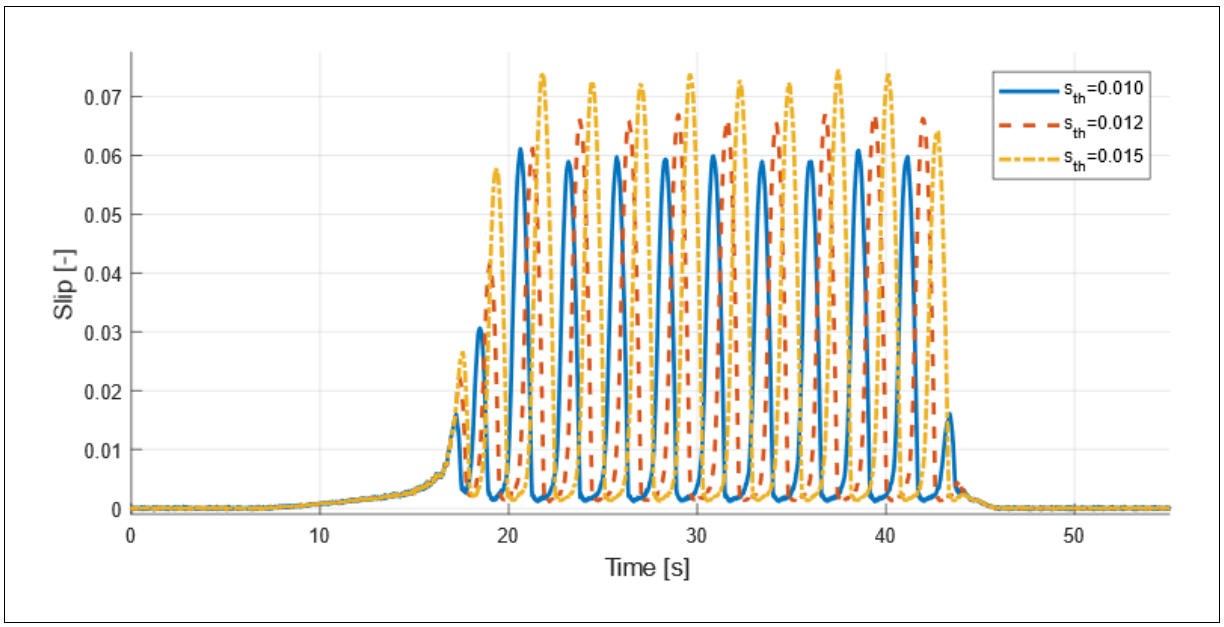

Simulation results of WSCST performed under grease contaminated test condition and different threshold values (v_r=20 km/h, A_{dec}=1, A_{inc}=1 and T_{min}=1%).

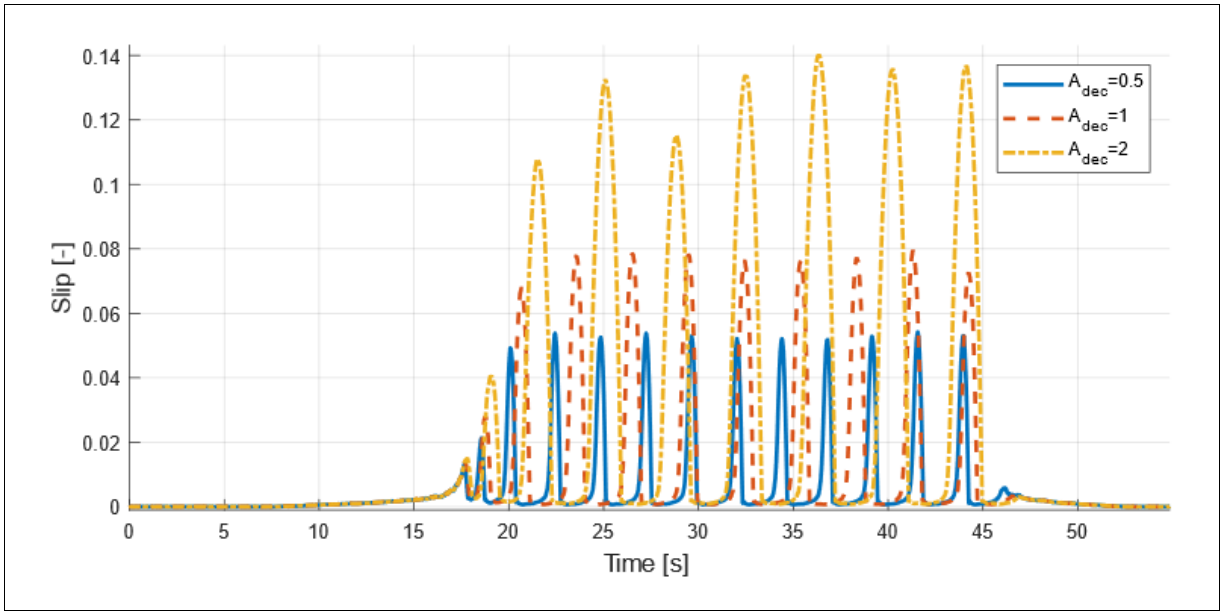

Simulation results of WSCST performed under water contaminated test condition and different A_{dec} parameters (v_r=20 km/h, s_{th}=0.008, A_{inc}=1 and T_{min}=15%).

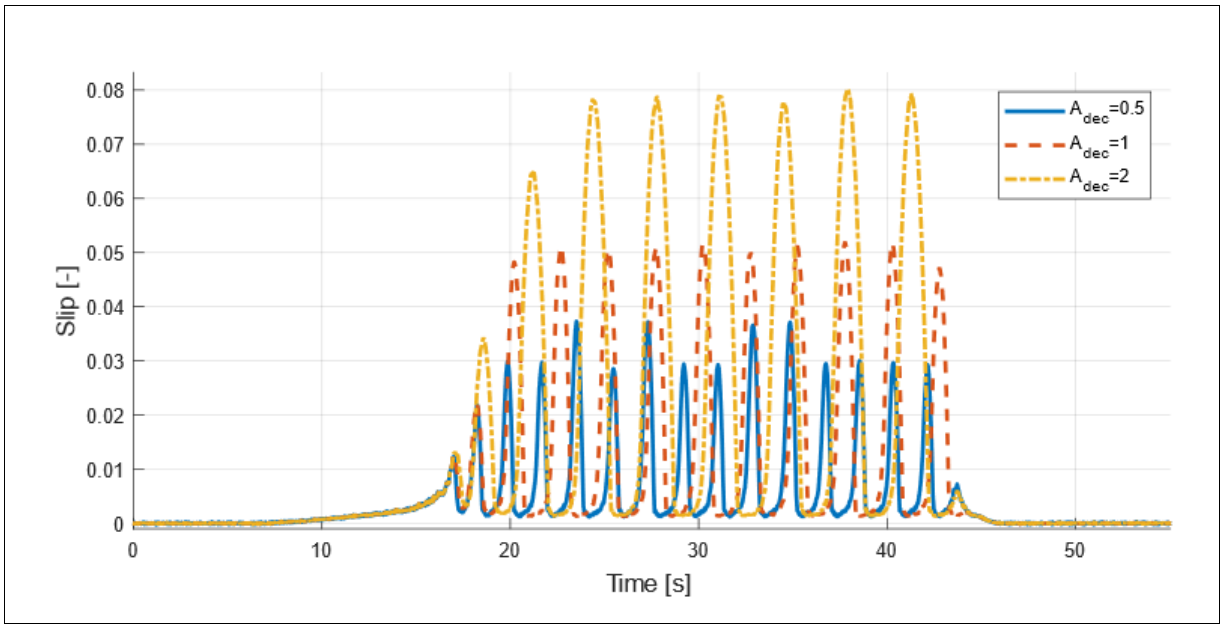

Simulation results of WSCST performed under grease contaminated test condition and different A_{dec} parameters (v_r=20 km/h, s_{th}=0.008, A_{inc}=1 and T_{min}=1%).

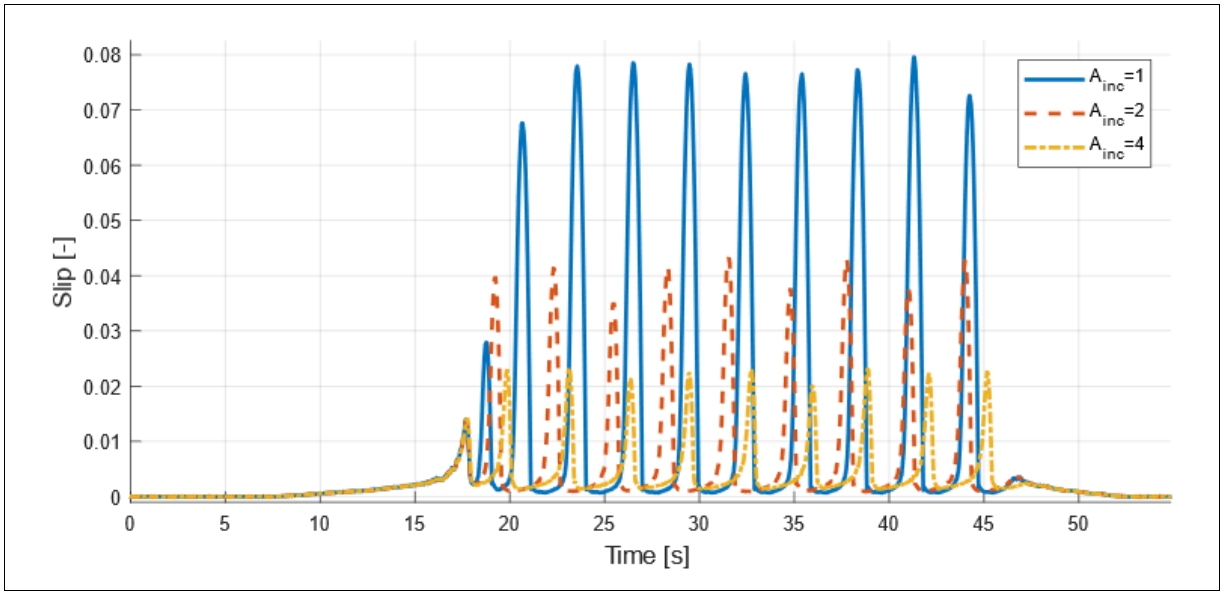

Simulation results of WSCST performed under water contaminated test condition and different A_{inc} parameters (v_r=20 km/h, s_{th}=0.008, A_{dec}=1 and T_{min}=15%).

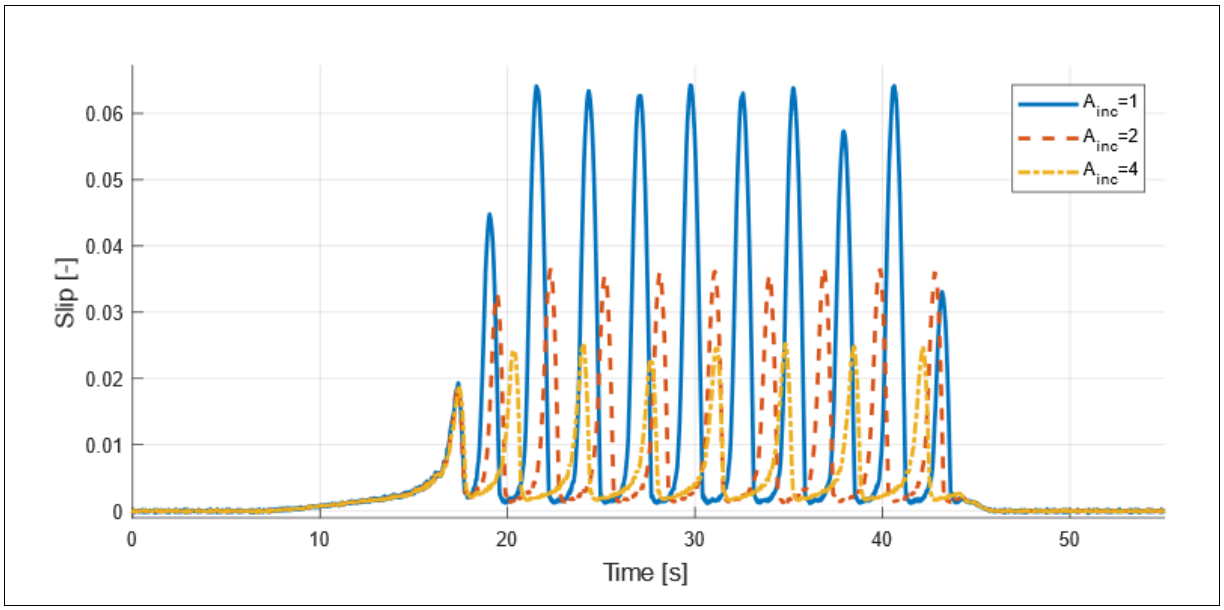

Simulation results of WSCST performed under grease contaminated test condition and different A_{inc} parameters (v_r=20 km/h, s_{th}=0.008, A_{dec}=1 and T_{min}=1%).

B-Wheel Slip Control Based on Multiple Thresholds

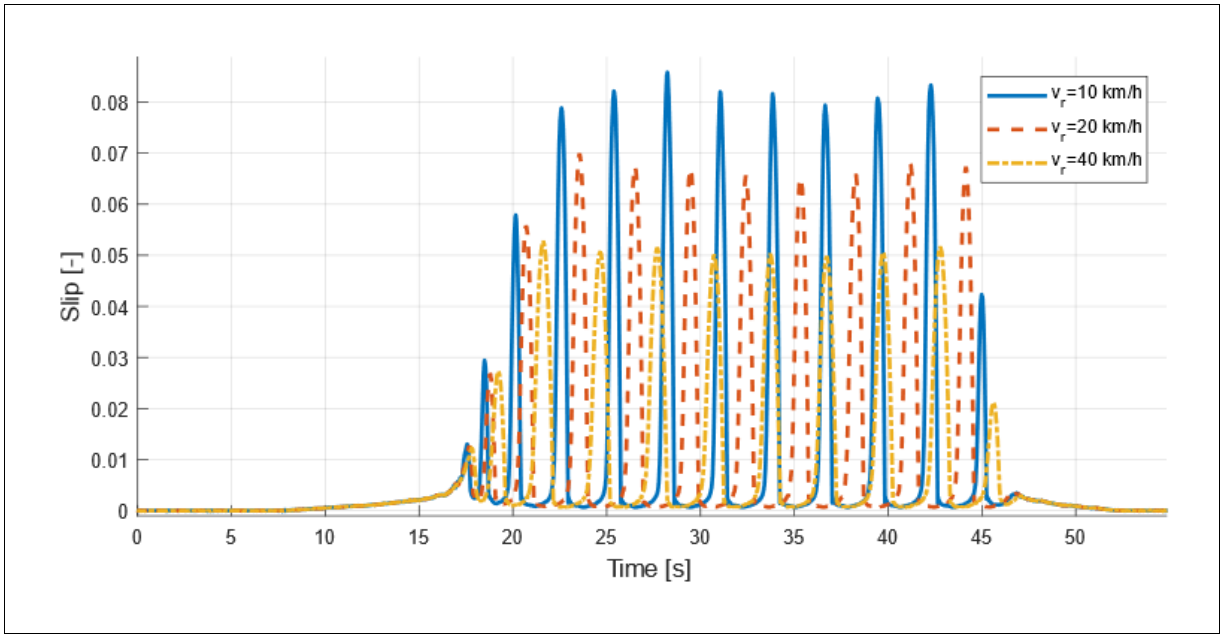

Simulation result of WSCMT performed under water contaminated test condition and different roller speeds (s_{th1}=0.006, s_{th2}=0.008, A_{dec}=1, A_{dec}=1 and T_{min}=15%).

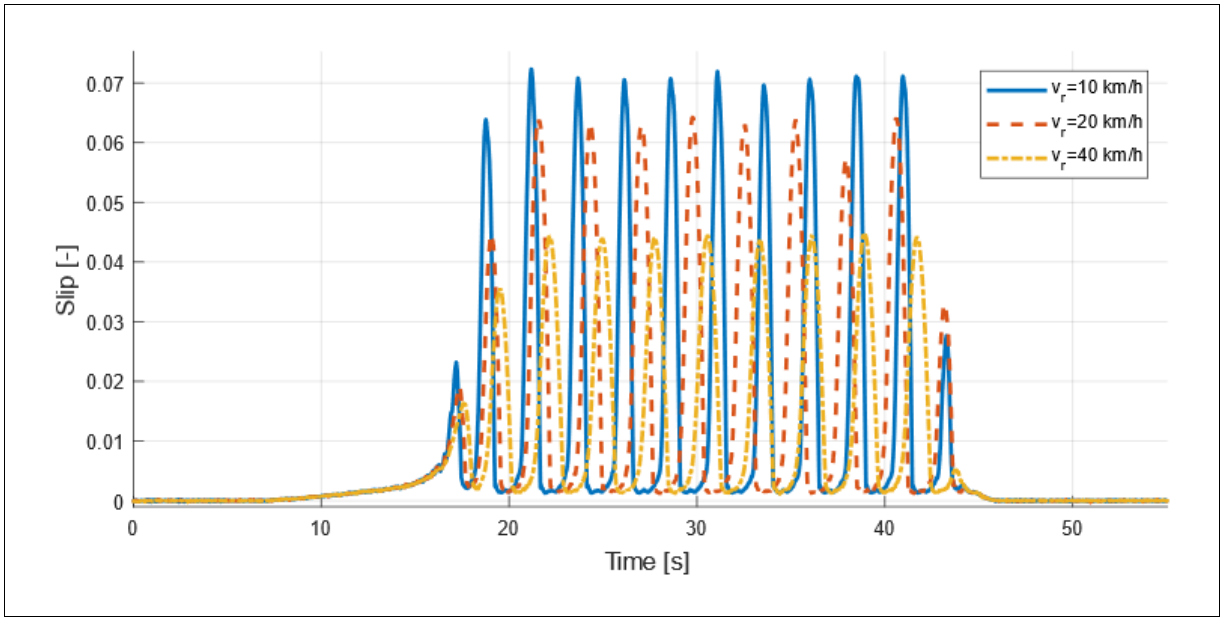

Simulation result of WSCMT performed under grease contaminated test condition and different roller speeds (s_{th1}=0.008, s_{th2}=0.012, A_{dec}=1, A_{dec}=1 and T_{min}=1%).

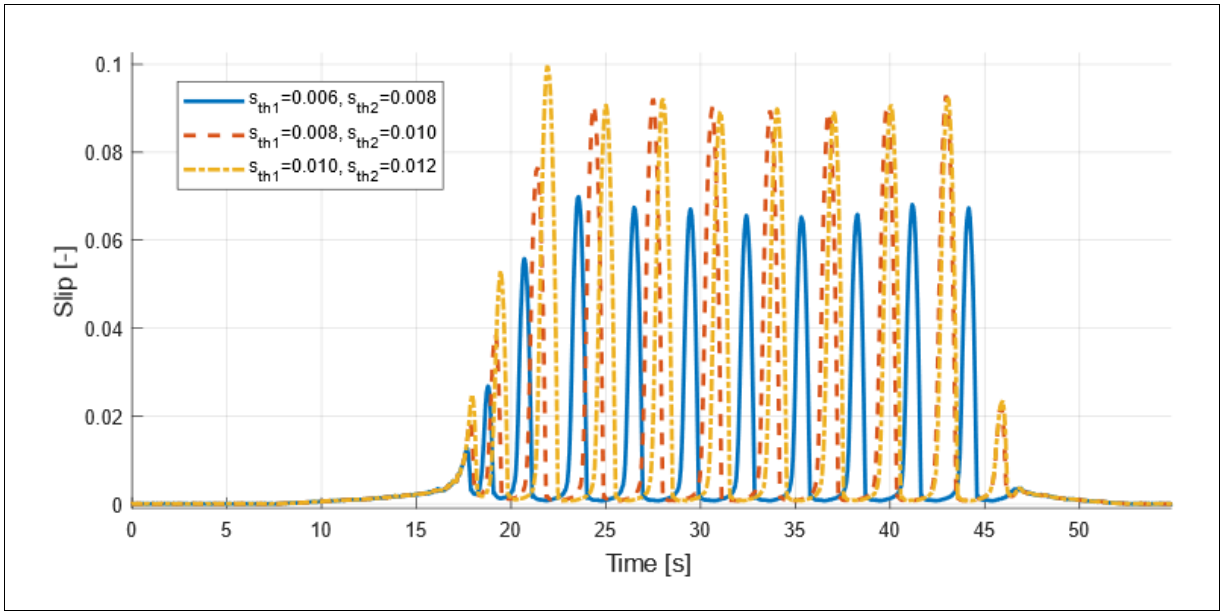

Simulation result of WSCMT performed under water contaminated test condition and different threshold values (v_r=20 km/h, A_{dec}=1, A_{dec}=1 and T_{min}=15%).

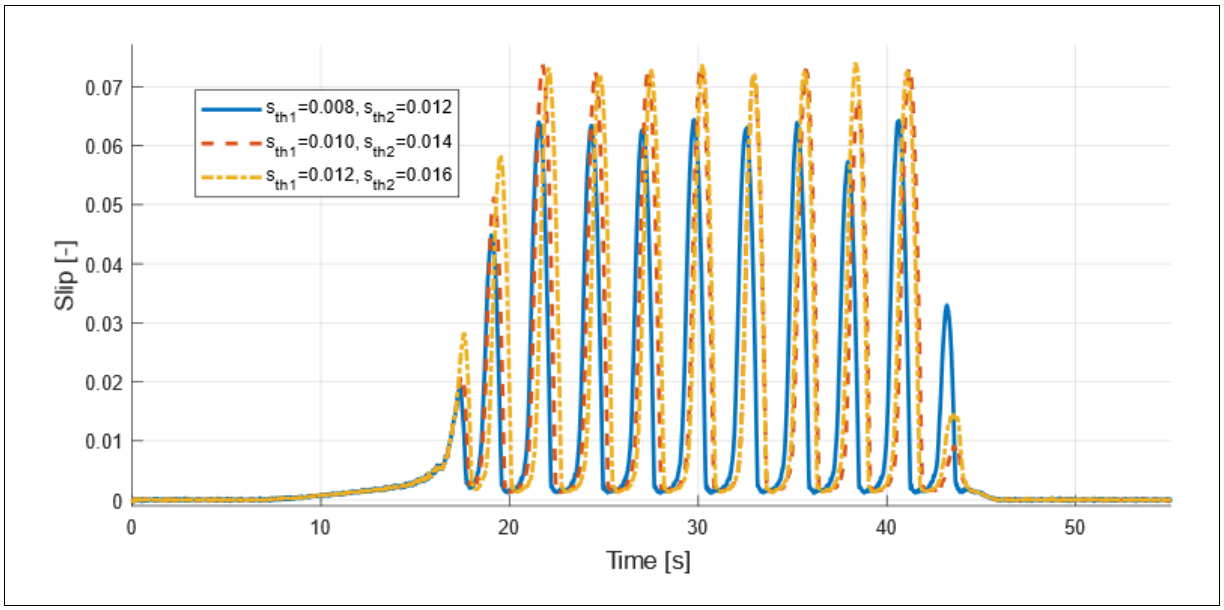

Simulation result of WSCMT performed under grease contaminated test condition and different threshold values (v_r=20 km/h, A_{dec}=1, A_{inc}=1 and T_{min}=1%).

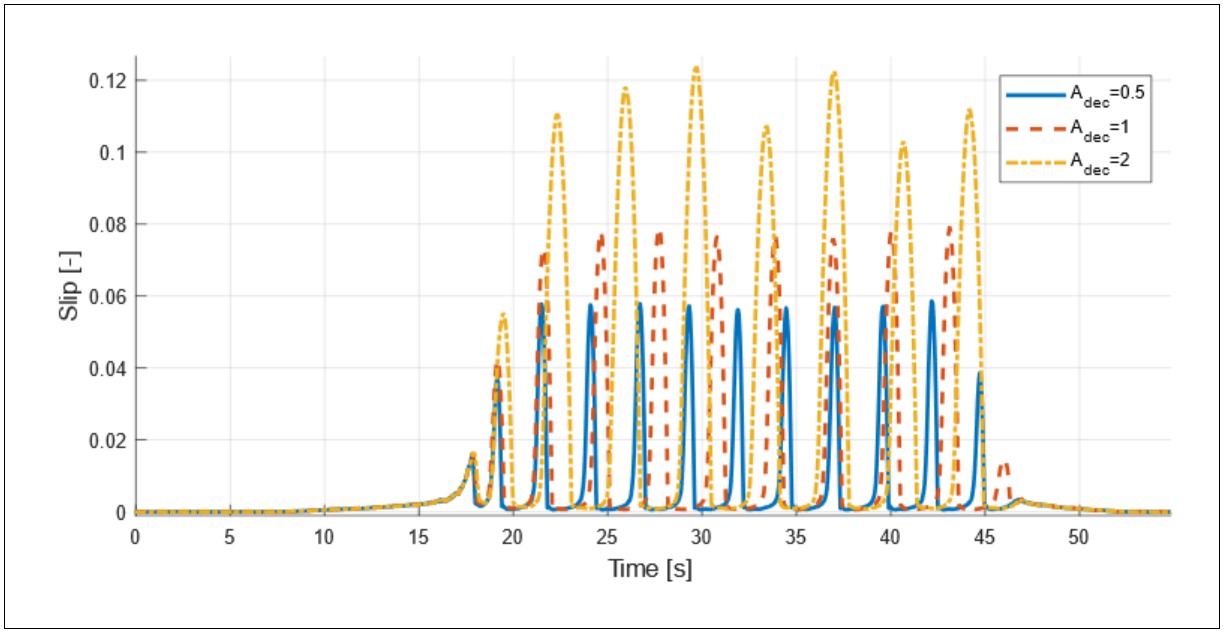

Simulation result of WSCMT performed under water contaminated test condition and different A_{dec} parameters (v_r=20 km/h, s_{th1}=0.006, s_{th2}=0.01, A_{inc}=1 and T_{min}=15%).

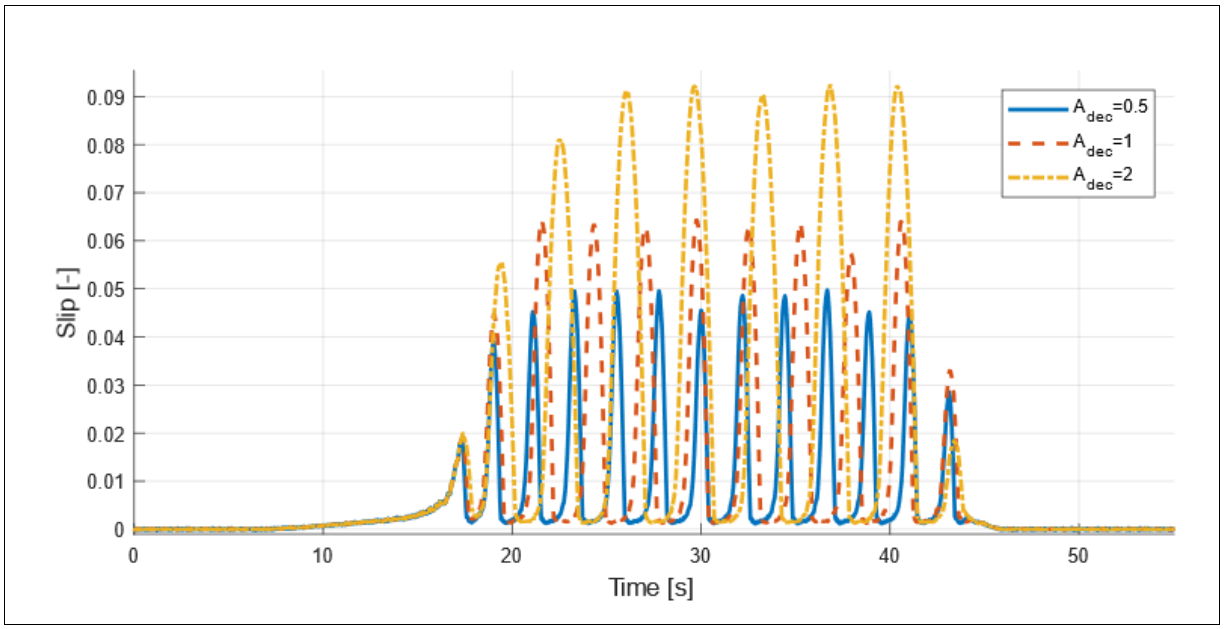

Simulation result of WSCMT performed under grease contaminated test condition and different A_{dec} parameters (v_r=20 km/h, s_{th1}=0.008, s_{th2}=0.012, A_{inc}=1 and T_{min}=1%).

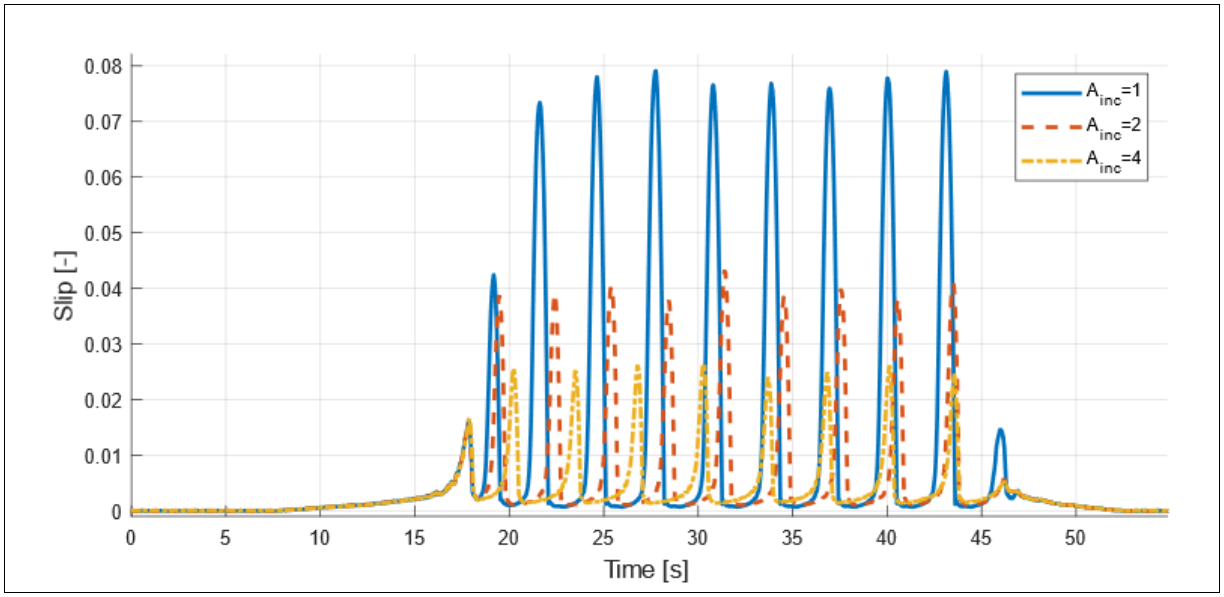

Simulation result of WSCMT performed under water contaminated test condition and different A_{inc} parameters (v_r=20 km/h, s_{th1}=0.006, s_{th2}=0.01, A_{dec}=1 and T_{min}=15%).

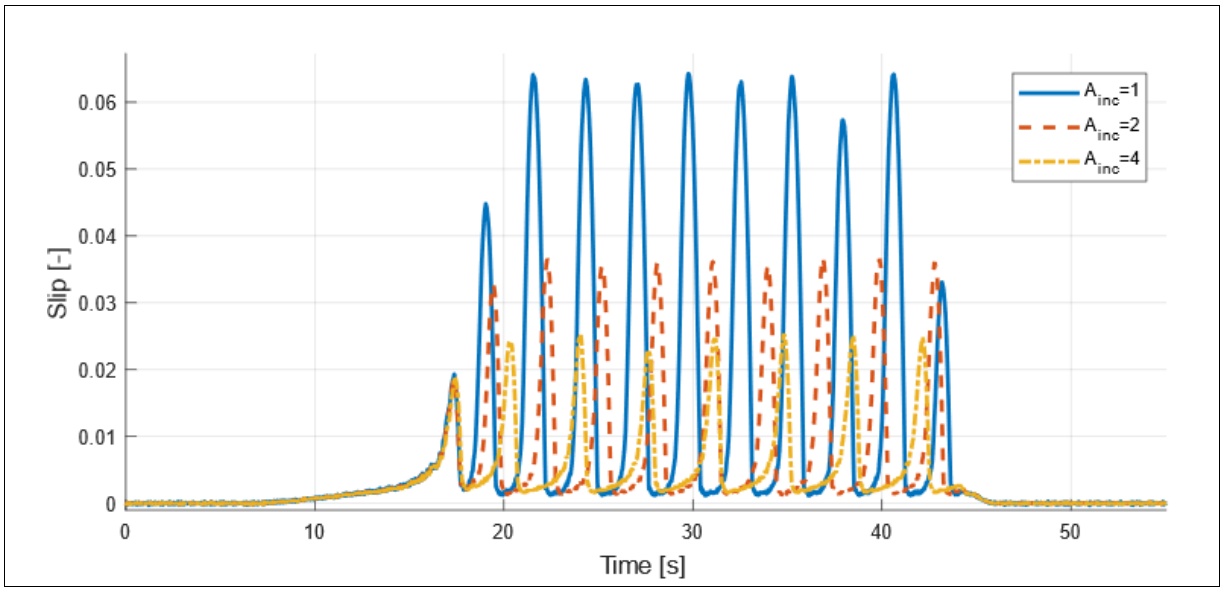

Simulation result of WSCMT performed under grease contaminated test condition and different A_{inc} parameters (v_r=20 km/h, s_{th1}=0.008, s_{th2}=0.012, A_{dec}=1 and T_{min}=1%).

C-Wheel Slip Control Based on Angular Acceleration of Wheel

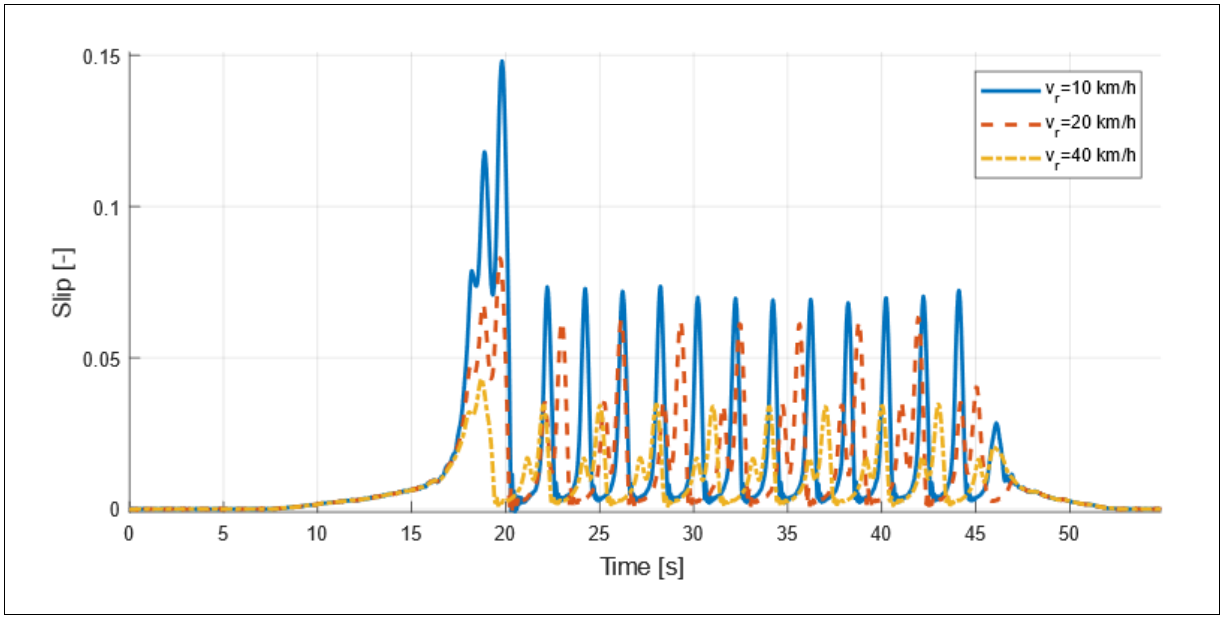

Simulation result of WSCAA performed under water contaminated test condition and different roller speed (α_{th}=0.75, A_{dec}=0.5, A_{inc}=1 and T_{min}=15%).

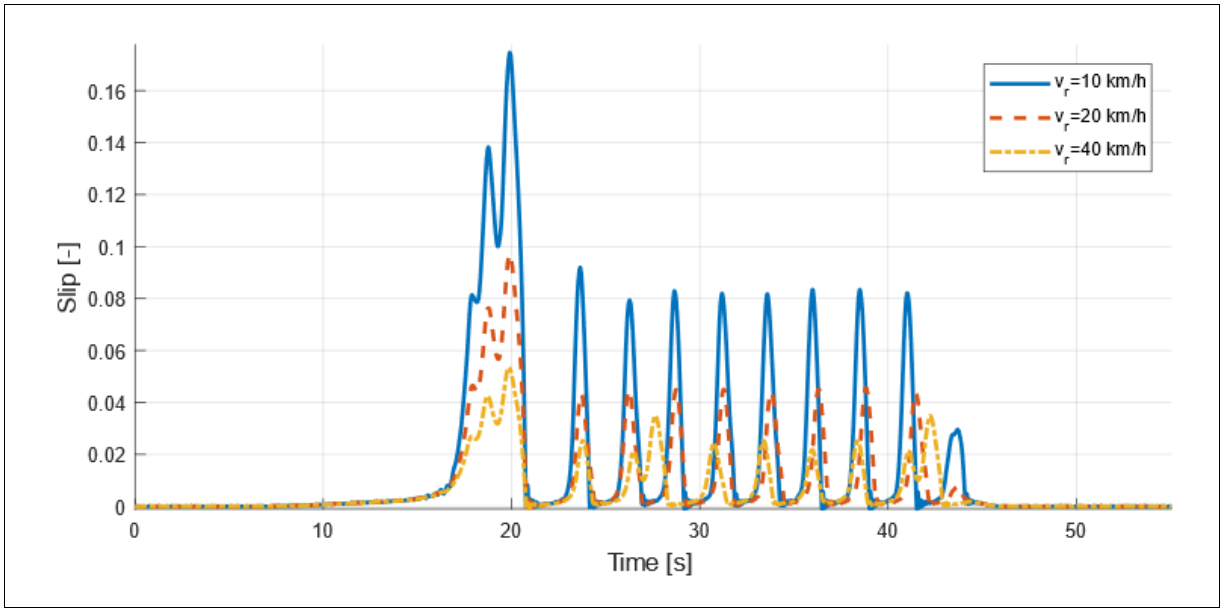

Simulation results of WSCAA performed under grease contaminated test condition and different roller speeds (α_{th}=0.75, A_{dec}=0.5, A_{inc}=1 and T_{min}=1%).

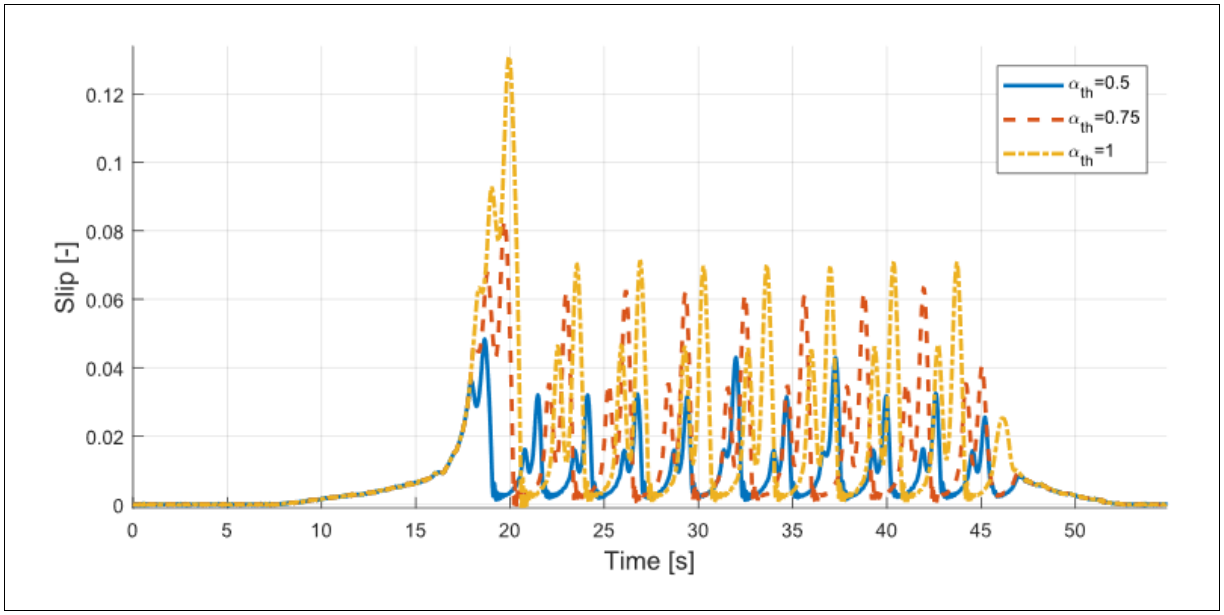

Simulation result of WSCAA performed under water contaminated test condition and different threshold values (v_r=20 km/h, A_{dec}=0.5, A_{inc}=1 and T_{min}=15%).

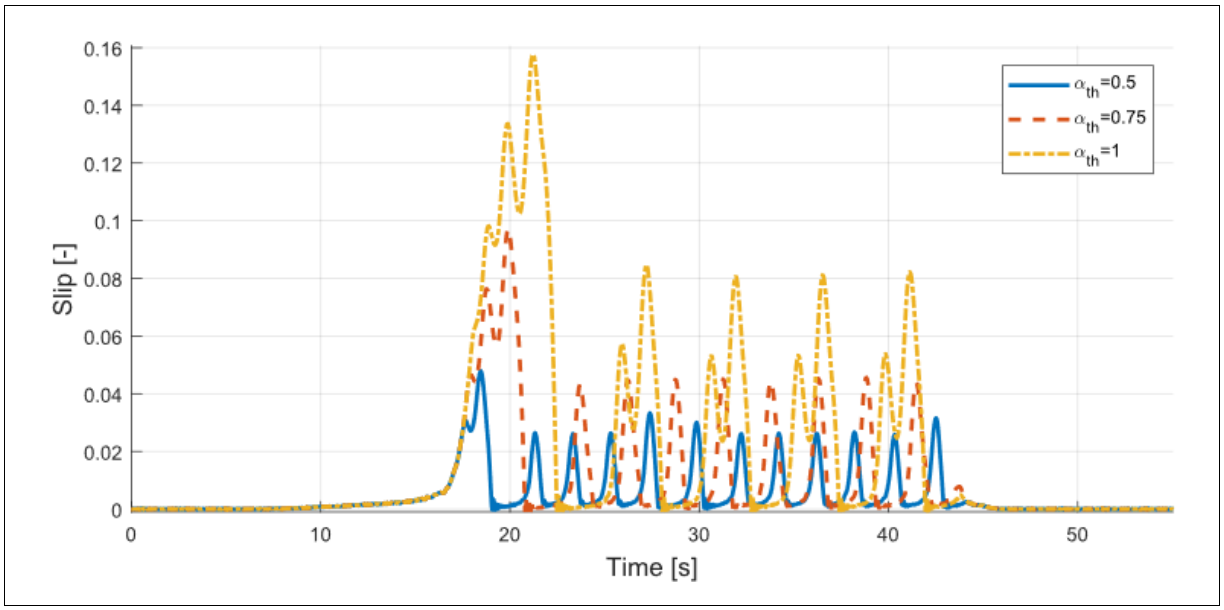

Simulation result of WSCAA performed under grease contaminated test condition and different threshold values (v_r=20 km/h, A_{dec}=0.5, A_{inc}=1 and T_{min}=1%).

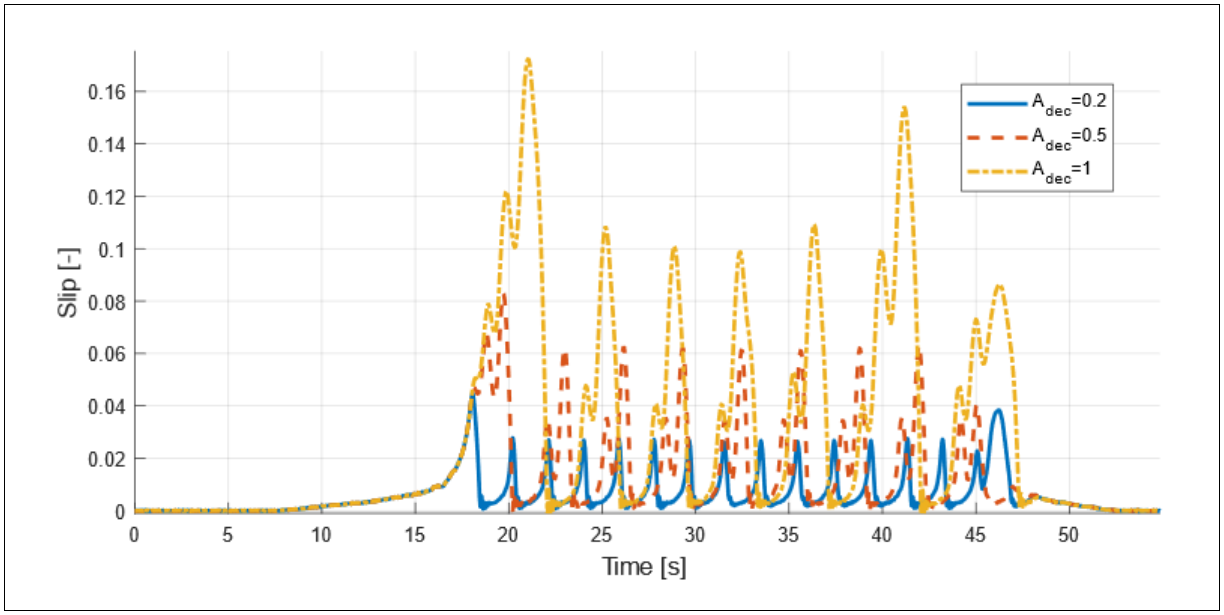

Simulation result of WSCAA performed under water contaminated test condition and different A_{dec} parameters (vs=20 km/h, α_{th}=0.75, A_{inc}=1 and T_{min}=15%).

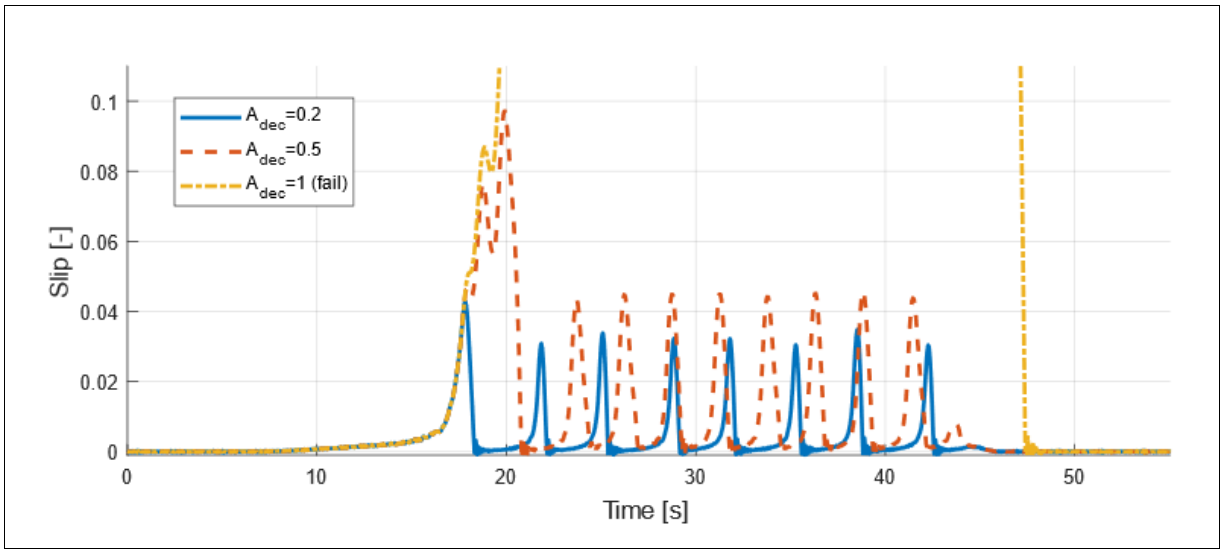

Simulation result of WSCAA performed under grease contaminated test condition and different A_{dec} parameters (vs=20 km/h, α_{th}=0.75, A_{inc}=1 and T_{min}=1%).

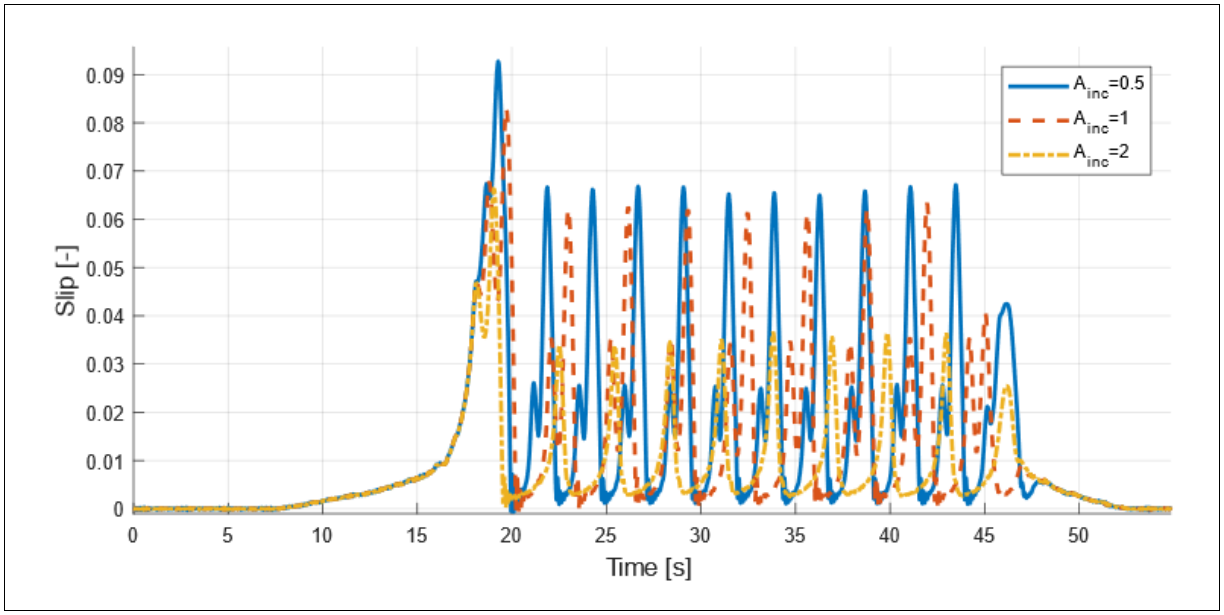

Simulation result of WSCAA performed under water contaminated test condition and different A_{inc} parameters (vs=20 km/h, α_{th}=0.75, A_{dec}=0.5 and T_{min}=15%).

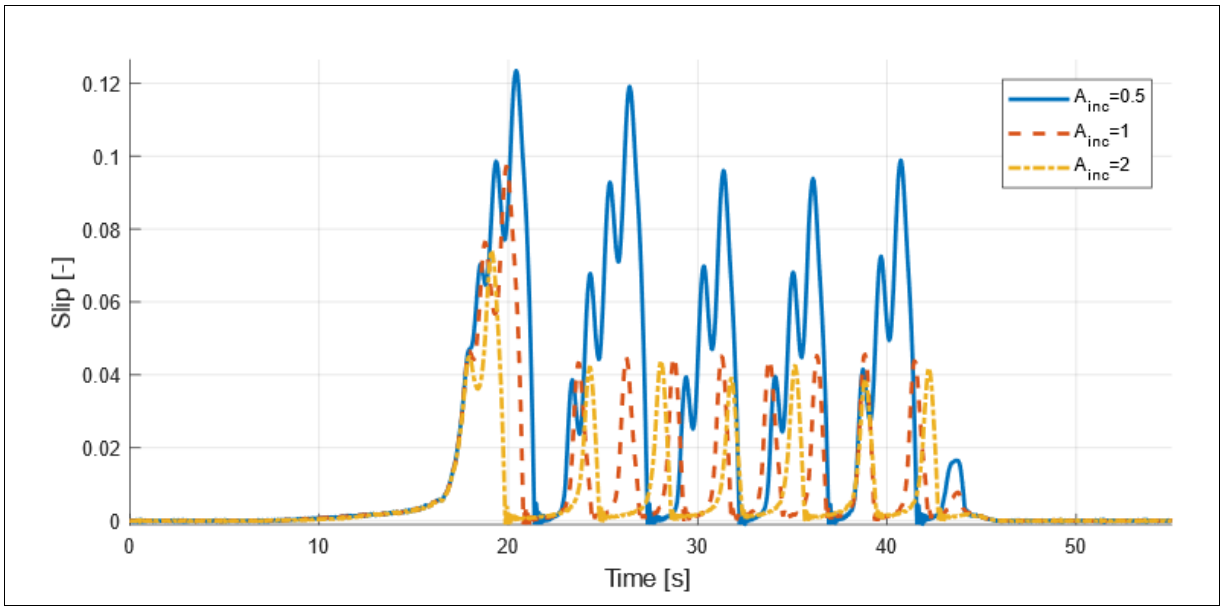

Simulation result of WSCAA performed under grease contaminated test condition and different A_{inc} parameters (vs=20 km/h, α_{th}=0.75, A_{dec}=0.5 and T_{min}=1%).

D-PI Wheel Slip Control

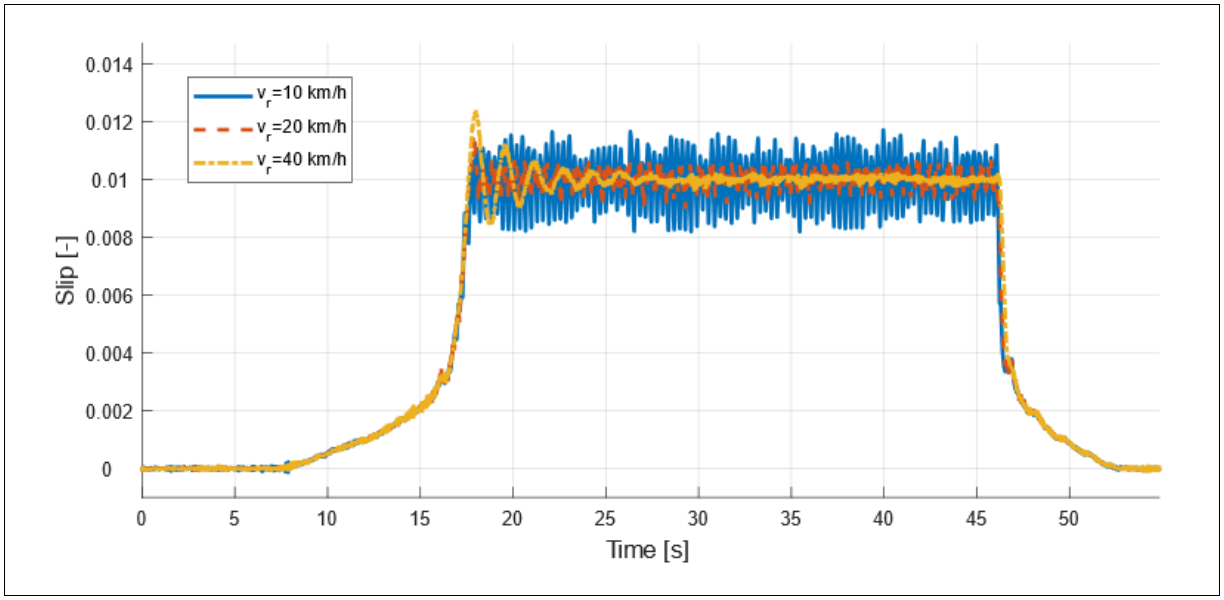

Simulation results of PI-WSC performed under water contaminated test condition and different roller speeds (s_d=0.01, K_p=200 and K_i=2000).

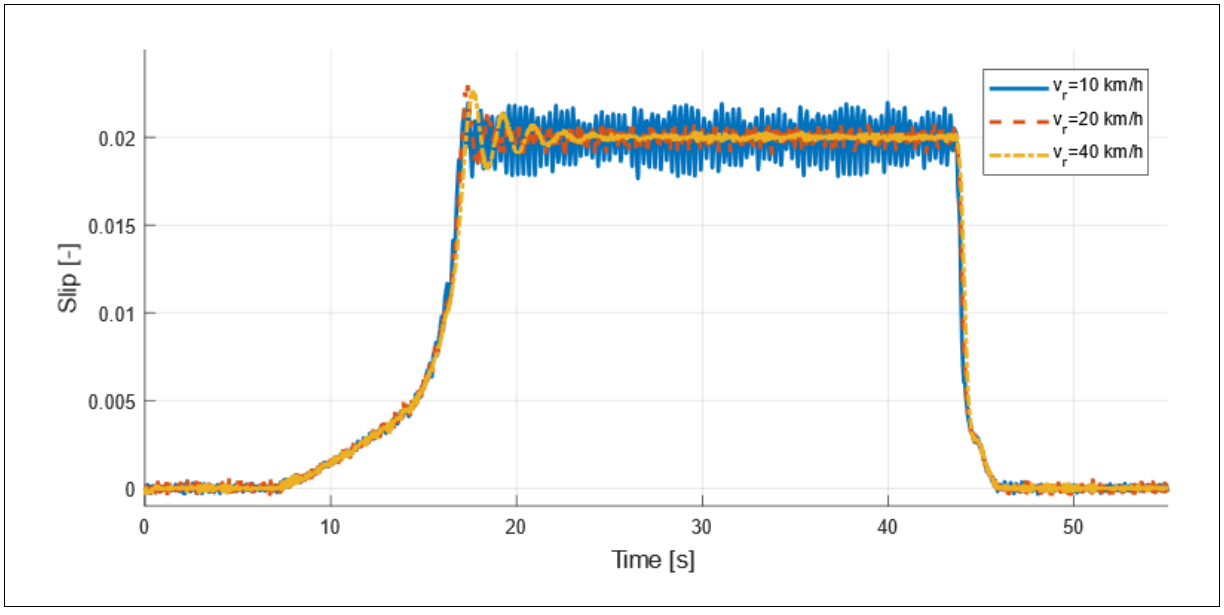

Simulation results of PI-WSC performed under grease contaminated test condition and different roller speeds (s_d=0.02, K_p=300 and K_i=2000).

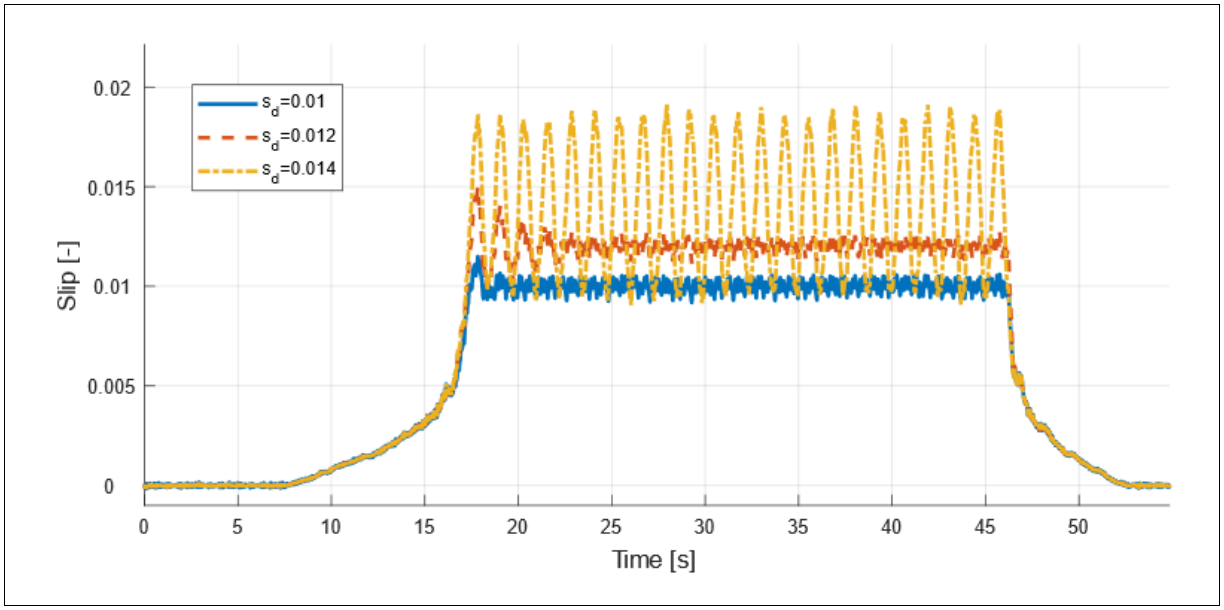

Simulation results of PI-WSC performed under water contaminated test condition and different desired wheel slip ratios (v_r=20 km/h, K_p=200 and K_i=2000).

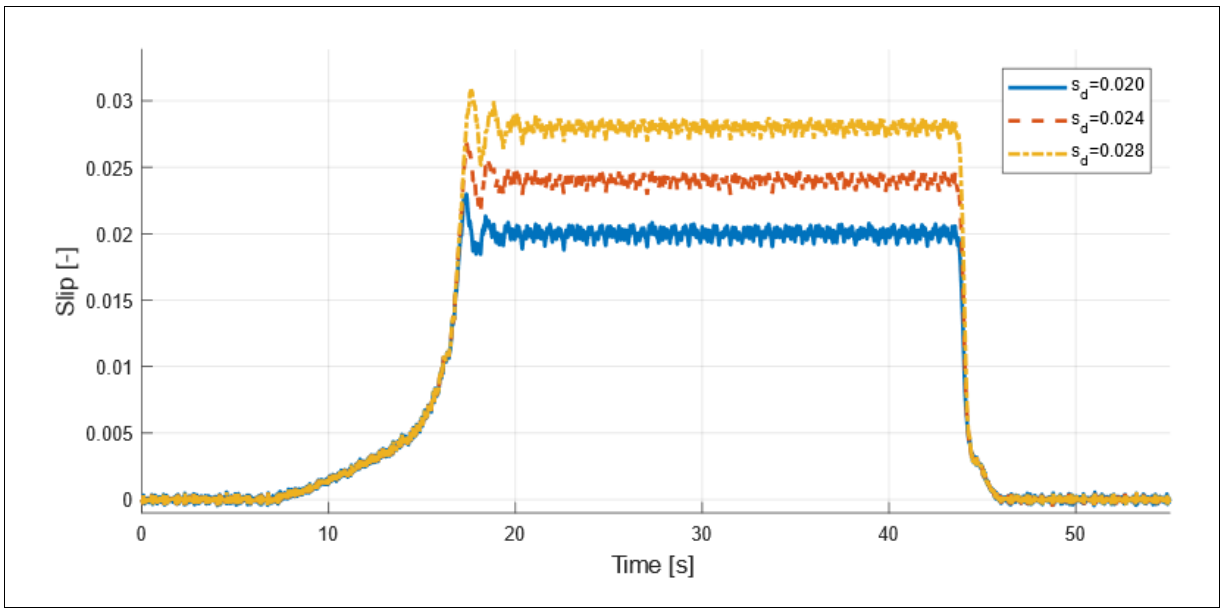

Simulation results of PI-WSC performed under grease contaminated test condition and different desired wheel slip ratios (v_r=20 km/h, K_p=300 and K_i=2000).

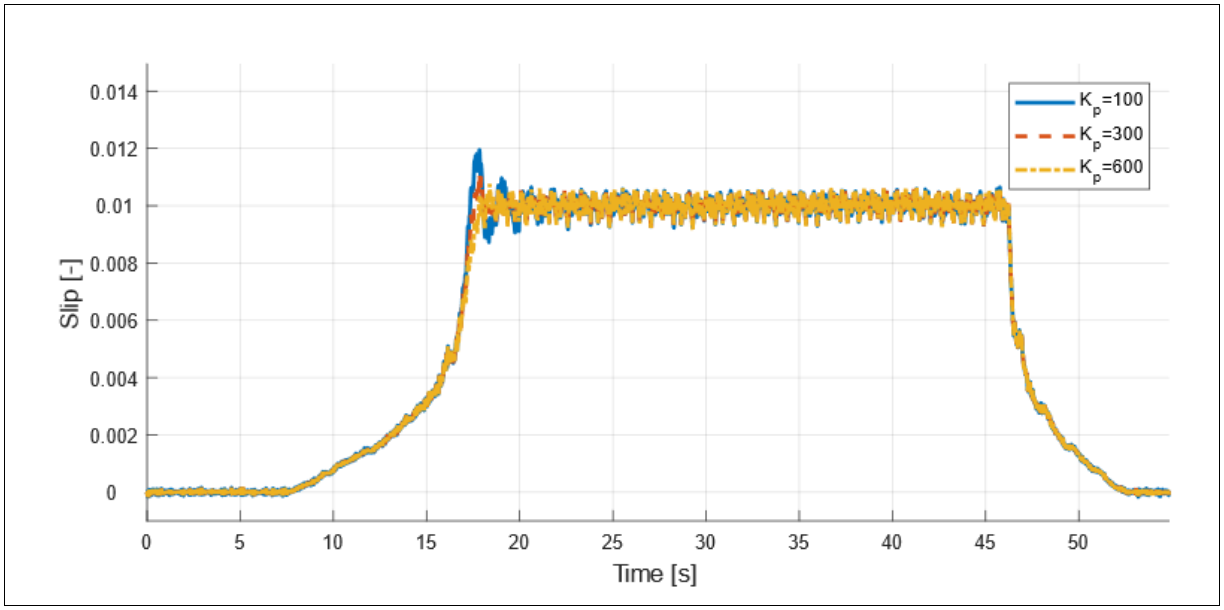

Simulation results of PI-WSC performed under water contaminated test condition and different K_p parameters (v_r=20 km/h, s_d=0.01 and K_i=2000).

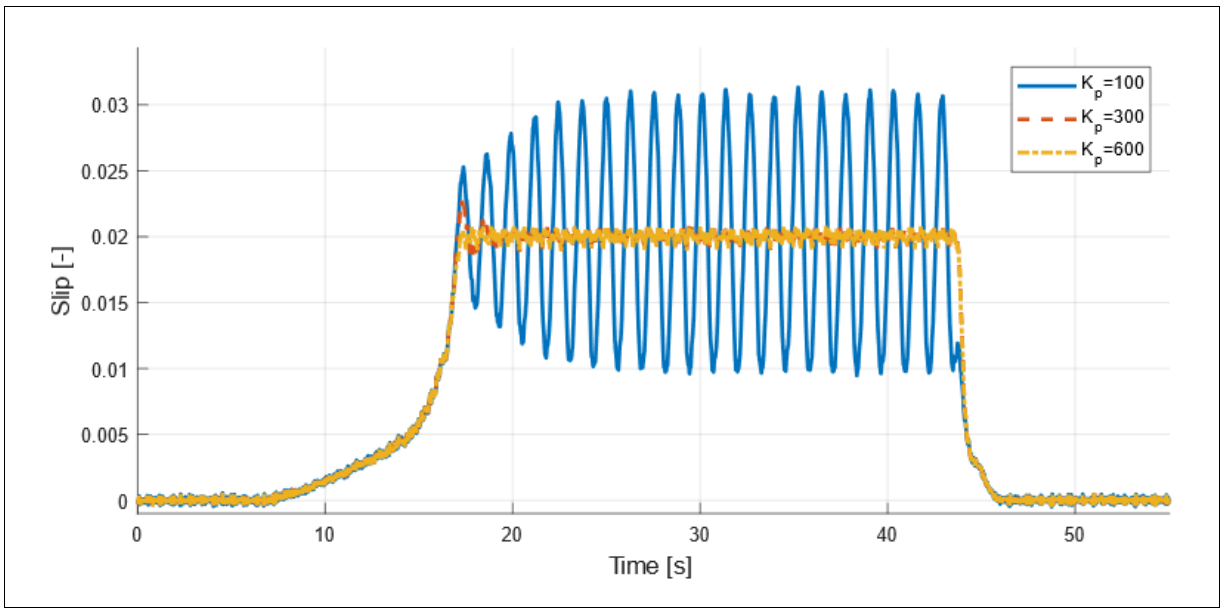

Simulation results of PI-WSC performed under grease contaminated test condition and different K_p parameters (v_r=20 km/h, s_d=0.02 and K_i=2000).

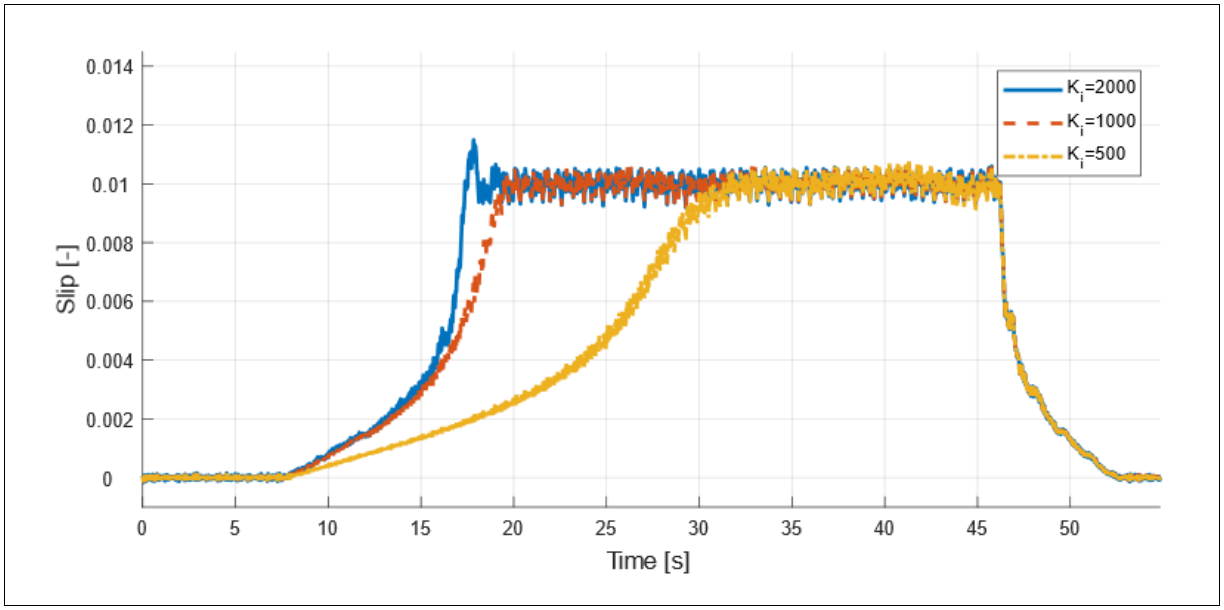

Simulation results of PI-WSC performed under water contaminated test condition and different K_i parameters (v_r=20 km/h, s_d=0.01 and K_p=200).

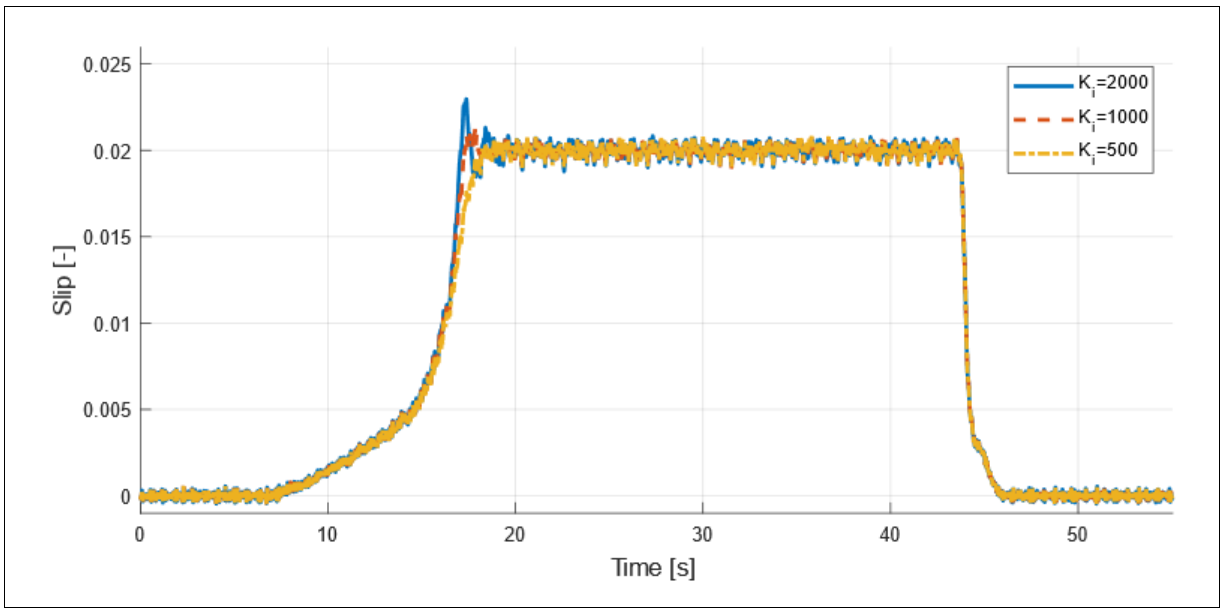

Simulation results of PI-WSC performed under grease contaminated test condition and different K_i parameters (v_r=20 km/h, s_d=0.02 and K_p=200).

E-Sliding Mode Wheel Slip Control

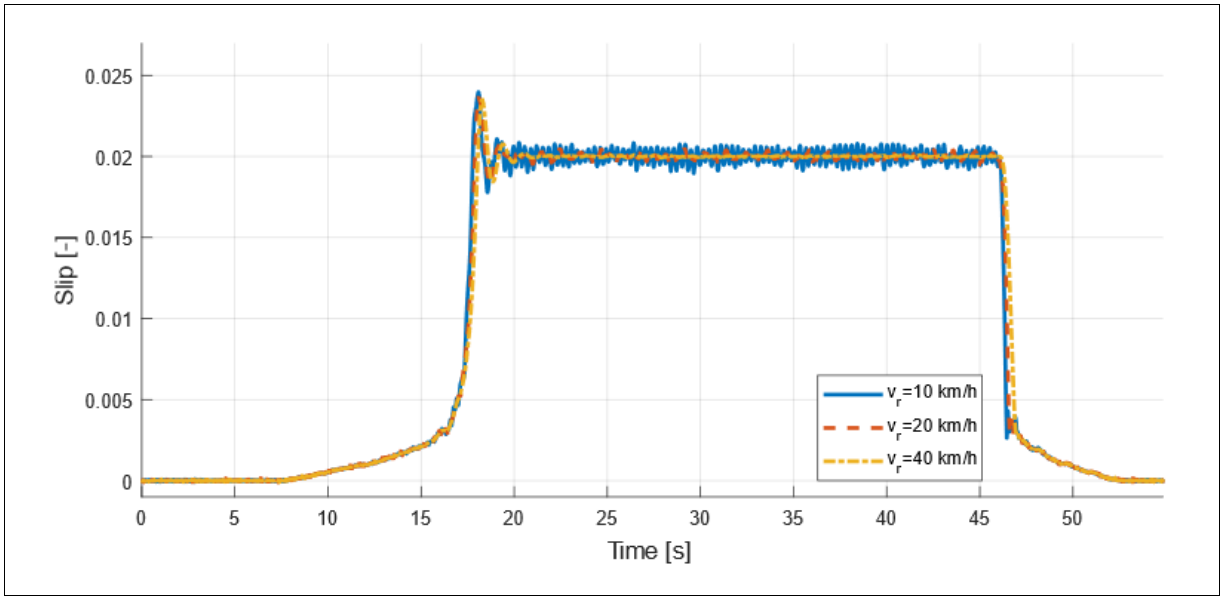

Simulation results of SM-WSC performed under water contaminated test condition and different roller speeds (s_d=0.02, D=10 and K=1).

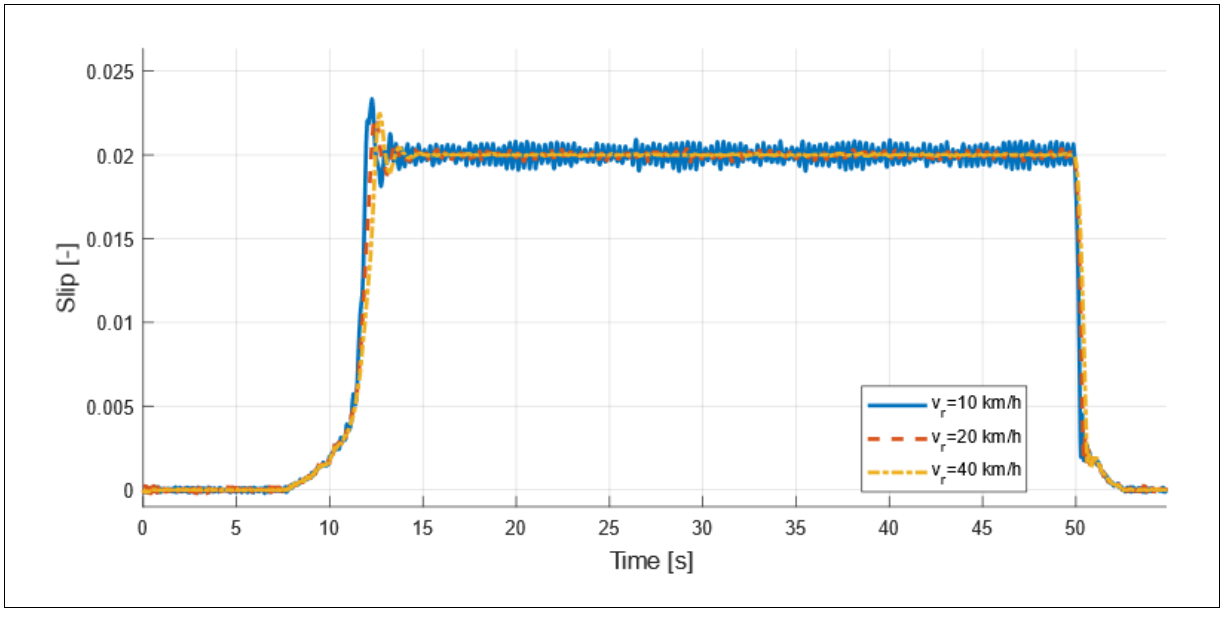

Simulation results of SM-WSC performed under grease contaminated test condition and different roller speeds (s_d=0.02, D=10 and K=1).

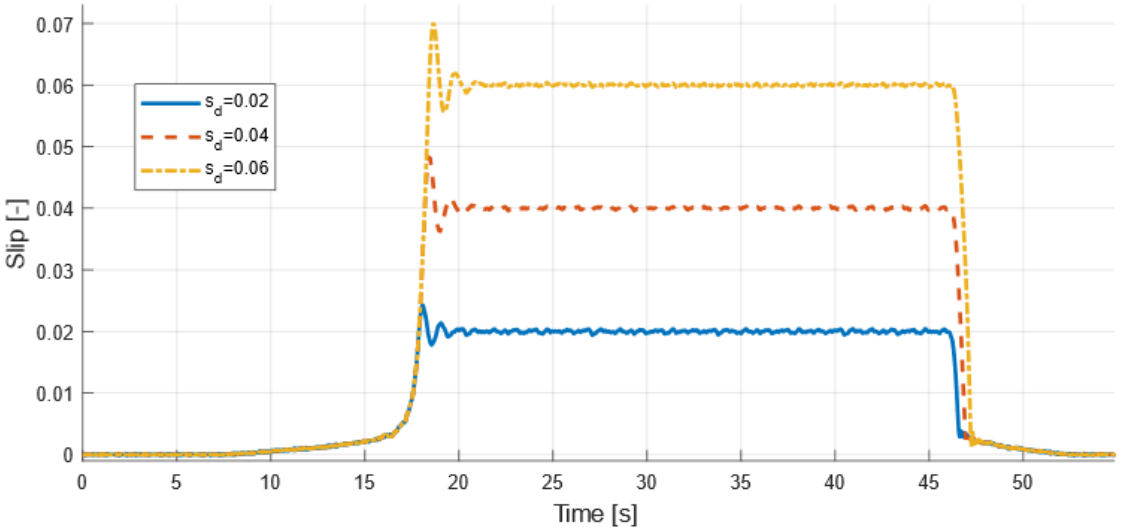

(a)

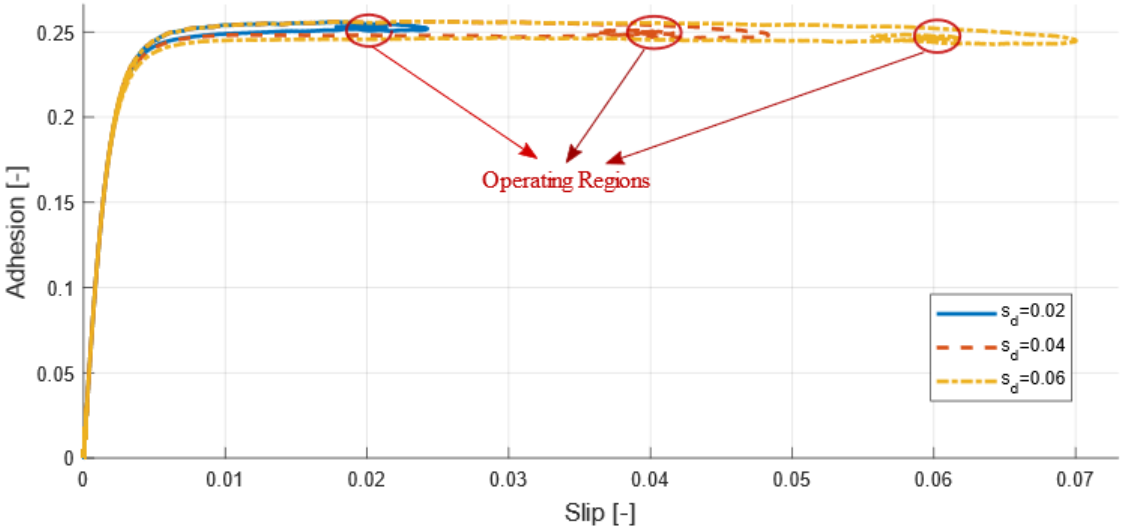

(b)

Simulation results of SM-WSC performed under water contaminated test condition and different slip wheel slip ratios (v_s=20 km/h, D=10 and K=1); (a) Wheel slips (b) Slip curves.

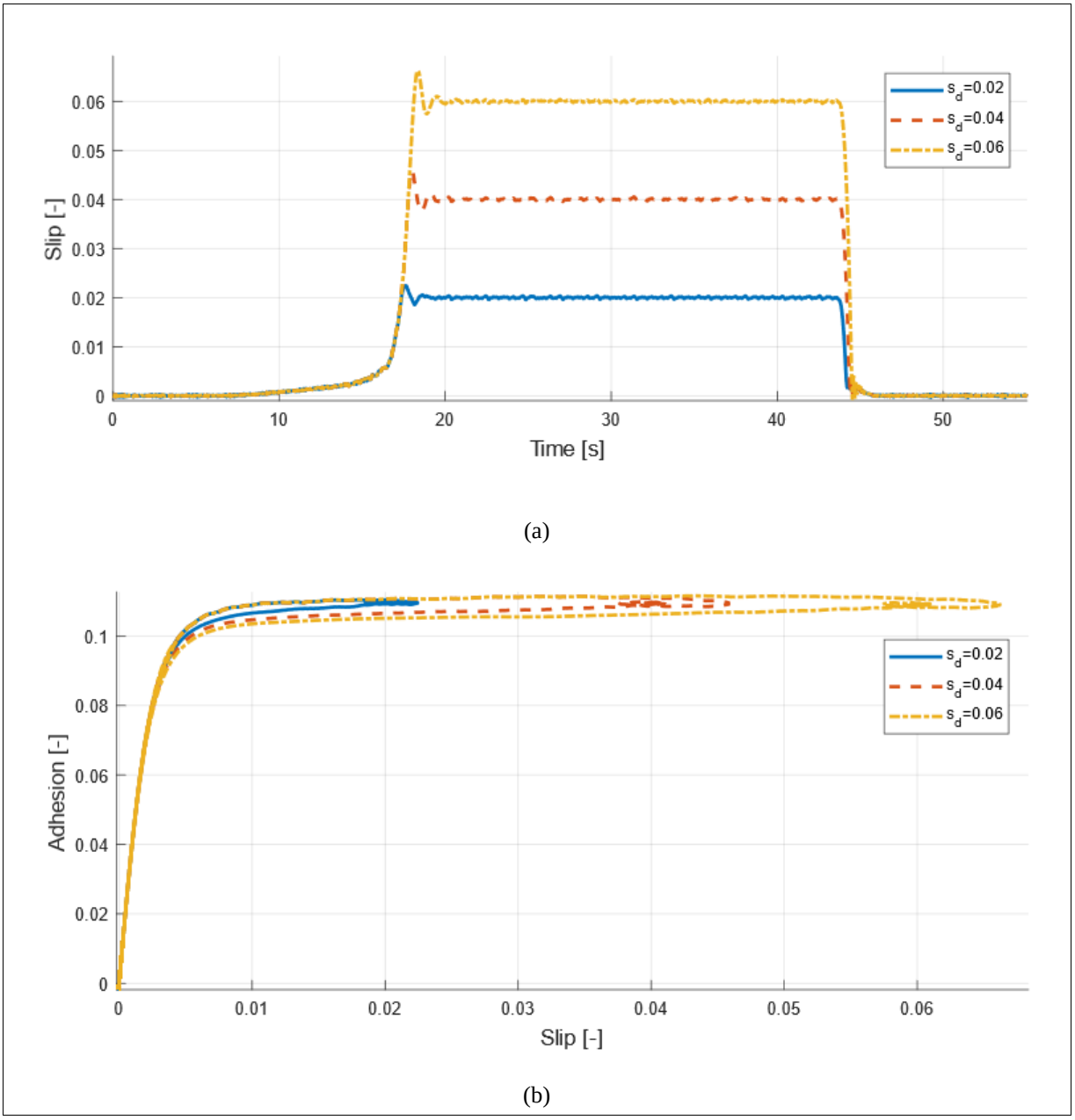

Simulation results of SM-WSC performed under grease contaminated test condition and different wheel slip ratios (v_s=20 km/h, D=10 and K=1); (a) Wheel slips (b) Slip curves.

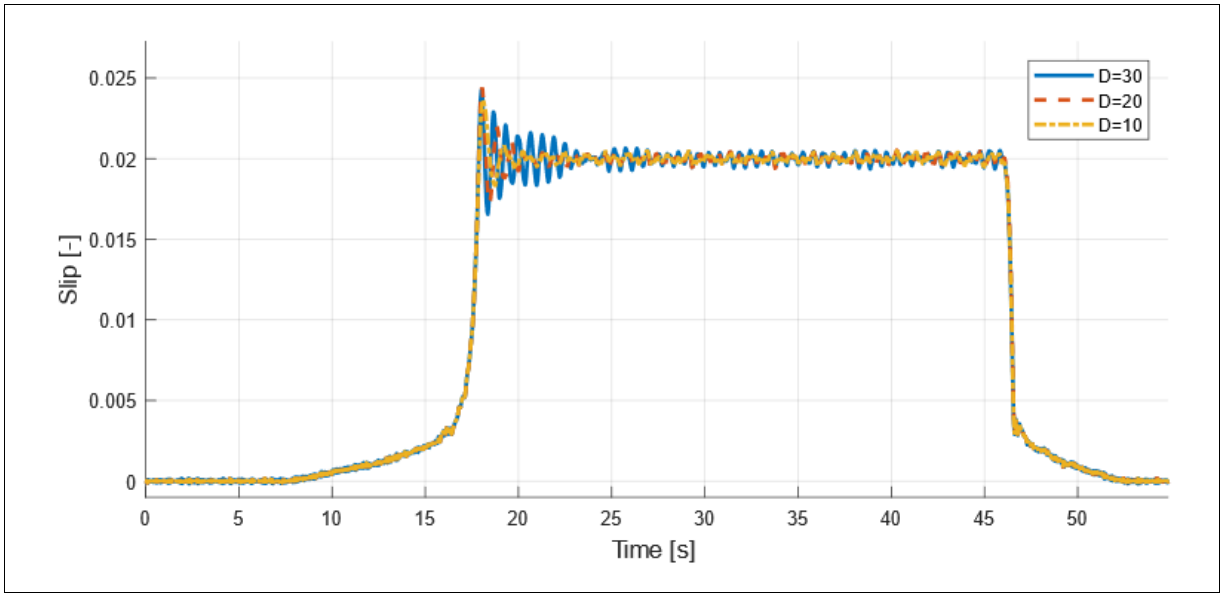

Simulation results of SM-WSC performed under water contaminated test condition and different D design parameters (v_s=20 km/h, s_d=0.02 and K=1).

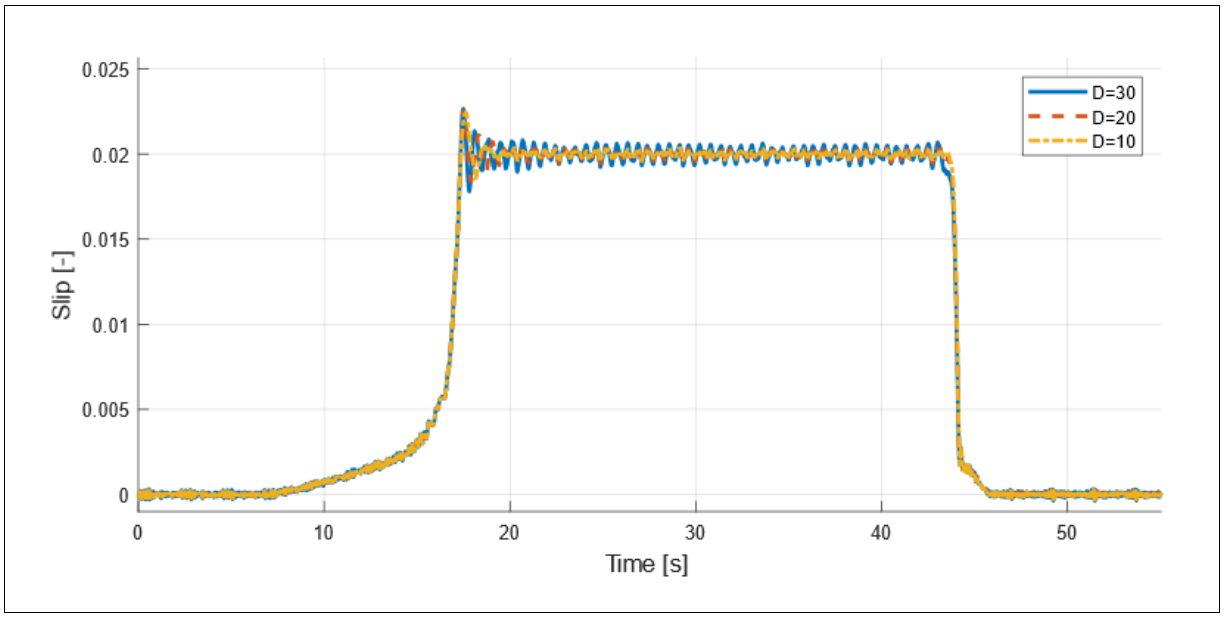

Simulation results of SM-WSC performed under grease contaminated test condition and different D design parameters (v_s=20 km/h, s_d=0.02 and K=1).

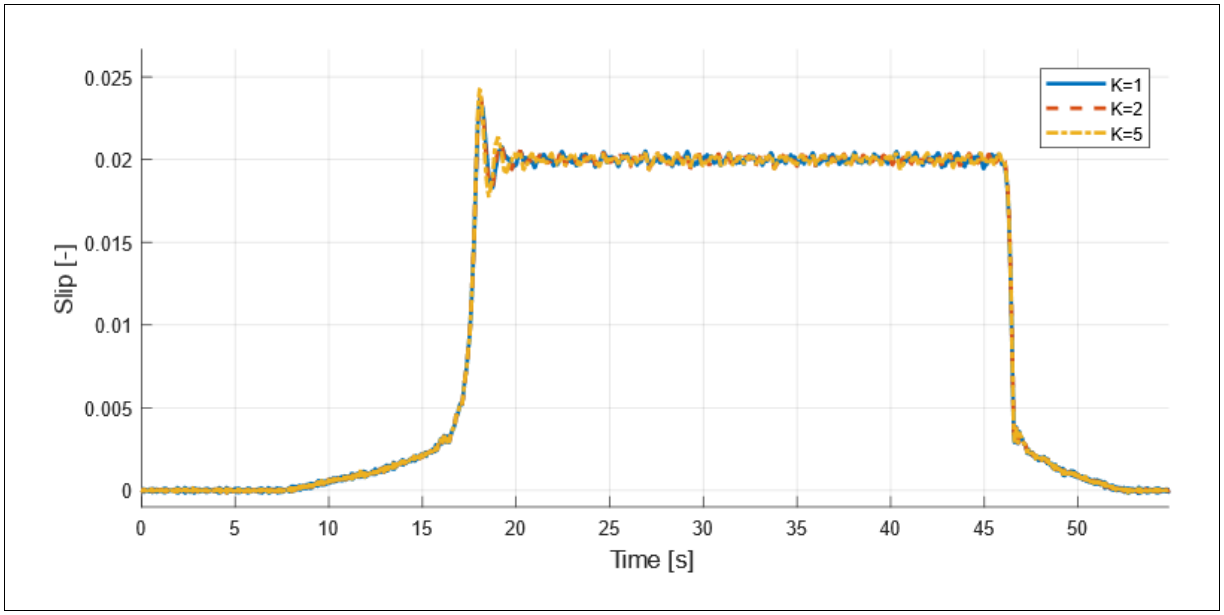

Simulation results of SM-WSC performed under water contaminated test condition and different K design parameters (v_s=20 km/h, s_d=0.02 and D=10).

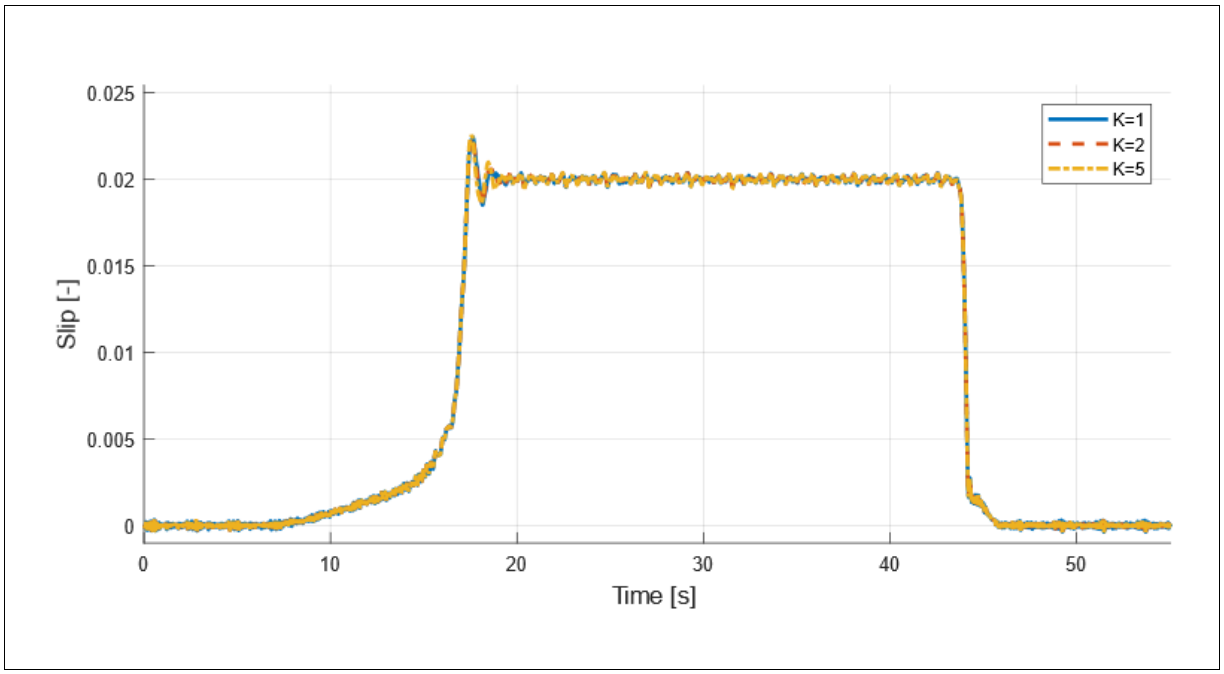

Simulation results of SM-WSC performed under grease contaminated test condition and different K design parameters (v_s=20 km/h, s_d=0.02 and D=10).